USING NONLINEAR OPTICAL PROPERTIES IN CONJUNCTION WITH CHEMICAL SYNTHESIS TO UNDERSTAND DEFECTS IN SELF-ASSEMBLED MOLECULAR FILMS

By

Wendy Christian Flory

A DISSERTATION

Submitted to
Michigan State University
in partial fulfillment of the requirements
for the degree of

DOCTOR OF PHILOSOPHY

Department of Chemistry

2000

ABSTRACT

USING NONLINEAR OPTICAL PROPERTIES IN CONJUNCTION WITH CHEMICAL SYNTHESIS TO UNDERSTAND DEFECTS IN SELF-ASSEMBLED MOLECULAR FILMS

By

Wendy Christian Flory

The potential utility of self-assembled monolayer and multilayer (SAM) thin films in applications such as optical information storage, photorefractives, and solid state microelectronics is generating a great deal of attention in the chemistry and materials science communities. The interest in these materials arises because of the ease of growth, the mild conditions for the formation of the self-assembled layers, and the structural and thermal stability of these assemblies, once they are formed. Because of the Zr-bisphosphonate interlayer linking chemistry, these films are self-terminating at each layer, allowing for the identity of individual layers to be controlled by macroscopic means. The zirconium-phosphate/phosphonate linkage is used because it is a thermally stable inorganic crystalline structure. The bulk properties of these films are currently being studied, but one issue that remains to be addressed is the quantification and characterization of defects in the formed layers. A novel approach to measuring defects on a molecular scale is to utilize the functional chemistry for orientational control in the growth of these films. By constructing these films with control over the orientation of each layer, a multilayer film can be assembled with either centrosymmetric or noncentrosymmetric bulk ordering. Theoretically, the $\chi^{(2)}$ nonlinear response of an

opposing bilayer structure should be zero because there is a center of inversion in the macroscopic assembly, and any surface second harmonic generation (SHG) signal observed from this film should be the direct result of defects.

Katz and coworkers developed a nonlinear chromophore for use in SAM assemblies. This chromophore (**1**) is a rigid azo dye with a large molecular hyperpolarizability giving rise to a large second harmonic signal from each monolayer. Functionalizing only one terminus with a phosphonate group controls the orientation of this chromophore. When this molecule is exposed to a zirconated surface, it adsorbs with the phosphonate group directed toward the surface. The exposed hydroxyl terminus of the chromophore is then phosphorylated. The second chromophore (**2**) is identical to the first except the functional groups at each end are exchanged. By synthesizing these chromophores so that they are functionalized selectively at each terminus, we can control the direction of the dipole moment for each formed layer. By assembling one layer each of chromophores **1** and **2**, we can construct a bilayer with a center of inversion. Quantifying the intensity of the SHG signal, which is present against a small background, we can work toward gaining an understanding of defect properties in ZP SAMs.

In Memory of Florence Wilhemina Schaus Christian

ACKNOWLEDGMENTS

I would first and foremost like to thank my advisor, Gary J. Blanchard, for the help and support he has given me while I was a graduate student. He has offered me his knowledge, patience, and understanding through the years and I will always be grateful for that. I would not have been able to learn as much as I have without Gary as an advisor. I would also like to thank the members of my committee; Prof. Marcos Dantus, Prof. Greg Baker, and Prof. Kris Berglund. It has been a pleasure having each of you as part of my committee.

I would also like to thank the guys from the machine and electronic shops, who have been a part of my research trek. Russ, Dick, Sam, Glenn, and Tom, you have all come through in quickly machining the parts that I've needed in the development of the laser systems over the years. Because of you I've become very good at making banana bread! Ron and Dave, thanks for the advice when I was building the circuitry for the system. And thanks, Ron, for the many great jokes through email!

To my mother, whose constant insistence that I go to college was the real driving force for me to not be afraid to follow my dreams, no matter what happens, thank you. Thanks to my father who also taught me that, even if I failed, it was okay. Both of you have taught me many important lessons in life. To my siblings and their spouses: Pam and Bryan, John and Sue, and Amy and Lonnie, thank you for always supporting me, sending me care packages when I'm down, and calling me just to say hello. These things meant a lot to me.

I would not have been the person I am today without the love and support from

my friends, who've always been there for me. Thanks to Jill, Dawn, Leslie, Michelle, and Andrea. You guys have been my confidants for a very long time. Dale, you've been a big part of my life here at MSU, thanks. Tom and Richard, my pseudo-parents(?), thanks for watching out for me, and hosting a lot of great parties! Bob, thanks for always having a positive outlook on life. To the rest of my MSU friends, Karen, Joann, Lynda, Shannon and Jeremy, Shawn, Lee and Carina, Kristi, and Lofy, thanks for the fun times! All of my friends will always be an important part of my life. To the many softball teams I've been apart of, I'll always remember all the great times we've had at Art's. Finally, to the past, present, and future Blanchard group members, good luck!

TABLE OF CONTENTS

LIST OF TABLES

LIST OF FIGURES

Chapter 1

INTRODUCTION

In recent years there has been a surge of research interest in processes that will chemically modify surfaces, which can then be used in applications such as solid-state electronics, electro-optic devices, and optical information storage.[1,2] The thin films that are built off of surfaces, either through physisorption or chemisorption, can be used for these applications only if the molecular construction can be controlled. Modifications of these surfaces have lead to the development of many clever synthetic routes aimed at inducing molecular orientation in these layered materials.

The first monolayer assemblies studied were Langmuir-Blodgett(LB) thin films[3-5] The LB technique involves the mechanical transfer of a compressed molecular monolayer at the air-liquid interface to a substrate. The monolayer is created through the use of amphiphilic molecules. These molecules form highly ordered monolayers when compressed laterally at the liquid interface and can be physisorbed onto a surface to form multilayer assemblies through sequential dipping of a substrate.[6] The drawbacks of this family of layered materials come from the relatively complex procedures for layer formation, their sensitivity to impurities, and the weak intermolecular interactions. Because their order derives from relatively weak van der Walls forces, they are not thermally stable, nor can persistent order be maintained indefinitely in multilayer assemblies.[7]

The most recently developed route to building thin films with molecular orientation is using self-assembled mono- and multilayers (SAM).[8-17] SAMs are thin

films built by chemically linking the functionalization groups of a substrate with a molecule that is in solution through covalent bonding. Noncovalent intermolecular forces enforce in-plane ordering of the layer. An excellent review article on SAMs discusses the various types of assemblies used, including alkanethiols on gold and organosilane and metal phosphonate binding chemistries.[18]

Thiols on metals such as Au and Ag were one of the first SAM systems to be explored as a means to control surface morphology.[18-20] Many studies of these systems have been reported.[21,22] While these films are highly ordered and are structurally and thermally stable, the thin film characteristics obtained depend sensitively on the metal substrate used in their formation. Thiol/gold monolayers suffer from long-term chemical stability limitations[23,24] and, until recently, the inability to form chemically-bound multilayer assemblies.[25]

Silane multilayers from silicon and silica substrates have also been investigated.[26-29] Alkylaminosilanes, alkylchlorosilanes, and alkylalkoxysilanes require a hydroxylated surface such as silica or alumina for the monolayer to form.[18] A high quality surface of this type is difficult to assemble because of the careful control needed to be maintained over the amount of water present during synthesis. Too little water will lead to incomplete layer formation, while too much water leads to polymerization of the solution.

SAMs made using metal-phosphonate (MP) chemistry have been studied for the last 12 years as a novel route to surface modified assemblies.[8,30-34] MP SAMs have robust physical properties with persistent structural anisotropy. These are very attractive features for using MP thin films in materials-based applications. Zirconium phosphonate

SAMs were first demonstrated by the Mallouk group, where layered structures from α,ω-alkanebisphosphonates were reported.[35] A typical deposition process procedure is as follows: a substrate is treated to produce a Zr^{4+}-rich surface and, when exposed to phosphonate moieties, the groups react forming an inorganic structure. The substrate is then dipped into a zirconium solution, allowing the exposed phosphonate to react, capping the molecular sheet and forming another zirconium rich surface. Multiple layer growth in a two-step fashion formed films that were quickly formed and robust over many layers. This work spurred a great deal of research effort on MP SAMs by several groups.[36-48] The films initially reported by the Mallouk group were centrosymmetric about the metal center because the direction of the organic moiety within the layer formed could not be controlled. Either of the phosphorylated ends could react with the zirconium surface.

Howard Katz *et al.* reported a scheme to incorporate molecular-level orientation within each layer by utilizing a three-step synthetic approach to the formation of the layers instead of the two step method reported initially.[8] The same ZP inorganic structure would still be used as the main construction, but instead of having both ends of the organic molecule phosphonated, Katz *et al.* used molecules that were phosphonated at one terminus, thereby controlling the orientation of the formed layer. The exposed terminus of the adsorbed molecule contained a hydroxyl moiety that could be reacted with $POCl_3$ to form a phosphate functionality. When reacted with a Zr^{4+} solution, the surface was ready to be reacted through the three step cycle again. Initially, this directional order was used to build films for use as nonlinear optical thin films. These assemblies exhibit nonlinear responses comparable to inorganic materials, such as $LiNbO_3$.[8] We have

chosen the three step synthetic strategy to explore a novel method to characterize the defect properties of SAMs.

With these various strategies of controlling thin films by chemical means, there is a growing interest in characterizing the defects within these assemblies.[49-53] The techniques most commonly used are electrochemistry, atomic force microscopy (AFM), and scanning electron microscopy (SEM). These methods probe a range of microscopic levels.[54-60] While the results for these measurements indicate defect sites to within the resolution of the instrument, little information is given about the physical or chemical properties of the defect structures. The object of this dissertation is to characterize and quantify defects in SAMs using a spectroscopic technique. We have chosen surface second harmonic generation (SSHG) to achieve the characterization based on the symmetry requirements for second order nonlinear processes. A centrosymmetric material in the presence of a strong electric field will not exhibit a second order nonlinear response. The idea is, using the appropriate chemistry to construct SAMs with a center of inversion within the assembly and therefore achieve control over the nonlinear response, as long as the response is dominated by electric dipole properties.

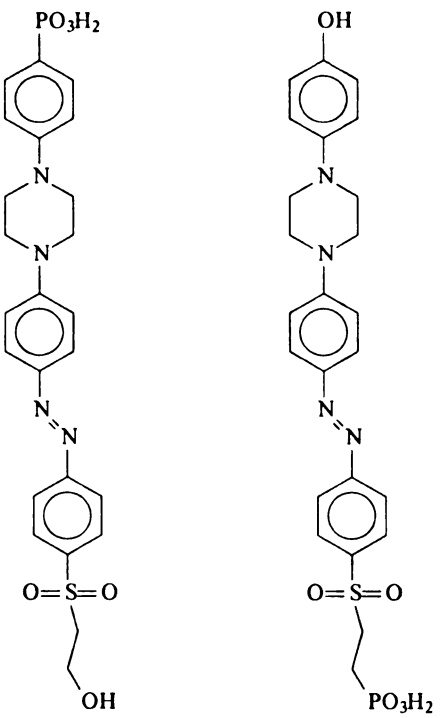

1 **2**

Figure 1.1 Structures of chromophores **1** and **2**.

We have chosen to use Zr-phosphate/phosphonate (ZP) chemistry in the assembly of our SAMs because of the structural versatility available with this system, combined with the high degree of control that can be exercised in multilayer assemblies.[35,61] We use a nonlinear optical chromophore developed by Katz and coworkers, (4-(4-(4-(4-((2-hydroxyethyl)sulfonyl)-phenyl)azo)phenyl)piperazinyl)phenyl)phosphonic acid, **1**, shown in Fig. 1.1. The nonlinear chromophore **1** is a rigid azo dye with a large second order nonlinear susceptibility, $\chi^{(2)}$. The second harmonic signal from layers of this chromophore is significant.[62,63] The complement to chromophore **1** is (2-(4-(4-(4-(4-hydroxy-phenyl) piperazinyl) phenyl) azo-phenyl) sulfonyl) ethylphosphonic acid, **2**.[64] This molecule is identical to **1** except that the terminal functional groups have been exchanged. By assembling one layer each of chromophores **1** and **2**, a bilayer film can be constructed that will have a center of inversion around the interlayer linking metal ion. If the film is defect-free (Figure 1.2a), the χ^2 response of this structure should be the same as the background because there is a center of inversion about the metal ion. If there are defects in the bilayer assembly (Figure 1.2b) there will not be complete cancellation of the dipole moments over two

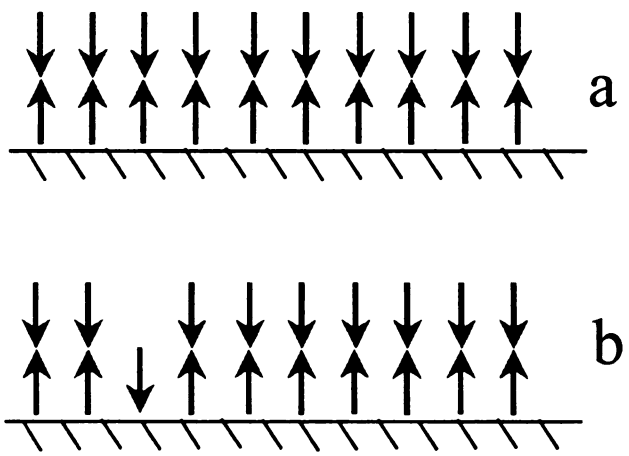

Figure 1.2 Bilayer structure of **1** and **2**. a- bilayer has perfect symmetry about the metal linkage and therefore cancellation of the dipole moments of each layer; b- bilayer has a vacancy defect site and will have an overall dipole moment and SSHG response for the assembly.

layers and the χ^2 signal will nonzero. Note that the signal is only present with defects, therefore we are trying to detect a nonzero signal against a dark background.

The first step of this dissertation project was to synthesize **2**. This chromophore is used in ZP thin films as a χ^2-active molecule and its structure ensures alignment relative to the surface. The steps used to synthesize this molecule, the resulting structural data, and selected thin film properties, as compared to chromophore **1**, are presented in Chapter 2.

Chapter 3 details the next step, which was the design, assembly, and troubleshooting of a surface second harmonic generation instrument for the nonlinear measurements. We use two different Nd:YAG lasers the source for fundamental (1064 nm) light. The lasers used operate in two different time regimes. The initial system used pulses in the ns time regime, the bulk of this work, however, involves the use of a ps Nd:YAG laser. We used both transmission and reflection configurations in the SSHG system design, with reflection from silicon wafers being used in the ns time regime and transmission being used in the ps time regime. The reflection experiments using the ps Nd:YAG laser with silicon wafers failed because of surface heating and ablation. For this reason, we switched to transmission measurements using fused silica substrates.

Chapter 4 discusses our results on selected multilayer structures of **1** and **2** built on silica substrates. The $\chi^{(2)}$ nonlinear response was characterized for bare fused-silica substrates, each chromophore chemisorbed to the substrate, and bilayers of opposing chromophore bilayers. While the results demonstrate that there was complete cancellation of the electric dipole moments for the bilayer assemblies, the $\chi^{(2)}$ responses of the two opposing bilayer systems are different and reveal the extent to which the "dipole

approximation"[65] is valid in these layered assemblies. From the data, we elucidate the role that quadrupolar terms play in the $\chi^{(2)}$ responses of thin interfacial films. This chapter discusses the complex and structural issues associated with the construction of layered interfaces, and presents the theory to support the experimental data.

In Chapter 5, the dependence of the nonlinear response as a function of multilayer structure is measured and characterized. We have shown that by spacing the individual layers of chromophores **1** and **2** apart using 1,12-dodecanediylbis(phosphonic acid), the SSHG signal is no longer decreased due to the induced center of inversion, but increases significantly. We have also inserted a spacer layer between the substrate and chromophore bilayers. These results are very different to those of bilayer assemblies adjacent to the substrate, presented in Chapter 4. The significance of these findings is that the molecular details of interface structure can have a profound effect on the measured response. We understand these data in the context of spatial variation in the dielectric response of the interface. It is this spatial variation that gives rise to nonlinearities in the induced polarization. The spatial profile of this variation influences the propagation of the fundamental and second harmonic electric fields. Because the chromophores **1** and **2** both have band tails at 532 nm, both the real and imaginary components of the dielectric gradient contribute to the observed signal.

Finally, chapter 6 concludes the findings of this body of data, and future directions of this project are discussed. There are a variety of directions that this project can now take to further investigate ZP SAMs or other interfacial chemistries. Modification of the SSHG system to image the surfaces is another possible route that this project can take. SSHG imaging gives surface morphology details on the μm scale.[66] By

using both SSHG intensity and imaging measurements to characterize surfaces, a great wealth of information can be gained.

A clear direction that this work must take is elucidation of the details involved in the theory of multilayer structures. Chapter 5 discusses possible explanations to the results of multilayer interfaces, but further work in this area is needed before concrete conclusions can be drawn. Once the details of the multilayer structures are understood, manipulations of thin films can then lead to selective control of the dielectric properties for use in materials-based applications.

Another possible avenue of exploration is the study of aggregation within a chromophore layer using SSHG as the measuring tool. It has been shown that varying the concentration of a chromophore within a single layer leads to island formation.[67,68] By using the nonlinear molecules presented on this thesis in conjunction with SSHG, noninvasive characterization to the degree of this inhomogenaity can be assessed.

1.1 Literature Cited

1. Xia, Y. N.; Whitesides, G. M.; *Annu. Rev. Mater. Sci.*, **1998**, 28, 153.

2. Collier, C. P.; Wong, E. W.; Belohradsky, M.; Raymo, F. M.; Stoddart, J. F.; Kuekes, P. J.; Williams, R. S.; Heath, J. R.; *Science*, **1999**, 285, 391.

3. Langmuir, I.; *J. Am. Chem. Soc.*, **1917**, 39, 1848.

4. Blodgett, K. B.; *J. Am. Chem. Soc.*, **1935**, 57,1007.

5. Florsheimer, M.; Kupfer, M.; Bosshard, C.; Looser, H.; Gunter, P.; *Adv. Materials*, **1992**, *4*, 795.

6. Gaines, G. L. *Insoluble Monolayers at Liquid-Gas Interfaces*; Interscience: New York, 1966.

7. Ulman, A. An Introduction to Ultrathin Organic Films: From Langmuir-Blodgett to Self-Assembly, 1st ed.; Academy Press: San Diego, 1991.

8. Katz, H. E.; Scheller, G.; Putvinski, T. M.; Schilling, M. L.; Wilson, W. L.; Chidsey, C. E. D.; *Science*, **1991**, *254*, 1485.

9. Marowsky, G.; Lupke, G.; Steinoff, R.; Chi, L. F.; Mobius, D.; *Phys. Rev. B*, **1990**, *41*, 4480.

10. Palto, S. P.; Blinov, L. M.; Yudin, S. G.; Grewer, G.; Schonholl, M.; Losche, M.; *Chem. Phys. Lett.*, **1993**, *202*, 308.

11. Kepley, L. J.; Crooks, R. M.; Ricco, A.; *Anal. Chem.* **1992**, *64*, 3191.

12. Swalen, J. P.; Allara, D. L.; Andrade, J. P.; Chandross, E. A.; Garoff, S.; Israelachvilli, J.; McCarthy, T. J.; Murray, R.; Pease, R. F.; Rabolt, J. F.; Wynne, K. J.; Tu, H.; *Langmuir* **1987**, *3*, 932.

13. Calvert, J. M.; Georger, J. H., Jr.; Peckerer, M. C.; Perhsson, P. E.; Schnur, J. M.; Scheon, P.; E.; *Thin Films* **1992**, *114*, 9188.

14. Dulcey, C. S.; Georger, J. H.; Krauthamer, V.; Stenger, D. A.; Fare, T. L.; Calvert, J. M.; *Science* **1991**, *252*, 551.

15. Kumar, A.; Biebuyck, H. A.; Abbott, N. L.; Whitesides, G. M.; *J. Am. Chem. Soc.* **1992**, *114*, 9188.

16. Vrancken, K. C.; Van Der Voort, P.; Gillis-D'Hammers, I.; Vansant, E. F.; Grobet, P.; J. Chem. Soc., Faraday Trans. **1992**, 88, 3197.

17. Pfleiderer, B.; Albert, K.; Bayer, E.; J. Chromatogr. **1990**, 506, 343.

18. Ulman, A.; *Chem. Rev.* **1996**, *96*, 1533.

19. Dubois, L. H.; Nuzzo, R. G.; *Annu. Rev. Phys. Chem.* **1992**, *43*, 437.

20. Xia, Y.; Whitesides, G. M.; *Angew. Chem. Int. Ed.* **1998**, *37*, 551.

21. Nuzzo, R. G.; Zegarski, B. R.; Dubois, L.H.; *J. Am. Chem. Soc.*, **1987**, 109, 733.

22. Xia, Y. N.; Whitesides, G. M.; *Annu. Rev. Mater. Sci.*, **1998**

23. Karpovich, D. S.; Blanchard, G. J.; *Langmuir* **1994**, *10*, 3315.

24. Schessler, H. M.; Karpovich, D. S.; Blanchard, G. J.; *J. Am. Chem. Soc.* **1996**, *118*, 9645.

25. Kohli, P.; Taylor, K. K.; Harris, J. J.; Blanchard, G. J.; *J. Am. Chem. Soc.*, **1998**, *120*, 11962.

26. Li, D.; Ratner, M. A.; Marks, T. J.; Zhang, C. H.; Yang, J.; Wong, G. K.; *J. Am. Chem. Soc.* **1990**, *112*, 7389.

27. Gun, J.; Iscovici, R.; Sagiv, J.; *J. Colloid Interface Sci* **1984**, *101*, 201.

28. Maoz, R.; Sagiv, J.; *J. Colloid Interface Sci.* **1984**, *100*, 465.

29. Maoz, R.; Sagiv, J.; *Thin Solid Films* **1985**, *132*, 135.

30. Cao, G.; Rabenberg, L. K.; Nunn, C. M.; Mallouk, T. M. *Chem. Mater.* **1991**, *3*, 149.

31. Hong, H.-G.; Sackett, D. D.; Mallouk, T. E. Chem. Mater. **1991**, 3, 521.

32. Thompson, M. E. Chem. Mater. **1994**, 6, 1168.

33. Byrd, H.; Snover, J. L.; Thompson, M. E.; Langmuir, **1995**, 11, 4449.

34. Cao, G.; Hong, H.G.; Mallouk, T. E.; *Acc. Chem. Res.*, **1992**, *25*, 420.

35. Lee, H.; Kepley, L.J.; Hong, H.; Mallouk, T.E.; *J. Am. Chem. Soc*, **1988**, *110*, 618.

36. Yonemoto, E. H.; Saupe, G. B.; Schmehl, R. H.; Hubig, S. M.; Riley, R. L.; Iverson, B. L.; Mallouk, T. E. *J. Am. Chem. Soc.* **1994**, *116*, 4786.

37. Katz, H. E.; Bent, S. F.; Wilson, W. L.; Schilling, M. L.; Ungashe, S. B. *J. Am. Chem. Soc.* **1994**, *116*, 6631.

38. Frey, B. L.; Hanken, D. G.; Corn, R. M. *Langmuir* **1993**, *9*, 1815.

39. Yang, H. C.; Aoki, K.; Hong, H.-G.; Sackett, D. D.; Arendt, M. F.; Yau, S.-L.; Bell, C. M.; Mallouk, T. E. *J. Am. Chem. Soc.* **1993**, *115*, 11855.

40. Vermeulen, L.; Thompson, M. E. *Nature* **1992**, *358*, 656.

41. Ungashe, S. B.; Wilson, W. L.; Katz, H. E.; Scheller, G. R.; Putvinski, T. M. *J. Am. Chem. Soc.* **1992**, *114*, 8717.

42. Cao, G.; Rabenberg, L. K.; Nunn, C. M.; Mallouk, T. M. *Chem. Mater.* **1991**, *3*, 149.

43. Katz, H. E.; Schilling, M. L.; Chidsey, C. E. D.; Putvinski, T. M.; Hutton, R. S. *Chem. Mater.* **1991**, *3*, 699.

44. Putvinski, T. M.; Schilling, M. L.; Katz, H. E.; Chidsey, C. E. D.; Mujsce, A. M.;

Emerson, A. B. *Langmuir* **1990**, *6*, 1567.

45. Rong, D.; Hong, H.-G.; Kim, Y.-I.; Krueger, J. S.; Mayer, J. E.; Mallouk, T. E. *Coord. Chem. Rev.* **1990**, *97*, 237.

46. O'Brien, J. T.; Zeppenfeld, A. C.; Richmond, G. L.; Page, C. J.; *Langmuir*, **1994**, *10*, 4657.

47. Ansell, M. A.; Zeppenfeld, A. C.; Yoshimoto, K.; Cogan, E. B.; Page, C. J.; *Chem. Mater.*, **1996**, *8*, 591.

48. Katz, H. E. *Chem. Mater.* **1994**, *6*, 2227.

49. Langmuir, I.; *Trans. Faraday Soc.*; **1920**, 15, 62.

50. Kleinfeld, Elaine R.; Ferguson, Gregory S.; *Chem Mater.*, **1996**, 8, 1575.

51. Chidsey, C. E. D., Loiacono, D. N.; *Langmuir*, **1990**, 6, 682.

52. Seshadri, K.; Froyd, K.; Parikh, A. N. Allara, D. L.; Lercel, M. J.; Craighead, H. G.; *J. Phys. Chem.*, **1996**, 100, 15900.

53. Patrick, David L.; Cee, Victor, J.; Purcell, Timothy, J.; Beebe, Thomas B. Jr.; *Langmuir*, **1996**, 12, 1830.

54. Sabatini, E.; Rubinstein, I.; *J. Phys. Chem.*, **1987**, *91*, 6663.

55. Sabatini, E.; Rubinstein, I.; Moaz, R.; Sagiv, J.; *J. Electroanal. Chem.*, **1987**, *219*, 365.

56. Finklea, H. O.; Snider, D. A.; Fedyk, J.; Sabatini, E.; Gafni, Y.; Rubinstein, I.; *Langmuir*, **1993**, *9*, 3660.

57. Finklea, H. O.; Snider, D. A.; Fedyk, J.; *Langmuir*, **1990**, *6*, 371.

58. Sabatini, E.; Cohen-Boulakia, J.; Bruening, M. L.; Rubinstein, I.; *Langmuir*, **1993**, *9*,

2974.

59. Janek, R. P.; Fawcett, W. R.; Ulman, A.; *Langmuir*, **1998**, *14*, 3011.

60. Zhao, Xiao-Mei; Wilbur, James L.; Whitesides, George M.; *Langmuir*, **1996**, 12, 3257.

61. Lee, H.; Kepley, L.J.; Hong, H.; Sohail, A.; Mallouk, T.E.; *J. Phys. Chem.*, **1988**, *92*, 2297.

62. Katz, H. E.; Wilson, W. L.; Scheller, G.; *J. Am. Chem. Soc*, **1994**, *116*, 6636.

63. Flory, W. C.; Blanchard, G. J.; *J. Am. Chem. Soc., in review.*

64. Flory, W. C.; Mehrens, S. M.; Blanchard, G. J.; *J. Am. Chem. Soc., in review.*

65. Guyot-Sionnest, P.; Shen, Y. R.; *Phys. Rev. B.*, **1987**, 35, 4420.

66. Florsheimer, M.; Kupfer, M.; Bossard, C.; Looser, H.; Gunter, P.; *Adv. Mater.*, **1992**, 4, 795.

67. Horne, J.C.; Huang, Y.; Liu, G. Y.; Blanchard, G. J.; *J. Am. Chem. Soc.*, **1999**, 121, 4419.

68. Horne, J.C.; Blanchard, G. J.; *J. Am. Chem. Soc.*, **1999**, 121, 4427.

Chapter 2

SYNTHESIS OF A NONLINEAR OPTICAL CHROMOPHORE FOR USE IN ORIENTED ZIRCONIUM PHOSPHATE/PHOSPHONATE MULTILAYER ASSEMBLIES

Summary

We report the synthesis of the nonlinear optical chromophore, (2-(4-(4-(4-(4-hydroxyphenyl)piperazinyl)phenyl)azophenyl)sulfonyl)ethylphosphonic acid, to be used in self-assembled multilayer (SAM) structures. This chromophore has been designed as the structural complement of a $\chi^{(2)}$-active chromophore first reported by Katz, Wilson, and Scheller [*J. Am. Chem. Soc.*, **1994**, *116*, 6636.]. The reason for synthesizing this structural complement is to explore the utility of structural "cancellation" of a surface $\chi^{(2)}$ optical response. We report the synthesis, structural data, and preliminary surface characterization data for the chromophore and its complement.

2.1 Introduction

There has been significant recent interest in creating nonlinear optical (NLO) materials by incorporating organic chromophores into interfacial or polymeric support structures. The resulting NLO materials have been reported to have $\chi^{(2)}$ responses on the same order as those characteristic of crystalline inorganic materials such as $LiNbO_3$.[1] The potential for self-assembling multilayer (SAM) structures to be used in electro-optic device applications or in solid state electronics has provided the impetus for the development of many clever synthetic routes aimed at inducing molecular orientation in layered materials. Such systems include Langmuir-Blodgett (LB) films,[2] polymer films,[3] and self-assembled mono- and multilayers.[1,4,5] Of these, SAMs appear to be the best choice for combining robust physical properties with persistent structural anisotropy. Using the appropriate chemistry, SAMs can be constructed one layer at a time, allowing control over the identity and orientation of the NLO chromophore within a given layer. An excellent review article on SAMs discusses the various types of assemblies used, including alkanethiols on gold and organosilane and metal phosphonate binding chemistries.[6]

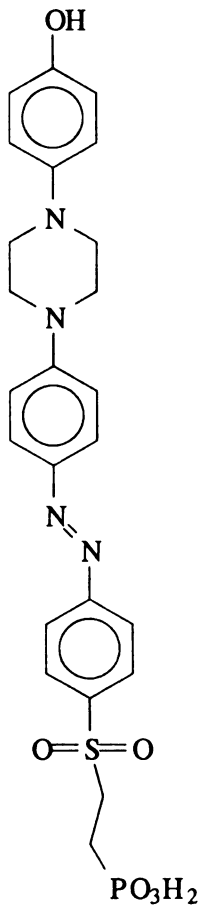

Figure 2.1
Chromophore **2**.

We have chosen to use Zr- phosphate/phosphonate (ZP) chemistry in the assembly of our SAMs[7,8] because of the structural versatility available with this system combined with the high degree of control that can be exercised in their assembly. Zr-phosphonate SAMs were first demonstrated by the Mallouk group, where layered

structures formed from α,ω-alkanebisphosphonates were reported.[7] The films reported initially by the Mallouk group were centrosymmetric about the layer center and were thus not viable as $\chi^{(2)}$-active interface materials. Katz *et al.* reported a scheme to incorporate molecular-level orientation within each layer by utilizing a three-step synthetic approach to the formation of the layers instead of the two step method reported initially.[7] It is this basic synthetic strategy that allows us to explore a novel way to characterize the defect properties of these SAMs.

Our motivation for the synthesis we report here is to use the $\chi^{(2)}$-active chromophores **1** and **2** (Figure 1.1) in the characterization of ZP SAMs. A significant question that remains to be answered for these interfaces is the quantification and characterization of vacancy and orientational defects within the layers. Our approach to answering this question is to construct a bilayer with two $\chi^{(2)}$-active chromophores that are identical in structure but opposed in orientation. The $\chi^{(2)}$ signal of a perfectly opposing bilayer structure should vanish because there is a center of inversion in the macroscopic assembly and any surface second harmonic generation (SSHG) signal that is observed will be the result of defects. The first step in this ongoing project is to synthesize and characterize the nonlinear chromophores, and that is the focus of this chapter.

Katz and coworkers synthesized the chromophore (4-(4-(4-(4-((2-hydroxyethyl)sulfonyl)-phenyl)azo)phenyl)piperazinyl)phenyl)phosphonic acid, **1**.[9] The nonlinear chromophore **1** is a rigid azo dye with a large second order hyperpolarizabilty, β. The second harmonic signal from a monolayer of this chromophore is usefully large. The orientational complement to chromophore **1** is (2-(4-(4-(4-(4-

hydroxyphenyl)piperazinyl)phenyl)-azophenyl)sulfonyl)ethylphosphonic acid, **2**, shown in Figure 2.1. This molecule is identical to **1** except that the terminal functional groups have been exchanged. By assembling a bilayer with one layer each of chromophores **1** and **2**, we can construct a nominally centrosymmetric bilayer with opposing dipolar orientation of the layers. We report on the details of the $\chi^{(2)}$ response for this system in chapter 4.

The focus of this chapter is on the synthesis of nonlinear chromophore **2**, the characterization of its linear optical properties and the ellipsometric determination of its layer thickness in a homogeneous multilayer structure. The synthetic route to chromophore **2** is shown in Figure 2.2. The optical and layer properties are compared to the response of **1**. The pair of complementary chromophores **1** and **2** were chosen because of their rigid structure, a characteristic that will minimize SSHG signal from intralayer sterically-mediated defects. Isomerization about the azo bond could, in principle, create *cis* conformers, but using 1064 nm light we do not excite these layers on resonance, so isomerization about the azo functionality is not likely to be a significant problem.

2.2 Experimental

Chemicals. All chemicals used were obtained in the highest purity grade available. (4-Acetlyaminobenzene)sulfonyl chloride, 2-chloroethanol, 2,3,4-collidine, $POCl_3$, $ZrOCl_2 \cdot 8H_2O$, triisopropyl phosphite, *p*-anisidine, bromotrimethylsilane, and $CDCl_3$ were obtained from Aldrich Chemical Co. *p*-Toluene sulfonyl chloride, sodium sulfite, and sodium bisulfite were obtained from Spectrum Chemicals. N,N-Bis-2-

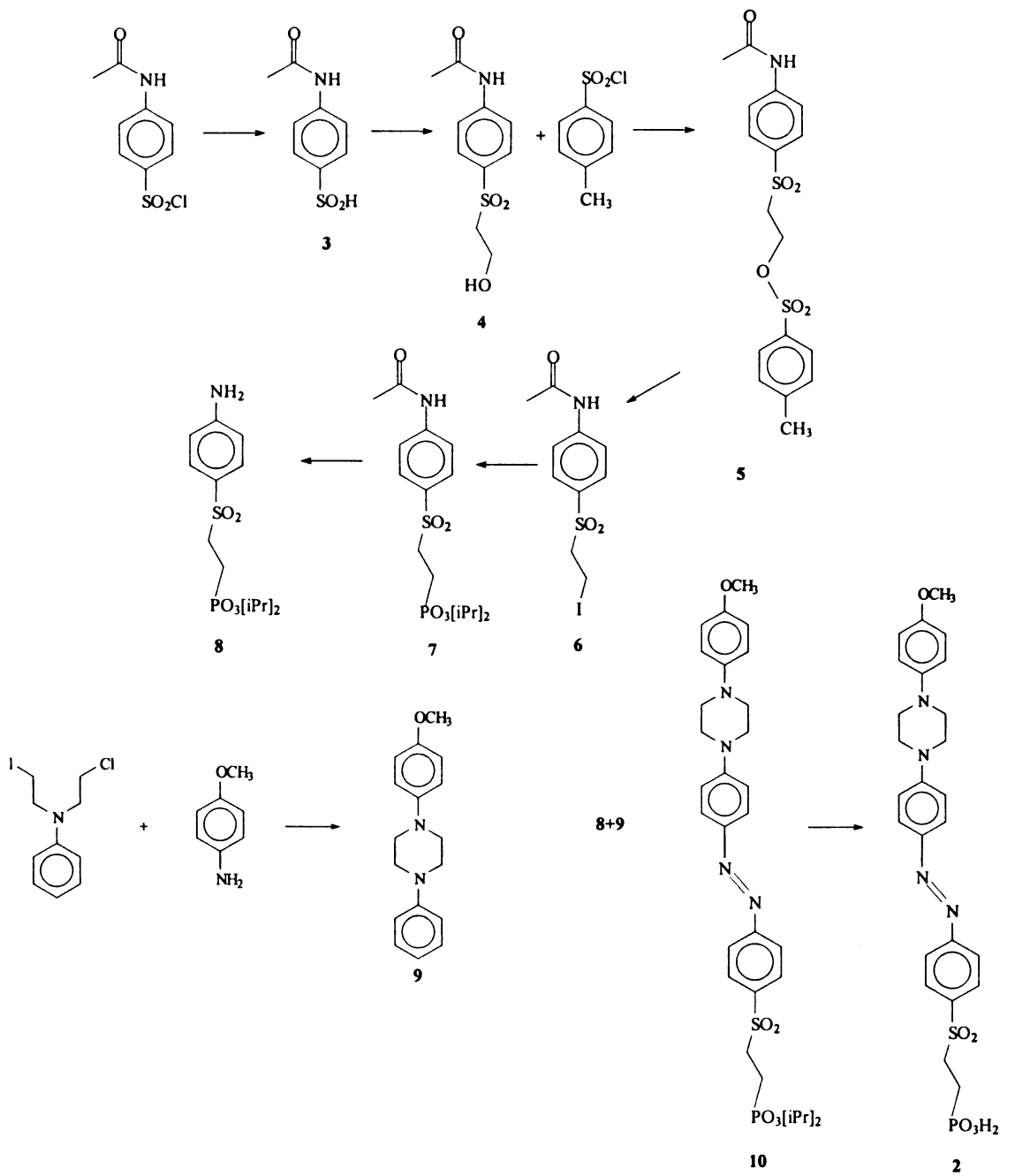

Figure 2.2 Synthetic route to Chromophore 2.

chloroethanol was obtained from Pfaltz & Bauer, d_6-DMSO was purchased from Isotec Inc., and 3-aminopropyltrimethoxysilane was purchased from United Chemical Technologies, Inc. All water used was distilled in-house. All chemicals were used as received except for triisopropyl phosphite, which was purified by drying over sodium under an inert atmosphere, followed by vacuum distillation.[10]

Measurements. ^{1}H NMR spectra of all compounds were taken with a Varian Gemini-300 MHz NMR spectrometer. Optical absorption measurements were made using a Hitachi U-4001 UV-visible absorption spectrometer. The thickness of chromophore layers bound to Si substrates was measured using an optical null ellipsometer (Rudolph AutoEL-II) operating at λ = 632.8 nm. The software used to calculate layer thickness was supplied by Rudolph. The complex refractive index of the individual layers was taken to be $\mathbf{n} = 1.61 + 0i$.[11]

Calculations. Semi-empirical and molecular mechanics calculations were performed on chromophores **1** and **2** using Hyperchem® v. 4.5 on a PC. Energy level calculations were performed on ground-state optimized structures using the PM3 parameterization.

Synthesis. The synthetic route is shown in Figure 2.2. For the compounds listed in the following section, the ^{1}H NMR spectral properties are summarized in Table 2.1. The syntheses described below are typical results for individual experiments. The absolute amounts of compounds used in each section are not limited by that reported here.

(4-acetylaminophenyl)sulfinic acid[12]**(3)** 50.1 g Na_2SO_3 (anh.) (400 mmol) was dissolved in 250 mL H_2O. (4-Acetylaminophenyl)sulfonyl chloride (47.7 g, 204 mmol)

was added slowly to the solution. The pH of the solution was maintained above 9 using 50% NaOH. After 2 hours, 60% H_2SO_4 was added dropwise until a white precipitate formed. The white precipitate was collected by vacuum filtration. The yield was 48.0 g (97%). Pure by NMR, FTIR, and MS.

(4-acetylaminophenyl)-β-hydroxyethyl sulfone[13] (**4**) 56.5 g of (4-acetylaminophenyl)sulfinic acid (284 mmol) and 21.9 g of NaOH (548 mmol) were added to 230 mL H_2O. Once dissolved, 45.0 mL of 2-chloroethanol (671 mmol) was added and the solution was refluxed for 2 hours. The solution was cooled gradually then placed in an ice bath and the resulting white crystals were collected by vacuum filtration. The filtrate was made slightly alkaline and was refluxed for an additional 2 hours with 10% NaOH added at intervals. One-third of the solvent was then removed by rotary evaporation, and the remaining solution was cooled in an ice bath. The crystals were collected by vacuum filtration and added to the first batch. A total of 62.8 g of product was obtained (91%). Pure by NMR, MS, and FTIR.

4-acetylaminophenyl-β-(p-toluenesulfonyloxy)ethyl sulfone[13] (**5**). *p*-Toluene sulfonylchloride (2.03 g, 10.6 mmol) was added to 2.25 g of (4-acetylaminophenyl)-β-hydroxyethylsulfone (9.25 mmol) in 9.5 mL of pyridine at 0°C. The solution was stirred for 2 hours at 0°C then poured into 30 mL of ice water. The precipitate was collected by vacuum filtration and then recrystallized from ethanol. A total of 3.08 g (83%) of white crystalline product was recovered. Pure by NMR.

4-acetylaminophenyl-β-iodoethyl sulfone[13] (**6**). 2.34 g NaI (15.4 mmol) was added to 3.08 g 4-acetylaminophenyl-β-(p-toluenesulfonyloxy)ethyl sulfone (7.72 mmol) in 23.4 mL of acetone. The solution was refluxed for 15 hours then poured into a

solution of 3.03 g of sodium bisulfite in 93 mL of H_2O. The crystalline product was collected by vacuum filtration. Total product obtained was 2.26 g (82%). Pure by NMR and MS.

(4-acetylaminophenyl)sulfonylethyldiisopropyl phosphonate (7). 27.0 mL of purified triisopropyl phosphite (109 mmol) was added to 25.7g of 4-acetylaminophenyl-β-iodoethyl sulfone (73.1 mmol) under Ar. The solution was refluxed for 5 hours at 145°C. The solution was cooled and excess triisopropyl phosphite and isopropyl iodide was removed by vacuum distillation. The remaining crystals were dissolved in ethanol and recrystallized. The product was collected by vacuum filtration and dried, yielding 22.6 g (79%) of white product. Pure by NMR and MS.

2-(4-aminophenyl)-sulfonylethyldiisopropyl phosphonate (**8**). 7.90 g of (4-acetylaminophenyl)sulfonylethyldiisopropylphosphonate (20.2 mmol) was refluxed at 75°C in 75 mL of 0.5M HCl for 48 hours. The solution was cooled and the precipitate collected by vacuum filtration. The precipitate was recrystallized from ethanol yielding 3.57 g (51%). Pure by NMR.

4-(4-methoxyphenyl)phenyl piperazine[14] (**9**). 7.27 g of N,N-bis-2-chloroethylaniline (33.5 mmol) was combined with 8.77 g of *p*-anisidine (71.1 mmol) in 25 mL of water:acetone (1:1), and refluxed for 2.5 hours. The solution was cooled in an ice bath and the crystals were collected by vacuum filtration. The product was recrystallized from ethanol, yielding 3.09 g of lustrous white platelets (35%). Pure by NMR and MS.

(2-(4-(4-(4-(4-methoxyphenyl)piperazinyl)phenyl)azophenyl)sulfonyl) ethyldiisopropyl phosphonate (**10**). The compound (**10**) was synthesized by formation

of an azo bond between (**8**) and (**9**). These functionalities were reacted by first forming the diazonium salt. This was done by dissolving 0.260 g of (**8**) (0.745 mmol) in 57 mL of 2M HCl and then slowly adding a solution of 150 mg of $NaNO_2$ in 13 mL of water at 0°C. After 15 minutes, the diazonium salt was added to 0.199 g of (**9**) (0.742 mmol) dissolved in 30 mL of propanoic acid:H_2O (1:5) at 0°C, producing an orange solution. Sodium acetate was added to increase the pH to ~ 4. The solution was stirred for 24 hours at 0°C, then slowly brought to room temperature. The liquid was decanted and the remaining precipitate was dissolved in 50 mL of CH_2Cl_2. This solvent layer was washed 3 times with 25 mL of 0.5 M HCl. After the third washing, 25 mL water was added and the CH_2Cl_2 layer was boiled off, leaving a red-orange precipitate. This solid was washed several times with 5:1 water:isopropanol to remove starting material. This solid was then purified by chromatography on 100 g of silica gel, eluting with acetone:toluene (1:1). The yield is 72.2 mg (15%). Pure by NMR.

(2-(4-(4-(4-(4-hydroxyphenyl)piperazinyl)phenyl)azophenyl)sulfonyl) ethyl phosphonic acid (2). 67.2 mg of (10) (0.011 mmol) was placed in a flask under Ar. To this, 8.0 mL of dried CH_2Cl_2 and 130 μL of dried pyridine were added. 620 μL Bromotrimethylsilane was added and the solution was allowed to stir at ambient temperature. After 24 hours, 10 mL of H_2O was added to hydrolyze the silanes. The CH_2Cl_2 layer was washed with 50 mL water and 50 mL 0.5M HCl. The CH_2Cl_2 evaporated and 53.0 mg of red-orange solid was collected (93 %). Pure by NMR and UV-Vis.

Surface Preparation. Si(100) wafers (Multi Crystal Optics, Inc.) and silica substrates were used. Si substrates were cleaned in piranha solution (3:1 H_2SO_4:H_2O_2 –

Table 2.1 ^{1}H NMR spectra of compounds in the synthesis of chromophore **2**.

Molecule (solvent)	Resonances
3 (d_6–DMSO)	2.02(s) ; 7.48(s) ; 7.52(d) ; 7.69(d) ; 10.16(s)
4 (d_6–DMSO)	2.08(s) ; 3.35(t) ; 3.62(m) ; 4.85(t) ; 7.79(s) ;10.38(s)
5 (d_6–DMSO)	2.08(s) ; 3.37(t) ; 3.61(t) ; 7.79(s) ; 10.38(s)
6 (d_6–DMSO)	3.15(t) ; 3.78(t) ; 7.8s(s) ;10.42(s)
7 (d_6–DMSO)	1.22(t); 1.88(m) ; 2.18(s) ; 3.22(m) ; 4.54(m) ; 7.84(s) ; 10.41(s)
8 (d_6–DMSO)	1.18(t) ; 1.84(m) ; 3.09(m) ; 4.52(m) ; 6.22(s) ; 6.64(d) ; 7.48(d)
9 (d_6–DMSO)	3.12(t) ; 3.24(t) ; 3.68(s) ; 6.82(m) ; 6.96(m) ; 7.22(t)
10 (d_6–DMSO)	1.19(t) ; 1.95(m) ; 3.40(m) ; 3.79(s) ; 3.81(t) ; 3.87(d) ; 4.53(m) ; 6.97(d) ; 7.17(d) ; 7.25(d of d) ; 7.42(d of d) ; 7.85(d) ; 7.98(d) ; 8.07(d)
2 (d_6–DMSO)	1.77(m) ; 3.88(m) ; 6.97(d) ; 7.17(d) ; 7.25(d of d) ; 7.42(d of d) ; 7.85(d) ; 7.98(d) ; 8.07(d)

caution- strong oxidizer!) for 10 minutes, rinsed with distilled water, placed in 2 M HCl for 10 minutes, and rinsed with water. The substrates were dried in a dry N_2 stream. Under an Ar atmosphere, 20 mL anhydrous octane was added to a vessel containing the substrate. The octane was heated to reflux and 3-aminopropyltrimethoxysilane was added to make a 1% v/v solution. After 10 minutes of reaction the substrate was removed and rinsed with warm hexane, then water. A N_2 stream was used to dry the surface. Silica surfaces were cleaned in piranha solution, dried, but were not primed.

Both surfaces were then phosphorylated. This was done under Ar, using a solution of 20 mM 2,3,4-collidine and 20 mM $POCl_3$ in anhydrous acetonitrile at ambient temperature. After 10 minutes, the substrates were removed, rinsed with acetonitrile and water and dried with N_2. The surfaces were then zirconated by immersing in aqueous 5 mM $ZrOCl_2$ solution for 10 minutes. The surfaces were rinsed with water and dried.

Chromophore Deposition. The chromophores were deposited on the substrates from a saturated solution of each dissolved in 1:4 DMF:EtOH. For Si wafers, the solution was kept acidic by adding dropwise 4 M HCl in dioxane. The temperature of each solution was held just below boiling while the surfaces were immersed for 10 minutes followed by rinsing with warm ethanol and drying with N_2. The phosphorylation and zirconation of the surfaces is repeated as described previously. To monitor layer adsorption, ellipsometric thickness was used for Si wafers and UV-Vis absorption was used for silica substrates.

2.3 Results and Discussion

We have synthesized and performed initial characterization of (2-(4-(4-(4-(4-hydroxyphenyl)piperazinyl)phenyl)azophenyl)sulfonyl)ethyl phosphonic acid, **2**, a new nonlinear chromophore developed for use in zirconium phosphate/phosphonate SAMs. As discussed in the Introduction, our motivation for this work is to construct multilayer assemblies with controlled orientations and, using surface second harmonic generation measurements, evaluate interface defect properties.[7] In addition to the synthesis of the chromophore, it is important to perform some basic characterization steps to ensure that appropriate layered structures can be made. We need to determine that the substitution of

the terminal groups in **2** relative to **1** does not alter the electronic spectroscopic response of the chromophore seriously. This is an important issue because unwanted resonance effects in nonlinear spectroscopic measurements can cause difficulty in interpretation. We also need to consider the ability of **2** to form layered structures in the same manner as **1**. We have synthesized **1** and report a comparison of the linear optical responses and ellipsometric thicknesses per layer for SAMs formed from each of these two compounds. The linear optical responses of chromophores **1** and **2** in ethanol are shown in Figure 2.3a. The absorption maxima for **1** and **2** in solution are 429 nm and 415 nm, respectively. The slight difference between the two chromophores is due to the position of the terminal functional groups and the influence each has on the π system of the chromophores. We have assembled layers of **1** and **2** separately on SiO_x substrates. In Figure 2.3b, we show the absorption spectra of layers of chromophores **1** and **2**, revealing very similar electronic structures. Both chromophores are dominated by a broad absorption band centered at 417 nm, with only very slight differences in the red edge of the spectra. The higher energy bands appear to be somewhat different for the two chromophores and the reason for this effect is not obvious by inspection. Semi-empirical calculations of the linear response for these two chromophores show the ordering and energies of the first three excited singlet states to be slightly different, especially in the region of the most prominent band(s) (Figure 2.4). These calculations provide some justification for the differences in the absorption data, but given the spectral widths of the absorption bands, making the comparison between experiment and calculation at any meaningful level is not feasible. By plotting the absorbance at 417 nm of each chromophore against the number of deposited layers, we recover slopes of 0.0567 ±0.001

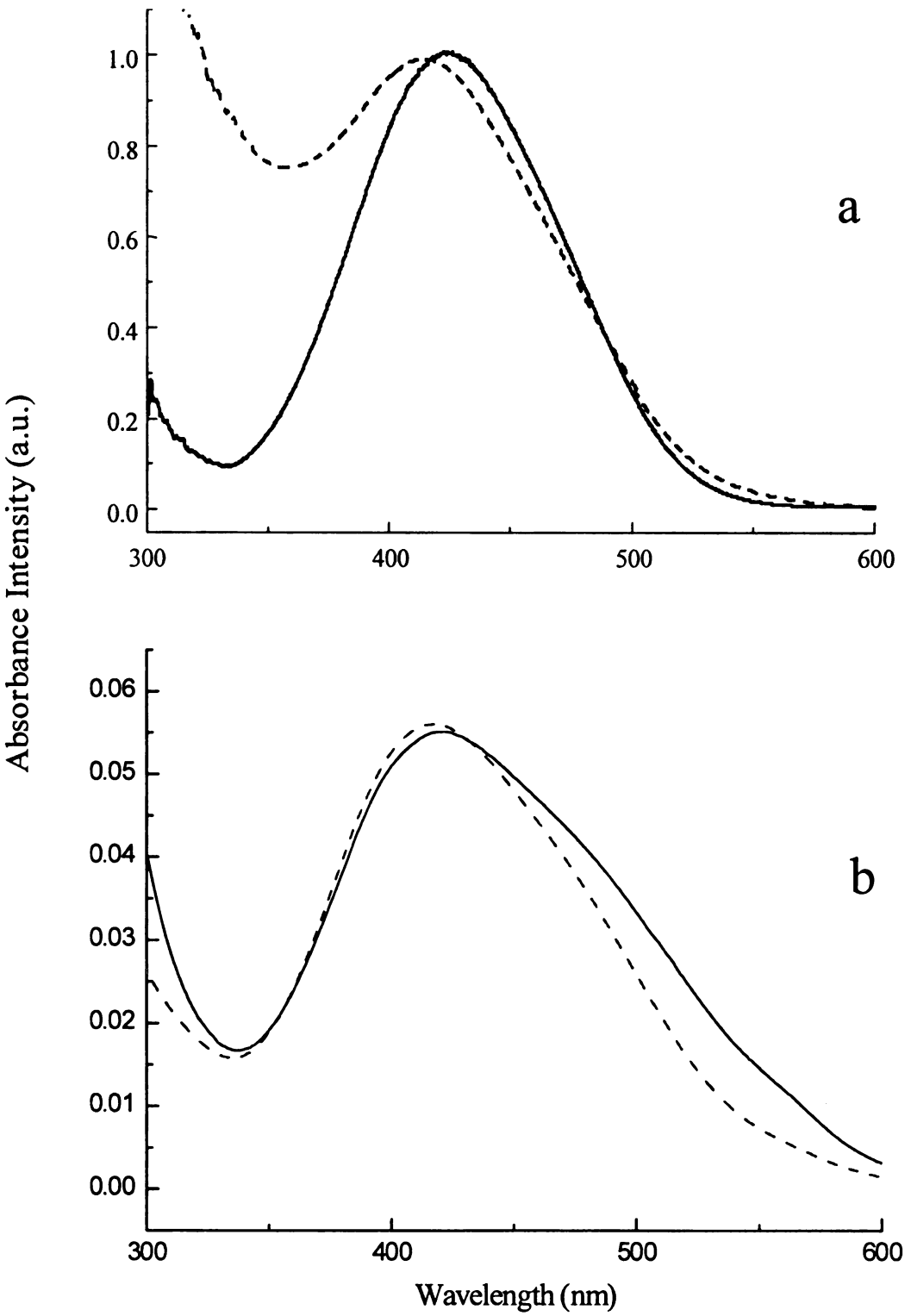

Figure 2.3 UV-Vis absorption spectra of (a) solution phase of **1** (solid blue) and **2** (dashed red); (b) the assemblies of 5 bilayers of **1** and **2** on fused silica.

and 0.0546 ± 0.0007 for **1** and **2**, respectively as shown in Figure 2.5a. These data demonstrate that the same concentration of chromophores is deposited in each layer, an important result for future uses of these chromophores in nonlinear applications. Because consistent build up is seen for each layer, we also conclude that priming the surface prior to chromophore deposition does not yield a more uniform surface coverage.

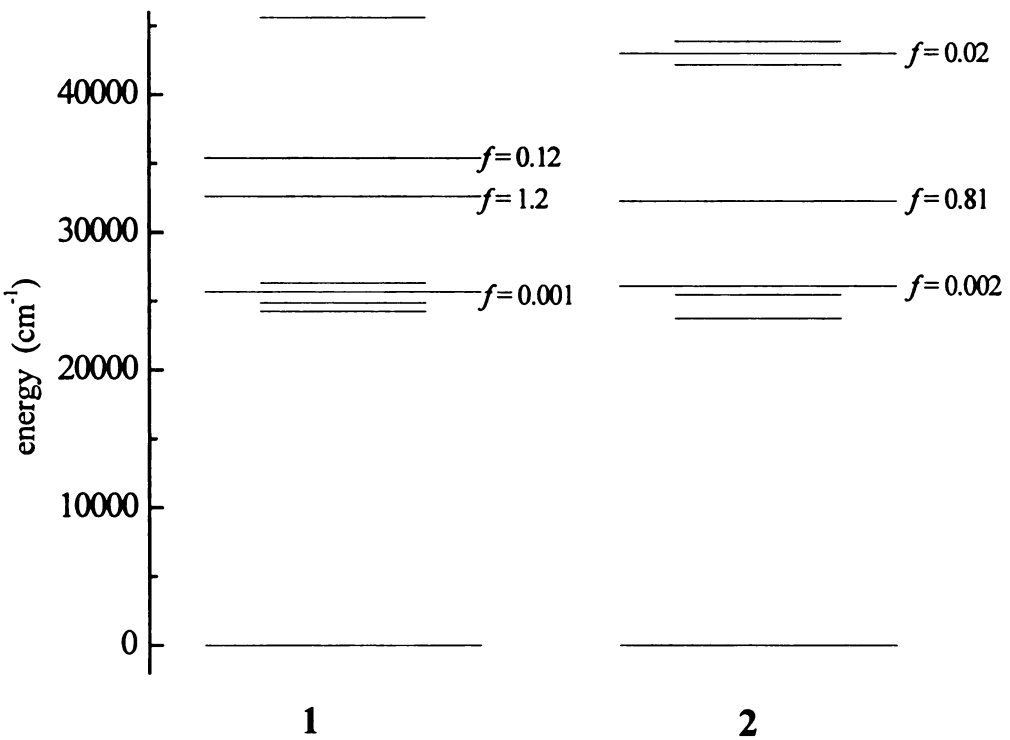

Figure 2.4 Semi-empirical calculations of the linear response for chromophores **1** (left) and **2** (right). Wide lines are singlet states, and calculated oscillator strengths for $S_i \leftarrow S_0$ transitions are indicated next to the upper state. Narrower lines indicate triplet states.

From the solution phase spectra, we extract ε_{max} = 207,600 L/mol-cm for **1** and given the same linear dependence of A on layer growth for **2**, we infer the same value of ε. Using the experimental data shown in Figure 2.5a, we estimate the surface loading density to be

1.6×10^{14} cm^{-2}-$layer^{-1}$.

From optical null ellipsometry, we recover a best-fit slope of 26.3 ± 0.5 Å/layer for chromophore **1** and 25.5 ± 0.4 Å/layer for chromophore **2**. (Figure 2.5b) These values are the same to within the experimental uncertainty. Our results are in good agreement with Katz and coworkers data on the layered growth of **1**.[15] The length of each molecule in its most stable conformation is calculated by molecular mechanics to be 27 Å. It has been reported previously that the thickness of a Zr-PO_3- linkage is 3.75 Å.[16] An average layer thickness of 25.6 Å indicates that the chromophores are tilted at an angle of ~20° from the surface normal, presuming full surface coverage. Katz *et al.* also reported this result for **1**. Because both chromophores tilt to similar angles when each is adsorbed into a layer, it can be assumed that assemblies of alternating layers of **1** and **2** will result in similar increases in the layer thickness. This finding also suggests that our approach to the measurement of defect densities in opposing bilayer structures is feasible with these complementary chromophores.

These chromophores are characterized by the same layer density, electronic structure, and tilt angle based on the linear response and ellipsometry data. We conclude that multilayers of **1** and **2** are structurally similar making them a good choice for investigations of the chemical structural contributions to the $\chi^{(2)}$ response of oriented ZP systems.

2.4 Conclusions

Chromophore **2** has been synthesized and characterized using ^{1}H NMR, UV-visible spectroscopy, and optical null ellipsometry. Layers of both **1** and **2** have been

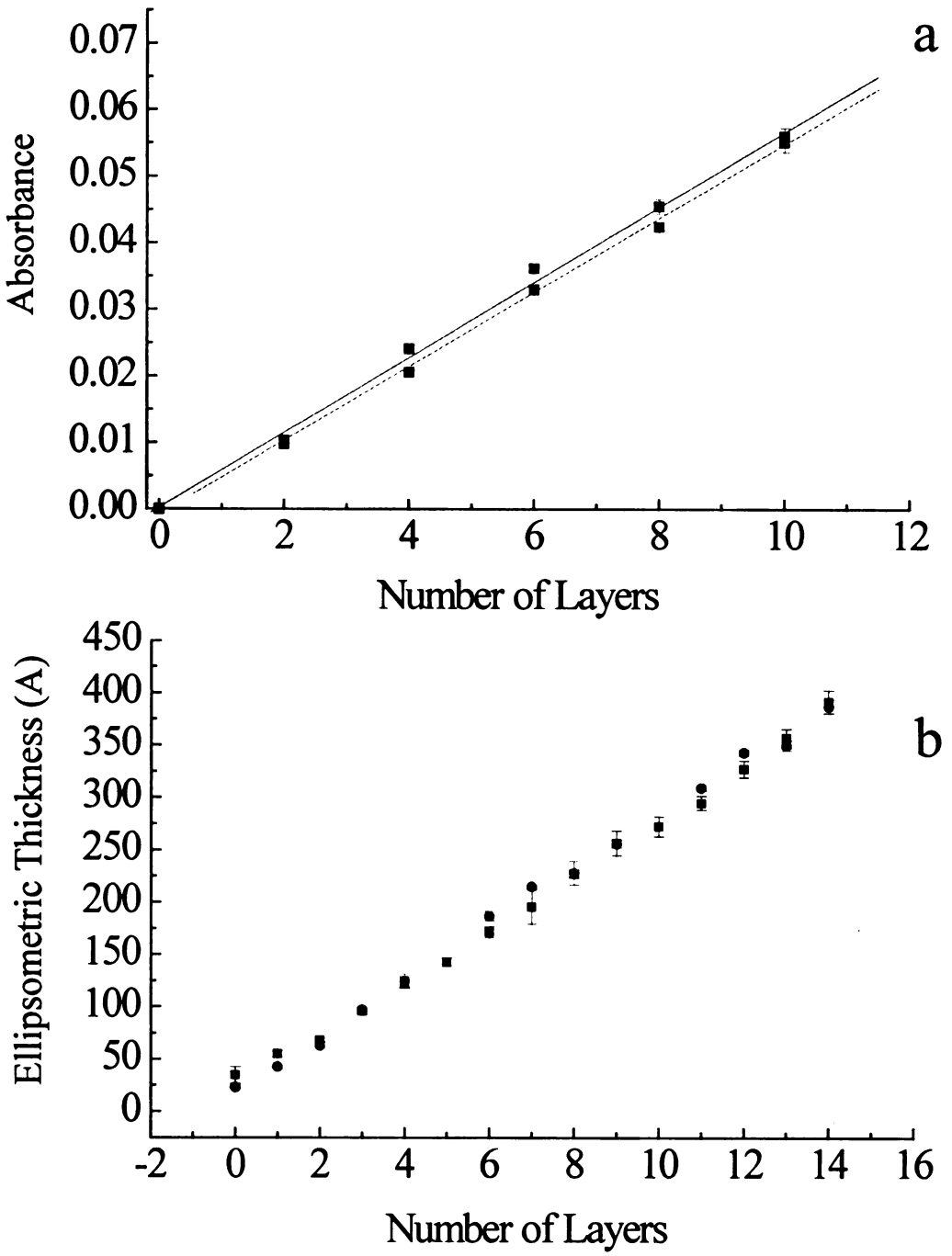

Figure 2.5 (a) Dependence of absorption on number of layers for both chromophores. See text for a discussion of these data. (b) Ellipsometric thicknesses of each layer for 15 layer assemblies of chromophores **1** (●) and **2** (■). The slopes of the best-fit line through these data are 26.3 ± 0.5 Å/layer for **1** and 25.5 ± 0.4 Å/layer for **2**. The y-intercept is a result of the primer layer.

built up on Si and silica wafers and each has an average thickness of 25.6 Å and an average tilt angle of ~20° from the surface normal assuming full coverage. Absorption data indicate a surface coverage of 1.6×10^{14} cm^{-2}-$layer^{-1}$. The chromophores exhibit very similar $\chi^{(2)}$ signals on silica substrates, as we detail in the next paper. The similar absorption and layer-forming characteristics of both chromophores make them ideal choices for surface second harmonic generation investigations aimed at characterizing and quantifying defect density and type in this family of SAMs.

2.5 Literature Cited

1. Katz, H. E.; Scheller, G.; Putvinski, T. M.; Schilling, M. L.; Wilson, W. L.; Chidsey, C. E. D.; *Science*, **1991**, *254*, 1485.
2. Florsheimer, M.; Kupfer, M.; Bosshard, C.; Looser, H.; Gunter, P.; *Adv. Materials*, **1992**, *4*, 795.
3. Zhu, X.; Chen, Y. M.; Li, L.; Jeng, R. J.; Mandal, B. K.; Kumar, J.; Tripathy, S. K.; *Opt. Commun.*, **1992**, *88*, 77.
4. Marowsky, G.; Lupke, G.; Steinoff, R.; Chi, L. F.; Mobius, D.; *Phys. Rev. B*, **1990**, *41*, 4480.
5. Palto, S. P.; Blinov, L. M.; Yudin, S. G.; Grewer, G.; Schonholl, M.; Losche, M.; *Chem. Phys. Lett.*, **1993**, *202*, 308.
6. Ulman, Abraham; *Chem. Rev.*, **1996**, *96*, 1533.
7. Lee, H.; Kepley, L.J.; Hong, H.; Mallouk, T.E.; *J. Am. Chem. Soc*, **1988**, *110*, 618.
8. Lee, H.; Kepley, L.J.; Hong, H.; Sohail, A.; Mallouk, T.E.; *J. Phys. Chem.*, **1988**, *92*, 597.
9. Katz, H. E.; Wilson, W. L.; Scheller, G.; *J. Am. Chem. Soc*, **1994**, *116*, 6636.
10. Perrin, D. D.; Armarego, W. L. F.; Perrin, B. R.; *Purification of Individual Organic Chemicals*, Pergmon Press, Oxford, 1980, 449.
11. Hanken, Dennis G.; Corn, Robert M.; *Anal. Chem.*, **1995**, *67*, 3767
12. Smiles,S.; Bere, C.M.; *Organic Syntheses*, Wiley, New York, 1941, Collect. Vol.1, 7.
13. Baker, B. R.; Querry, M. V.; *J. Org. Chem.*, **1950**, *15*, 413.
14. Popov, D.; *C. R. Acad. Bulg. Sci.*, **1966**, *19*, 1163.

15. Flory, W. C.; Blanchard, G. J.; *J. Am. Chem. Soc., in review.*

16. Katz, H. E.; Schilling, M. L.; Chidsey, C. E. D.; Putvinski, T. M.; Hutton, R. S. *Chem. Mater.* **1991**, *3*, 699.

Chapter 3

LASER SYSTEMS FOR SURFACE SECOND HARMONIC GENERATION MEASUREMENTS

Summary

We report on the laser systems used for the surface second harmonic generation (SSHG) measurements. We use Nd:YAG lasers (1064 nm) as our fundamental light source and detect the second harmonic signal (532 nm). We present the system design, characteristics, and some example data from each of the systems used. Two time regimes were used as well as two configurations, reflection and transmission geometries. The details of these systems as well as preliminary work to interface the laser system to a personal computer are presented.

3.1 Introduction

With the discovery of masers and then lasers[1] came the ability to generate harmonic frequencies from materials because of the high electric field intensities that these light sources produce.

$$P = \chi^{(1)}E + \chi^{(2)}E^{*}E + \chi^{(3)}EE^{*}E + \cdots(\text{bulk})$$
$$\mu = \alpha E + \beta E^{*}E + \gamma EE^{*}E + \cdots(\text{molecular})$$

Equation 3.1

Equation 3.1 describes the induced polarization for a medium in an electric field on microscopic (μ) and macroscopic (P) scales. For a low intensity electric field ($<10^2$ W/cm^2), the higher order terms can be neglected and the response is described using only the linear portion of the equation ($\chi^{(1)}$, α). For high intensity illumination ($>10^5$ W/cm^2), the electrons within the system can no longer oscillate with the electric field, and the expanded form of the equation needs to be used to describe the induced polarization of the system. One result of the expanded form of this equation is that moieties containing a center of inversion will not exhibit even harmonic responses. This is because the $\chi^{(2)}$ tensor elements of a material with a center of inversion are zero in the dipole approximation.

The first nonlinear term is $\chi^{(2)}$, the second order nonlinear susceptibility, is related to β, the first hyperpolarizability. An assembly of β-active molecules aligned appropriately will give an area with an overall dipole moment, yielding a $\chi^{(2)}$ signal. If this same molecule is dissolved in solution, there will be no $\chi^{(2)}$ response because there is orientational averaging in the bulk.

The driving force for using second harmonic generation (SHG) in these experiments is the symmetry restriction described above. Our intent is to build bilayer systems purposefully incorporating a center of inversion and thereby turning off any SHG

from defect-free portions of the thin film. In principle, any residual response arises from defects within the bilayer system.

The focus of this chapter is to describe the development of the laser systems used for the surface SHG measurements. We use the 1064 nm light generated by Nd:YAG lasers as our fundamental light source. Two different time regimes, ns and ps, have been used to generate the SHG signal. We have also used reflection geometry for films built on Si and transmission geometry for films built on fused silica substrates. A Labview® program was written and a peak track-and-hold circuit was built to interface the laser system to a personal computer. These items are detailed in this chapter.

3.2 Experimental

Two different Nd:YAG lasers were used for this thesis. A Q-switched ns Nd:YAG (Quanta-Ray DCR) and Q-switched, mode-locked ps Nd:YAG (Quantronix 416) were used as sources of fundamental (1064 nm) light. The details of these laser systems are presented in section 3.3. The data presented characterizes each of the systems, but the majority of the results were acquired using the Q-switched, mode-locked Nd:YAG system.

Surface Preparation. Si(100) wafers (Multi Crystal Optics, Inc.) and silica substrates were used. Si substrates were cleaned in piranha solution (3:1 H_2SO_4:H_2O_2 – *caution- strong oxidizer!*) for 10 minutes, rinsed with distilled water, placed in 2 M HCl for 10 minutes, and rinsed with water. The substrates were dried in a dry N_2 stream. Under an Ar atmosphere, 20 mL anhydrous octane was added to a vessel containing the substrate. The octane was heated to reflux and 3-aminopropyltrimethoxysilane was

added to make a 1% v/v solution. After 10 minutes of reaction the substrate was removed and rinsed with warm hexane, then water. A N_2 stream was used to dry the surface. Silica surfaces were cleaned in piranha solution, dried, but were not primed. Both surfaces were then phosphorylated. This was done under Ar, using a solution of 20 mM 2,3,4-collidine and 20 mM $POCl_3$ in anhydrous acetonitrile at ambient temperature. After 10 minutes, the substrates were removed, rinsed with acetonitrile and water and dried with N_2. The surfaces were then zirconated by immersing in aqueous 5 mM $ZrOCl_2$ solution for 10 minutes. The surfaces were rinsed with water and dried.

Chromophore Deposition. The chromophores were deposited on the substrates from a saturated solution of each dissolved in 1:4 DMF:EtOH. For Si wafers, the solution was kept acidic by adding dropwise 4 M HCl in dioxane. The temperature of each solution was held just below boiling while the surfaces were immersed for 10 minutes followed by rinsing with warm ethanol and drying with N_2. The phosphorylation and zirconation of the surfaces is repeated as described previously. To monitor layer adsorption, ellipsometric thickness was used for Si wafers and UV-Vis absorption was used for silica substrates.

3.3 Results and Discussion

ns Q-switched Nd:YAG laser system

The first laser system used for this work was a ns Q-switched Nd:YAG laser (Quanta-Ray DCR). A schematic of the ns SHG system in reflection mode is shown in Figure 3.1. The laser produces ~14W average power at 1064 nm with 5ns pulses at 10

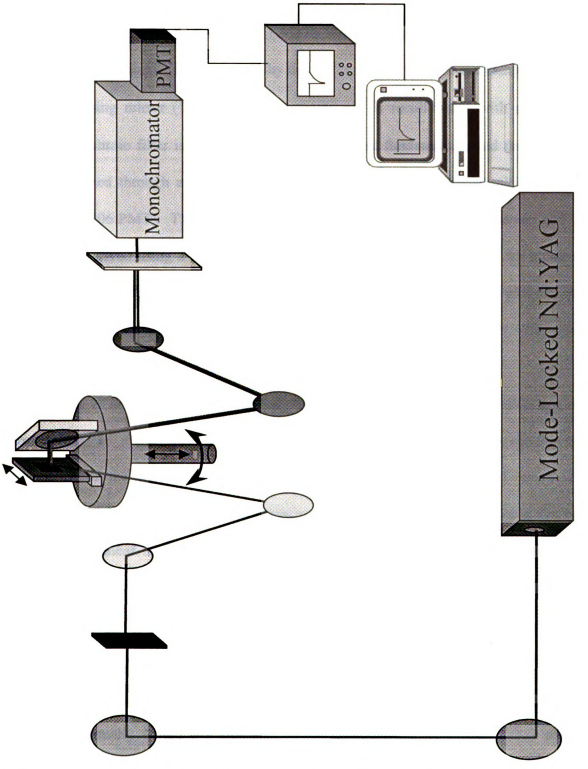

Figure 3.1 Q-switched ns Nd:YAG and mode-locked ps Nd:YAG laser systems. Reflection geometry was used and the fundamental light was focused onto the sample and them recollimated. A dichroic filter was used to remove the fundamental before the 532 nm light was detected.

Hz. The 1064 nm pulse train is directed through a 1 mm spatial filter. The beam, having an average power of 13 mW (intensity= $1.65x10^7 W/cm^2$), is passed through a color filter (RG 630) to remove any SHG generated by the optics, is focused onto the sample using a dichroic focusing mirror (100 μm focal diameter),and is recollimated with a dichroic mirror. A dichroic filter is used to remove the residual fundamental, and the 532 nm beam is directed through a monochromator (Spex) and then to a photomultiplier tube (Hammatsu 1106 PMT). The detector output is buffered using a voltage follower, and is then read and saved using a digital signal analyzer (Tektronix DSA 602A). An incident angle of 61° with respect to the surface was used for all measurements. The plotted data are the average of three readings, each being an average of 1024 single scans. The ratio of the signal vs. bare reference substrate is plotted to normalize the signal.

Katz *et al.* has reported previously on the second order nonlinear response of chromophore **1**.[2] Our data are consistent with his and we observe a square-law dependence of the second harmonic intensity with increasing number of layers for chromophore **1** built off of Si(100) substrates. This is an expected result for a system where the nonlinear medium is significantly thinner than the coherence length of the incident light source. The data we present (Figure 3.2) demonstrate this relationship and show that the system is sufficiently ordered to allow the square-law relationship to be observed for this chromophore. The drawback to using this system for this body of work was the heating of the surface and surface mount. Much of the incident energy was dissipated thermally within the substrate. It was thought that this extra energy could create defect contributions to the SSHG signal not originally related to the surface synthesis. The use of a ps laser to reduce the amount of energy per pulse was the next

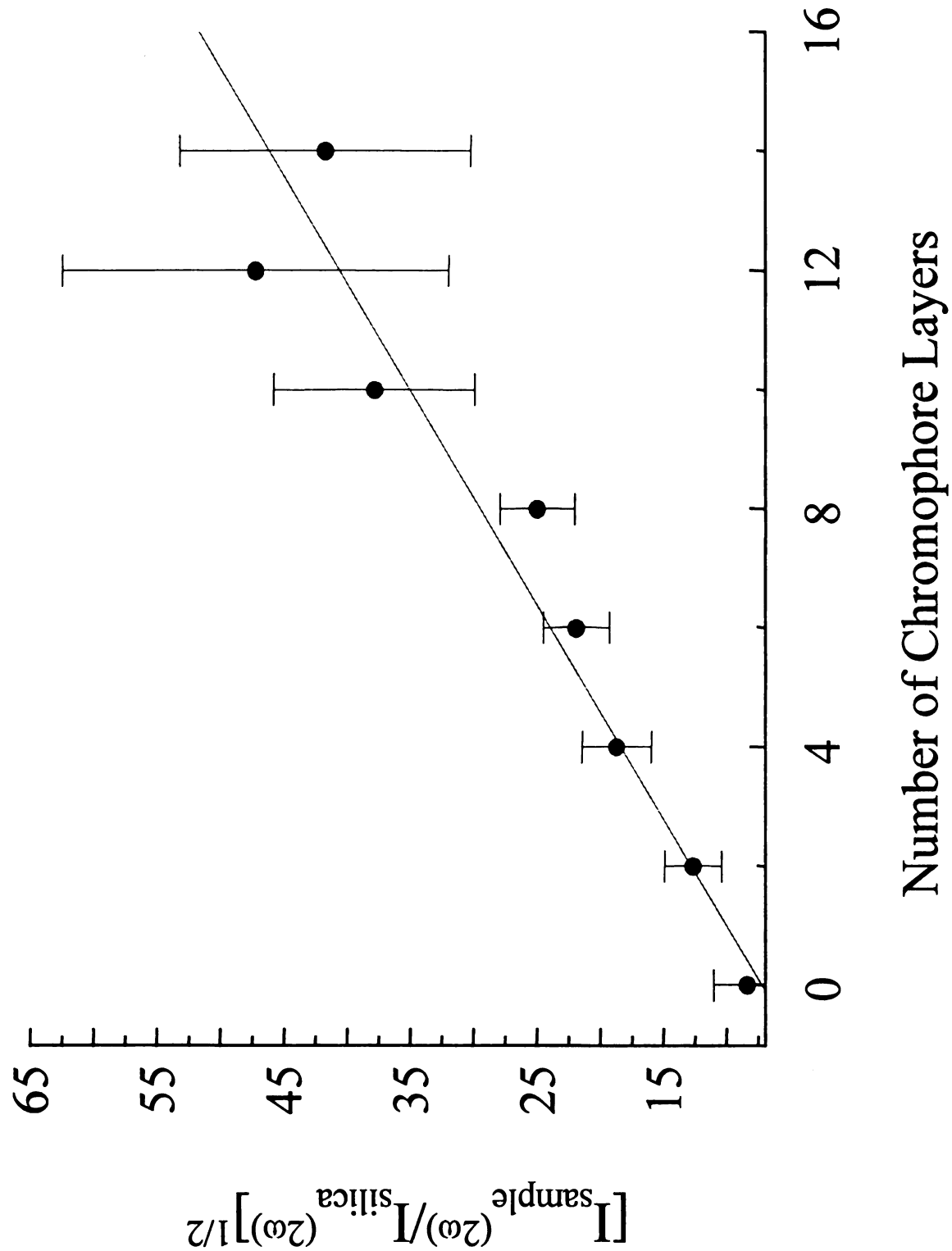

Figure 3.2 Plot of square law dependence of the SSHG signal vs. number of chromophore layers for the Q-switched ns Nd:YAG laser system. Chromophore **1** is chemisorbed on a Si(100) substrate.

step in the building of the SSHG system.

ps mode-locked Nd:YAG laser system

The Nd:YAG laser (Quantronix 416) produces ~10 W average power at 1064 nm when mode locked. The mode-locked pulse train produces a 100 ps pulse at a repetition rate of 80 MHz. The 1064 nm beam is attenuated using a polarizing beamsplitter cube (CVI) in conjunction with a polarization rotator. The beam, with an average power of 200 mW, is then directed through the same reflection mode optical train as described for the ns Nd:YAG laser system (Figure 3.1).

When a silicon substrate was at the focal point of the focusing mirror, the damage threshold was exceeded and the surface was ablated. When the beam remained collimated and directed onto the surface using a flat mirror, no signal was detected because the incident intensity was not sufficient to generate a detectable SSHG signal. An intermediate, defocused arrangement allowed signal detection without destruction of the substrate. This finding is consistent with the ns system and the intensities needed to observe a SSHG signal. The first data from this system came from layers of chromophore **1** built on silicon substrates and the raw data for the SSHG response of eight layers are plotted in Figure 3.3a. The reference SHG signal was taken simultaneously from a KDP crystal. A zero-signal line is drawn in red for ease of reading. The linear relationship between the square- root of the SHG intensity vs. number of layers was seen (Figure 3.3b), demonstrating that the system is sufficiently ordered, but the offset of the signal from zero remains an issue. The downfall of this configuration is the small signal obtained, even for many chromophore layers. In order

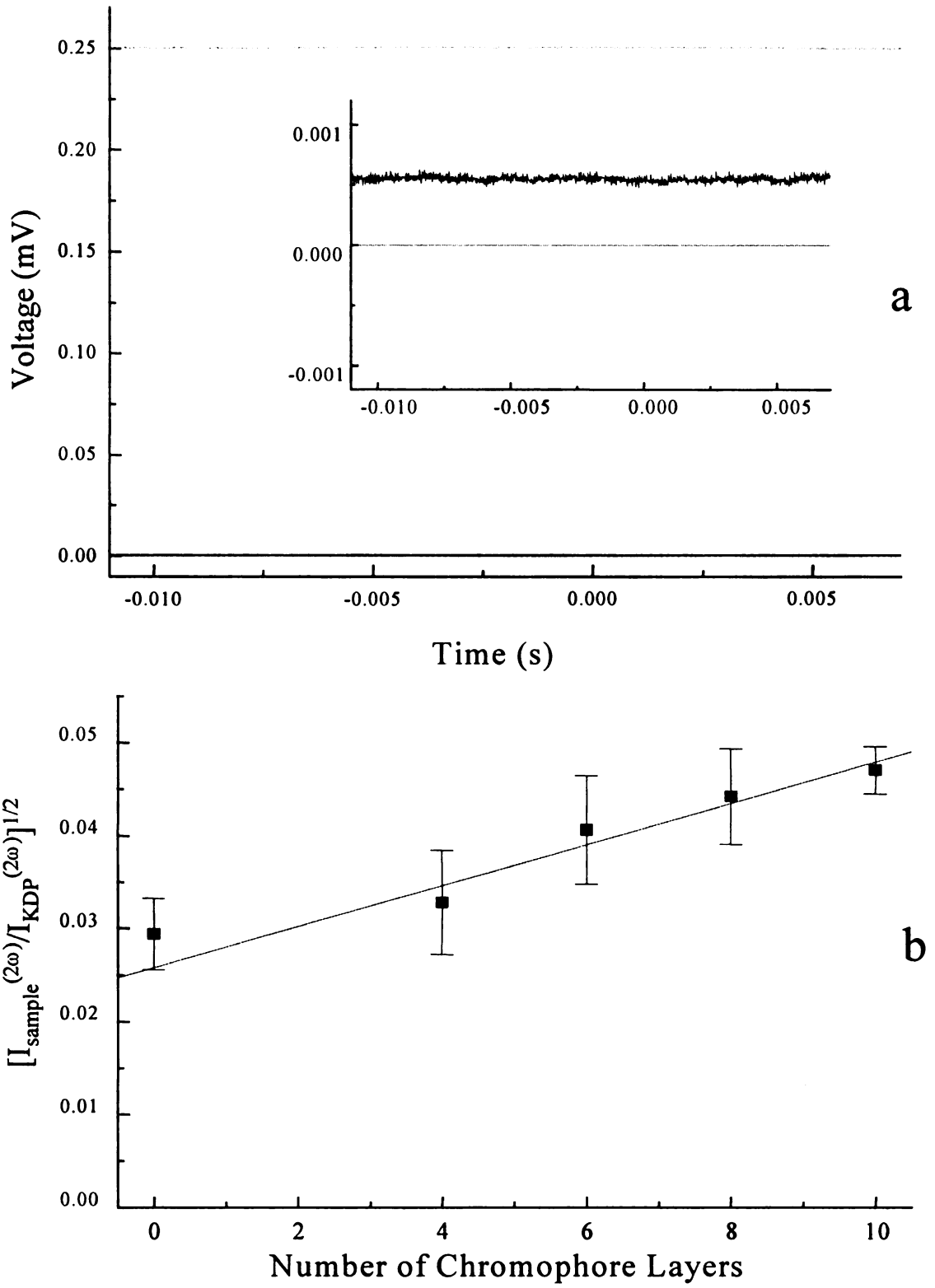

Figure 3.3 Mode-locked ps Nd:YAG laser system (a) raw data demonstrating the small signal. (KDP reference; SSHG signal from chromophore **1** on Si substrate; V=0); (b) plot of square law dependence of the SSHG signal vs. number of chromophore layers

for the system to be sensitive to a small SHG signal generated from defects alone, the $\chi^{(2)}$ signal from individual chromophore layers must be large. Since the peak power on the sample at the focal point damaged the surface, a modification to the system to reduce the duty cycle and increase the peak intensity without damage to the surface was needed. We report two alternatives below.

ps mode-locked Nd:YAG laser system with pulse compression

Optical pulse compression is a technique used to achieve ultrashort pulses by using self-phase modulation to expand the pulse frequency width, then manipulation of the "chirp" on the pulse using either a grating and a prism or a grating pair.[3-7] By decreasing the pulse width in time, very high peak powers can be achieved. We compressed the 100 ps pulses to ~10 ps pulses, but could not sustain the pulse integrity because of the instability of the system. The input pulse would heat the tip of the fiber and eventually burn the cladding, distorting the tip, and ruining the end. Stable compressed pulses, before the fiber damage could only be maintained for one hour. We abandoned the idea of compression to achieve high peak powers.

Q-switched, mode-locked ps Nd:YAG laser system

We installed a Q-switch on the mode-locked Nd:YAG laser to give an envelope of mode-locked pulses with high peak power. The pulse profile of the Q-switched mode-locked pulse is shown in Figure 3.4. A Q-switched, mode-locked Nd:YAG laser (Quantronix model 416) produces ~1.4W average power at 1064 nm with a 2 μs envelope at 500 Hz. The mode-locked pulses (80 MHz repetition rate) within the 2 μs envelope are

characterized by a 100 ps pulse width. Each 2 μs envelope contains 2.8 mJ total energy, with the maximum ps pulse in the envelope having ~125 μJ pulse energy.[8] A schematic of the surface SHG system is shown in Figure 3.5. The 1064 nm pulse train is directed

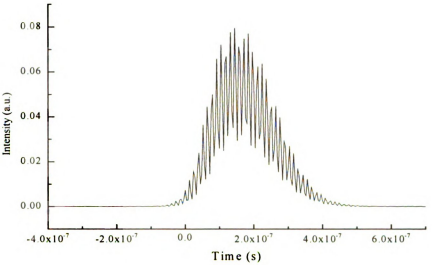

Figure 3.4 Pulse envelope of a Q-switched, mode-locked pulse. The mode-locked pulses (80 MHz repetition rate) are characterized by a 100 ps pulse width.

through a 2 mm spatial filter and a polarization rotator, then through a focusing lens and a color filter (RG 610) to remove any 532 nm light generated by the optics. The 1064 nm beam is focused onto the sample (~100 μm focal diameter), and is then recollimated. After the recollimating lens, three dichroic mirrors are used to separate the fundamental from the second harmonic light. The second harmonic light is directed into a 0.25 m monochromator (Fisher) and is detected with a PMT (Hammatsu 466). The

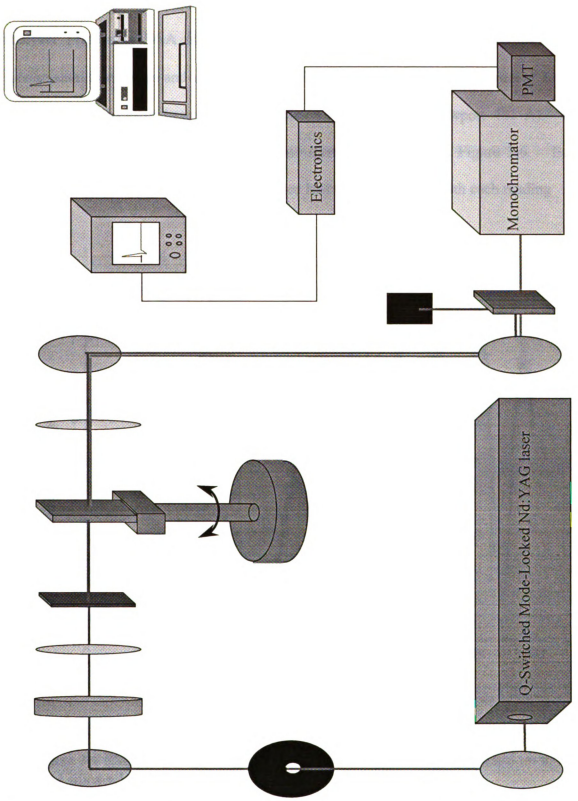

Figure 3.5 Q-switched, mode-locked Nd:YAG laser based system for SSHG experiments. Transmission mode i shown.

resulting transient is amplified (Ortec Model 451) and then stored using a digital signal analyzer (Tektronix DSA 602A). The sample is located at the focal point of the fundamental laser beam and is rotated manually about its vertical (y) axis from 0° to 70° relative to the incident beam using a precision rotation stage (Newport 481 A). The angular dependence of the second harmonic intensity is shown in Figure 3.6. Each experimental datum point is the result of three individual readings, with each reading

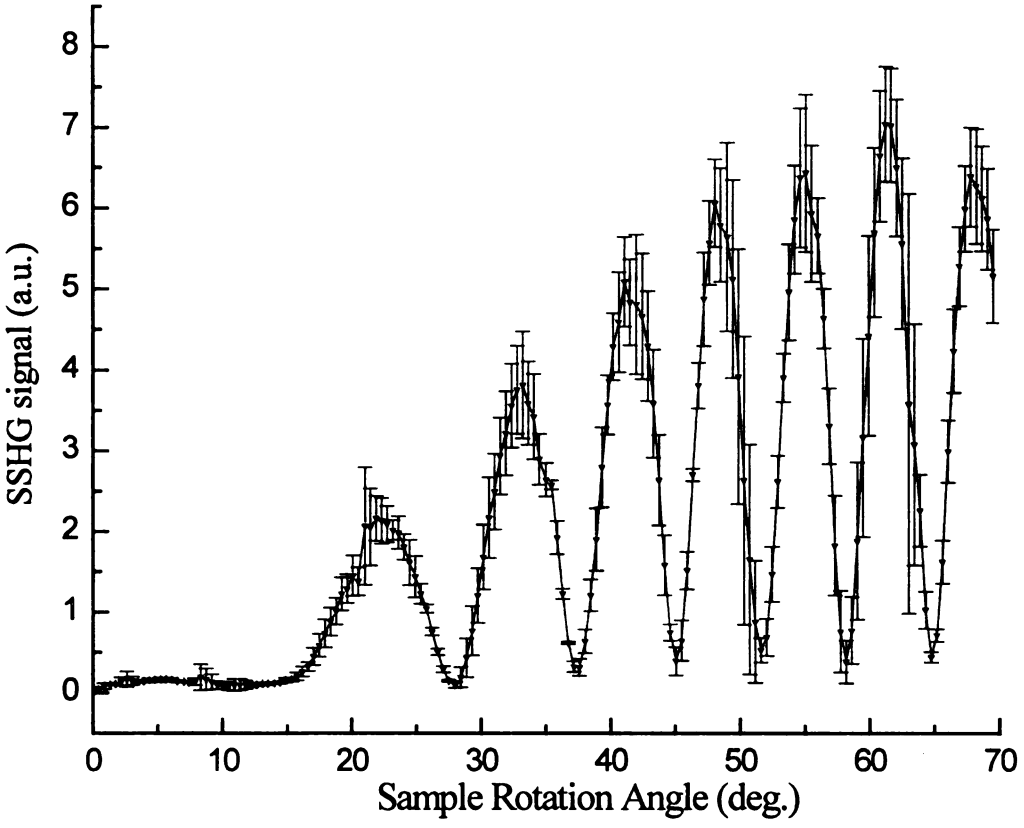

Figure 3.6 SSHG signal for three bilayers of chromophore **2** chemisorbed on a fused silica substrate.

being an average of 532 scans of the amplified transient recorded by the digital signal analyzer. The complete scan is normalized by referencing it to a scan of a reference bare fused silica substrate.

Data from the transmission mode geometry scanned from 0°-70° angle of incidence are shown in Figure 3.6. These data are from a quartz substrate with 3 bilayers

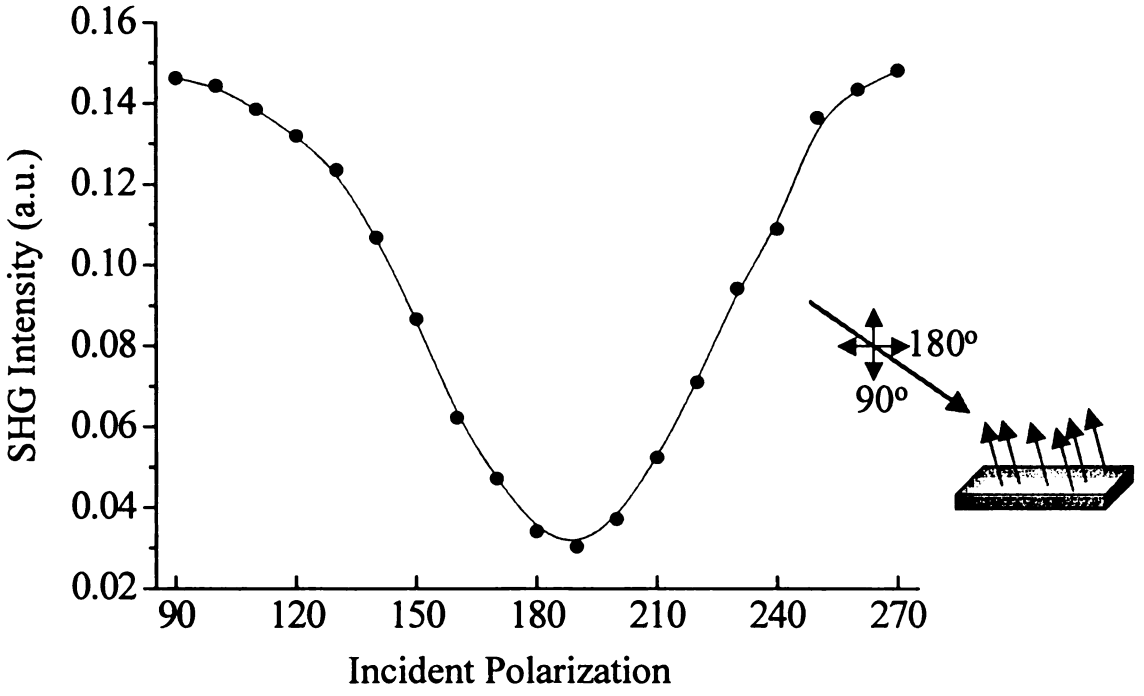

Figure 3. 7 Polarization dependence of the SSHG signal of chromophore **1** adsorbed onto Si(100). The inset cartoon depicts the coupling efficiency of the polarization to adlayers with their induced dipole moments normal to the surface.

of **2** chemisorbed to the surface. A complete interpretation of these data are presented in chapter 4. The data were taken with the 1064 nm light polarized at 90° with respect to the surface. A plot of the polarization dependence is shown in Figure 3.7 for chromophore **1** chemisorbed on silicon. The polarization dependence of the SSHG signal for chromophore **1** is shown in Figure 3.7 inset.

The next step in this project was to interface the laser system directly to a personal computer using Labview®. It was quickly determined that the data acquisition (DAQ) board that we had was slow compared to the temporal width of the detector output pulse. The DAQ board could only detect pulses with durations greater than 20 μs while the detector output pulse was 2 μs. I built a circuit to hold this peak value in time so that Labview® could detect the pulse.

Peak Track-and-Hold Circuit.

A peak track and hold circuit originally designed by John Rugis (MSU) electronics shop, was built to track and hold the voltage output amplitude of a PMT for an amount of time that allows the AT-MIO-16-L9 board sufficient time to read this value. The schematic of a modified version of the original circuit is shown in Figure 3.8. The holding time was chosen to be 88 μs, so that two channels could be sampled simultaneously with 8-10 points forming each waveform depending on the scanning rate of the Labview® program.

Figure 3.8 (inset) shows the relative timing between the trigger, input pulse, and the output pulse. A TTL input is needed to trigger the circuit. We used the analog output of the laser Q-switch driver as the trigger after converting it to a 5V signal with an inverting amplifier (LF357N). The duration of the trigger signal is 1 μs. The trigger is the signal input to a retriggerable monostable multivibrator (74LS123). The output is a square wave with a time dependence related to the resistor (R) and capacitor (C) used. We used R_T = 267 kΩ and C_{EXT} = 1000 pF to give a holding time of 88 μs as calculated

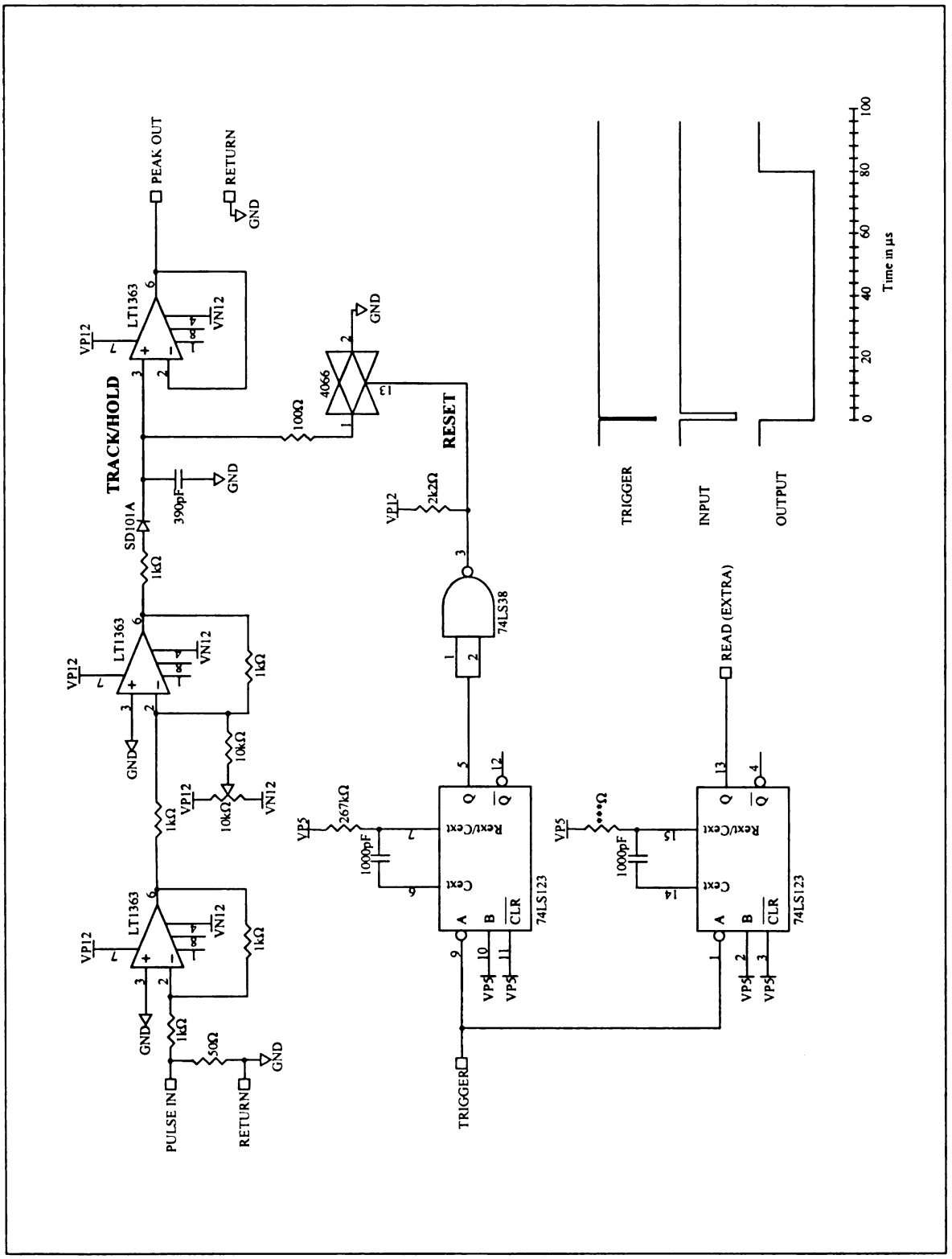

Figure 3.8 Peak track-and-hold circuit schematic used for computer interfacing. The details of this circuit are discussed in the text.

using equation 3.2:

$$T_w = 0.33 * R_T * C_{EXT} (1 + 0.7/R_T) \qquad \textbf{Equation 3.2}$$

This is the timing window that starts and resets the peak track and hold circuitry. The output Q from the multivibrator is the input to a bilateral switch (4066). When Q is high (H) the switch is on or tracking the pulse, and turns off or resets when Q is low (L). The time between the Q→H and Q→L is T_W.

The input pulse is sent into a high-speed inverting amplifier (LT1363) with a gain of one. The experimental signal travels through a fast diode where it charges a capacitor. This capacitor is isolated and therefore holds this charge while the bilateral switch is in the on position. The charged capacitor is isolated from the AT-MIO-16-L9 board through a voltage follower. This is a buffer that allows the held voltage to be read by the board without the capacitor losing its charge. When the bilateral switch turns off, the capacitor is shunted to ground, and discharged. This process resets the circuit, which waits for the next trigger/pulse input.

Labview® Code

A program was written that would read the data from the AT-MIO-16-L9 board, and plot this array as a waveform. This program was written using the icon-based programming software, Labview® from National Instruments. The program collects a scan of data in time and saves it as an array, saves the array, and resets itself and waits for the next trigger/pulse input. As it collects the arrays of data, it averages them. It then saves the array as an ASCII file, which can then be processed by a graphing program.

The program can be found in Appendix A.

The first step is to initialize the program. This is done with the AI CONFIG subVI, one of several subVIs included in Labview®'s software package. This subVI configures the hardware and allocates a buffer for the input. Here the device number and the buffer size are determined.

The AI START subVI sets the parameters such as trigger type, scan rate, and the number of scans to acquire. The program is externally triggered by the signal from the Q-switch. It is triggered by the falling edge of the square wave. The scan rate and number of scans are variable parameters that are connected to the front panel of the program so that they can be selected by the user.

The AI READ subVI is where the data from the AT-MIO-16-L9 channel 0 or 1 is read by the program. It reads the channel values and fills the allocated buffer at a rate determined by the set parameters. The array has a number of columns depending on how many channels are scanned. (*i.e.* if two channels are scanned, there will be two columns of data in the array). This array is sent to a bundle function, which plots the data points of the array depending on the time, set by the inverse of the scan rate. This data is also sent to a shift register at the edge of the for loop, where it is saved and then added to the next collected array. The summed array of all of the scans is divided by the number of scans giving a final array that is the average waveform of the scans. This array is plotted for the user, and is also sent to out of a second for loop. This array is broken down into individual columns, depending on the number of channels read, transposed, and saved with a second column of time values. The data is saved as an ASCII file, with values for X and Y. This is to make it very simple to call this data into a plotting program and

graph it.

Interface Troubleshooting

Each of the components works independently, but there were several problems encountered with interfacing the peak track-and-hold circuit to the Labview® program. The details and possible solutions to each are presented. The interfacing software and hardware are not currently being used due to these problems, but are presented for future reference.

One problem with the circuit is that when there is no input signal, the 390 pF holding capacitor charges to a voltage of 150 mV. This signal could be present because there may be an offset in this first op amp that is charging the capacitor in time. If this is the problem, then a voltage follower can be inserted between the first op amp and the diode to compensate for this offset.

Another problem between the interfacing of the laser system with the personal computer, is that the PULSE IN signal arrives so quickly after the trigger, Labview® misses the first two points of the waveform. One way to delay the read time is to trigger a TTL channel on the AT-MIO board and delay the TTL output of this channel by ~10 μs. Then the TTL out of this channel can be sent into the external trigger input that triggers Labview® to read.

One problem with the Labview® code is that it sometimes gives an error code when running the program. The error is an "overFlowErr" with a description of "at a time of the update clock for the input channel, the device-resident memory was unable to accept additional data- one or more data points may have been lost". This error could be

the result of the data not being transferred to Labview® before the next data is available to be read. The reason for this situation is not completely clear, but the overall conclusion of this interfacing using the current laser system is to obtain a faster DAQ board for fast data acquisition.

3.4 Conclusions

The systems developed for surface second harmonic generation measurements have been described. Two different time regimes were used and also two different geometries. The laser system used for measurements reported in the following chapters is a Q-switched, mode-locked Nd:YAG laser and measurements are made in transmission mode. It has been characterized and data obtained from this system are used for the study of defects and layered structure effects in self-assembled multilayer zirconium phosphate/phosphonate films. A peak track-and-hold circuit was built and a program using Labview® software was written in order to interface the laser system to a personal computer. Several problems with these components need to be solved before they can be used with this system.

3.5 Literature Cited

1. Franken, P. A.; Hill, A. E. Peters, C. W.. Weinreich, G.; *Phys. Rev. Lett.*, **1961**, 7(4), 118.

2. Katz, H. E.; Wilson, W. L.; Scheller, G.; *J. Am. Chem. Soc*, **1994**, *116*, 6636.

3. Shank, C.V.; Fork, R.L.; Yen,R.; Stolen, R. N.; Tomlinson, W. J.; *Appl. Phys. Lett.*, **1982**, 40(9), 761.

4. Nikolaus, B.; Grischkowsky, D.; *Appl.Phys.Lett.*, **1983**, 42(1),1.

5. Choi, Kee-Ju; Gustafson, Terry L.; *IEEE J. Quantum Electron.*, **1989**, 25(12), 2441.

6. Tomlinson, W. J.; Stolen, R. N.; Shank, C.V.; *J. Opt. Soc. Am. B.*, **1984**, 1(2), 139.

7. Nikolaus, B.; Grischkowsky, D.; *Appl.Phys.Lett.*, **1983**, 43(3),228.

8. *Quantronix, Model 416 Lasers, Technical Manual*; Quantronix Corporation, Smithtown, NY, pp. 1-3.

Chapter 4

STRUCTURAL CONTRIBUTIONS TO SECOND-ORDER OPTICAL NONLINEARITIES IN ORIENTED INTERFACIAL MULTILAYERS

Summary

We report on the characterization of Zr-phosphate/phosphonate (ZP) self-assembled multilayer structures using surface second harmonic generation measurements. Two structurally complementary $\chi^{(2)}$-active chromophores that can be deposited with orientational control relative to the substrate were used. These chromophores produce multilayer $\chi^{(2)}$ responses identical in magnitude but of opposite sign. O\opposing bilayers formed with these chromophores were used to produce two different structural motifs, each with a local center of inversion about the ZP interlayer bonding plane. The $\chi^{(2)}$ responses of these two bilayer systems are different and reveal the extent to which the dipole approximation is valid in these layered assemblies. Our data elucidate the role that quadrupolar terms play in the $\chi^{(2)}$ responses of thin interfacial films. This work illustrates the complex and subtle structural issues associated with the design and construction of layered interfaces, and provides a means to evaluate the vacancy and orientational defect density in layered materials.

4.1 Introduction

Self-assembled mono- and multilayer structures (SAMs) have received a great deal of attention in the materials community for fundamental as well as more near-term reasons.[1-9] An overarching goal of this effort has been to make the connection between molecular-scale organization, interface chemical identity, and macroscopic materials properties. A tremendous amount has been learned about interfacial monolayers and the associated measurement technology using the alkanethiol/gold system.[10-12] While studies of this archetypal system have led to profound advances in our understanding of organic-modified interfaces, thiol/gold monolayers suffer from long-term chemical stability limitations[13,14] and, until recently, the inability to form chemically-bound multilayer assemblies.[15] These limitations have been a driving force for research to identify alternative layer growth strategies, with both silane[2,16-18] and Zr-phosphate/phosphonate (ZP) chemistry[19-35] proving successful and versatile. The interest in SAMs based on ZP interlayer linking chemistry arises from their ease of assembly, the mild conditions used in the formation of these layers, and their structural and thermal stability, once formed. Recent work on ZP-based SAMs has pointed to limitations in their properties (*e.g.* mesoscopic ordering, optical response) that are mediated by structural defects.[36,37] The characterization of defects in mono- and multilayer interfaces is central to understanding SAM properties and is an area of interface and materials science that remains to be explored more fully. For alkanethiol/gold monolayers, cyclic voltammetry and impedance measurements have proven to be valuable tools in detecting the presence of vacancy defects.[38-43] For multilayers, electrochemical methods are not generally as useful owing to the short-range nature on the electron tunneling process responsible for

the experimental signal. We are investigating a means to study defects in multilayer assemblies using nonlinear spectroscopic methods. For many optical methods, the characteristic response of surface defects is small compared to the bulk material contribution, limiting the utility of spectroscopy for such investigations. We are interested in measuring vacancy and substitution defects in layered interfaces by utilizing the functional chemistry of selected second order nonlinear chromophores to control their orientation during layer growth. We have chosen $\chi^{(2)}$ measurements because of their intrinsic surface-selectivity.[44] By constructing interfaces with specific, predetermined orientation of the chromophore nonlinear transition moment within each layer, multilayer films can be assembled to produce either centrosymmetric or non-centrosymmetric bulk ordering to first approximation. The $\chi^{(2)}$ nonlinear response of a centrosymmetric bilayer structure will be null to within the validity of the electric dipole approximation. This dipolar cancellation allows examination of the residual $\chi^{(2)}$ response in the context of vacancy and substitution defects and higher order multipole contributions to the experimental signal against a nominally dark background. The resolution of the contributions to the $\chi^{(2)}$ response of opposing bilayers is an important first step in establishing this means of defect characterization in layered materials.

We use two compounds to explore the utility and practical limitations of chemically-based cancellation of the second order nonlinear response. The first is the $\chi^{(2)}$-chromophore (4-(4-(4-(4-((2-hydroxyethyl)sulfonyl)phenyl)azo)phenyl)piperazinyl) phenyl)phosphonic acid, **(1)**, reported by Katz and coworkers and designed for its combined rigid structure and large first hyperpolarizability, β.[33] The second compound, (2-(4-(4-(4-(4-hydroxyphenyl)piperazinyl)-phenyl)azophenyl)sulfonyl)ethylphosphonic

acid, **(2)**, is the structural complement of **1**, where the functional groups at the termini have been exchanged. The synthetic route to **2** is reported in the preceding paper,[45] and the structures of both molecules are shown in Figure 1.1. We report on the surface second harmonic generation (SSHG) response of multilayer assemblies of these chromophores for several different bilayer structural arrangements. Following a brief discussion of the experimental details, we consider the results of our experiments on these complementary chromophores in the context of the physical and chemical origins of the nonlinear response. We discuss the form of the SSHG signal and how that signal is related to the several contributions to the second order nonlinear susceptibility, $\chi^{(2)}$. We find direct evidence for the role of electric quadrupolar contributions to our data, with the magnitude of the quadrupole contribution depending sensitively on the chemical functionality in the vicinity of the ZP linking moieties.

4.2 Experimental

Synthesis. The synthesis of chromophore **2** is detailed in chapter 2 and the synthesis of chromophore **1** was reported by Katz *et al.*[33] All chemicals used were obtained in the highest purity grade available and the procedures reported in the literature were followed.

Surface Preparation. Fused silica substrates were cleaned in piranha solution (3:1 H_2SO_4:H_2O_2 – *caution - strong oxidizer!*) for 10 minutes and rinsed with distilled water. The substrates were then dried in a N_2 stream and introduced to a reaction vessel. The surfaces were phosphorylated under an Ar atmosphere using a solution of 20 m<u>M</u> 2,3,4-collidine and 20 m<u>M</u> $POCl_3$ in anhydrous acetonitrile at 20°C. After 10 minutes the

substrates were removed, rinsed with acetonitrile and water and dried with N_2. The surfaces were then zirconated by immersion in an aqueous 5 mM $ZrOCl_2$ solution for 10 minutes. The zirconated substrates were rinsed with water and dried.

Chromophore Deposition. Chromophores **1** and **2** were deposited on zirconated substrates from a saturated solution (~ 0.2 mM) of the appropriate chromophore dissolved in 1:4 DMF:EtOH. Deposition of each layer was from a solution containing either **1** or **2**, but not both. The temperature of each deposition solution was maintained slightly below boiling while the zirconated substrates were immersed for 10 minutes, followed by rinsing with warm ethanol and drying with N_2. Subsequent phosphorylation and zirconation of the chromophore-containing surfaces was performed as described above. Before measurement of adlayers for $\chi^{(2)}$ activity, terminal OH groups were phosphorylated. To monitor layer adsorption, the UV-visible absorbance spectrum of the sample was measured after each deposition cycle, and in all cases linear growth was observed.

Surface Second Harmonic Generation Laser System The details of the SSHG laser system are given in chapter 3.

4.3 Results and Discussion

The purpose of this chapter is to evaluate the use of structural cancellation at interfaces as a means of creating a nominally null $\chi^{(2)}$ background, making possible the characterization of interface vacancy and orientational defect density. We provide an overview of the relevant theory and discuss our experimental findings in the context of the contributions to the angle-dependent surface SHG data. We consider the nonlinear

response of the bare fused silica substrate first, then the same surface with layers of each chromophore adsorbed. With that information in hand, we present our data on two opposing bilayer structures; [SiO_x-**1**-**2**] and [SiO_x-**2**-**1**]. Their SSHG responses are not identical, pointing to the role and chemical identity of an adlayer quadrupole contribution to the experimental signal.

Many surface SHG experiments are performed in reflection mode,[46-49] with the angle of incidence of the fundamental electric field being the independent experimental variable. The form of the signal in these experiments is an incidence-angle dependent intensity of the reflected second harmonic light. The specific form of the data can, under favorable circumstances, be used to estimate the average tilt angle of the nonlinear chromophore relative to the surface normal and the magnitude of the experimental signal can be used to determine the value(s) of selected $\chi^{(2)}$ tensor elements. For SSHG transmission measurements on transparent substrates,[50-54] such as those we report here, the form of the experimental signal is somewhat more complicated and optical interference and transmission/reflection effects must be accounted for. We detail these effects below and discuss how information on interface properties can be obtained from our data.

We consider the system shown in Figure 4.1, where the incident electric field at frequency ω and polarized along the x-axis and propagates along the z-axis. The sample, composed of a transparent substrate, has interfacial layers present on both the front and back surfaces. The sample is rotated about the y-axis and the resultant second harmonic signal intensity is recorded as a function of rotation angle. Four effects contribute to the

data. The first is the angle-dependence of the reflection and transmission properties of the sample at both the fundamental and second harmonic frequencies. The second effect is optical interference between second harmonic light generated at the front and back

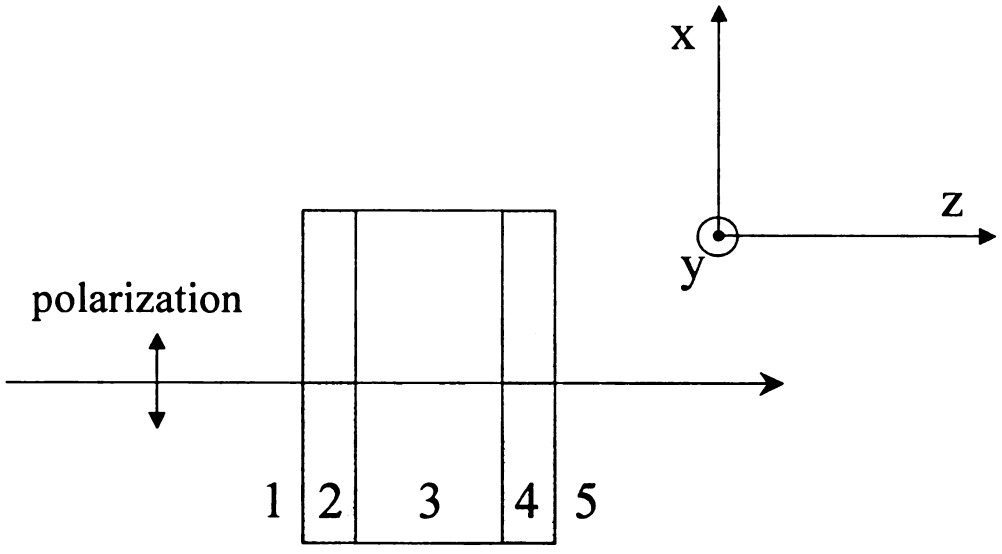

Figure 4. 1 Model system of thin films on both sides of a substrate. 1 and 5 are air; 2 and 4 are interfacial thin films; 3 is the substrate.

faces of the sample. Both the first and second effects are understood in the context of simple optical phenomena. The third and fourth features are the magnitude and shape of the envelope function of the SHG data. These quantities are related to the second order nonlinear susceptibility, $\chi^{(2)}$, and the orientation and angular distribution of the dominant $\chi^{(2)}$ tensor element(s) for the sample under consideration.

Optical effects. The angular dependence of the SHG signal we recover is oscillatory with respect to the angle of incidence of the fundamental electric field (Figure 4.2). This pattern appears to be outwardly similar to that produced by Maker fringes,[54-56] but it cannot be accounted for using Maker's treatment because the coherence length of

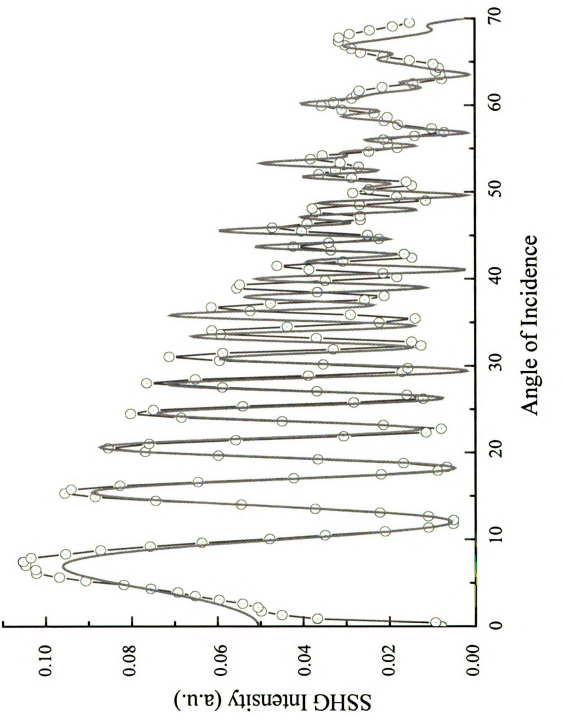

Figure 4.2 Surface SHG for a clean fused-silica substrate vs. angle of sample rotation (magenta) (0° is the condition where the incident electric field is propagates along the surface normal axis) plotted with the model (green) for three components of the etalon effect.

the light source we use is long relative to the thickness of the portion of the sample that generates the second harmonic signal. The origin of the signal shown in Figure 4.2 is interference between the second harmonic light generated at the front and back interfaces of the transparent substrate.[50,52,53] For the model system shown in Figure 4.1, we can decompose the induced polarization at 2ω into the components that arise from nonlinear interactions at each interface (layers 2 and 4, Figure 4.1),[57,58]

$$E^{2\omega} = E_2^{2\omega} + E_4^{2\omega} \qquad \textbf{Equation 4.1}$$

For $E^{2\omega}$ generated at each interface, we must account for the angular dependence of reflection and transmission, dispersion in each of the media and the thickness of the interface layer.

$$E_2^{2\omega} = \left(E^{\omega}\right)^2 \left(T_{12}^{\omega} R_2^{\omega}\right)^2 T_{23}^{2\omega} R_2^{2\omega} T_{34}^{2\omega} T_{45}^{2\omega} \left(\frac{4\pi\chi^{(2)}}{\left(\eta_{f_2}^{\omega}\right)^2 - \left(\eta_{f_2}^{2\omega}\right)^2}\right) \times \exp\left(i\phi_{f_2}\right) \exp\left(i\ell_f \frac{2\omega}{c}\right)\left(\eta_{f_2}^{\omega} \cos\theta_{f_2}^{\omega} - \eta_{f_2}^{2\omega} \cos\theta_{f_2}^{2\omega}\right) - 1 \qquad \textbf{Equation 4.2}$$

$$E_4^{2\omega} = \left(E^{\omega}\right)^2 \left(T_{12}^{\omega} R_2^{\omega} T_{23}^{\omega} T_{34}^{\omega} R_4^{\omega}\right)^2 T_{45}^{2\omega} R_4^{2\omega} \left(\frac{4\pi\chi^{(2)}}{\left(\eta_{f_4}^{\omega}\right)^2 - \left(\eta_{f_4}^{2\omega}\right)^2}\right) \times \exp\left(i\phi_{f_4}\right) \exp\left(i\ell_f \frac{2\omega}{c}\right)\left(\eta_{f_4}^{\omega} \cos\theta_{f_4}^{\omega} - \eta_{f_4}^{2\omega} \cos\theta_{f_4}^{2\omega}\right) - 1 \qquad \textbf{Equation 4.3}$$

where l_f is the film thickness, the terms η are the refractive indices of the films 2 and 4 at the frequencies indicated in the superscripts, the angles θ are the angles of refraction for the layer at the frequencies indicated, and the terms ϕ are the phase angles of the light at 2ω relative to the fundamental at each interface. The R and T terms are the Fresnel

transmittance and reflectance coefficients for a TM-polarized electric field at the interfaces indicated.[59]

$$t_{mn}^{TM} = \frac{2\eta_m \cos\theta_m}{\eta_n \cos\theta_m + \eta_m \cos\theta_n} \qquad T_{mn}^{TM} = \left(\frac{\eta_n \cos\theta_n}{\eta_m \cos\theta_m}\right)\left(t_{mn}^{TM}\right)^2$$

$$r_{mn}^{TM} = \frac{\eta_n \cos\theta_m - \eta_m \cos\theta_n}{\eta_n \cos\theta_m + \eta_m \cos\theta_n} \qquad R_{mn}^{TM} = \left(r_{mn}^{TM}\right)^2$$

Equation 4.4

The second harmonic light generated at interfaces 2 and 4 is initially in phase with the fundamental electric field at the same interfaces. The term that dominates the observed angular-dependence of the signal is the phase mismatch between the second harmonic light generated at interfaces 2 and 4 resulting from dispersion in the substrate. This phase relationship is given by[52]

$$\Delta\phi = \left(\phi_{f_2} - \phi_{f_4}\right) = \frac{2\omega}{c} d\left(\eta_s^{2\omega} \cos\theta_s^{2\omega} - \eta_s^{\omega} \cos\theta_s^{\omega}\right) \qquad \textbf{Equation 4.5}$$

where d is the substrate thickness. The oscillatory nature of the signal can be accounted for quantitatively using Eq. 4.5. With this information, $I^{2\omega} = (E^{2\omega})^2$ can be calculated as a function of the incidence angle of the fundamental electric field. We show the experimental second order response of a bare fused silica substrate in Figure 4.2 along with the calculated signal based on Eqs. 4.1-4.5. We note the presence of several different oscillating components and account for the presence of these components by considering that the substrate will act as an etalon. This is an expected phenomenon. The incident electric field makes multiple passes in the substrate, with the relative contribution from each odd-numbered pass (for a transmission measurement) depending on the angle of incidence in a manner dependent on the flatness of the SiO_x substrate and the Fresnel factors. The data shown in Figure 4.2 provide important insight into the

dominant contributions to the $\chi^{(2)}$ response for this system, and we will return to a discussion of this point after considering the chemical contributions to the nonlinear response.

Chemical effects. The chemical properties of the system that we sense with surface SHG measurements are the relative magnitudes of the several contributions to the first hyperpolarizability of the system and the distribution of orientations of the $\chi^{(2)}$-active species. Recent work by Simpson and Rowlen has treated the issue of $\chi^{(2)}$-chromophore orientation in surface second harmonic generation experiments.[60-62] Among the important findings of their work is that the chromophore tilt angle recovered experimentally converges to a "magic angle" of 39.2° with respect to the surface normal as the orientational distribution broadens. The actual treatment of the distribution can be complex, depending on its functional form, and it is typically assumed that the distribution is relatively narrow. In this limit, the dependence of the SHG response on chromophore tilt angle will scale with $\cos^2\langle\theta\rangle$, where $\langle\theta\rangle$ is the average angle between the incident electric field polarization vector and the chromophore nonlinear transition moment. For a molecule with its transition moment oriented along the surface normal, the maximum signal will occur when the incident electric field polarization vector is aligned with the substrate normal. The minimum signal for this condition will occur for the electric field propagating along the surface normal axis. The orientation-dependence of our data is manifested most prominently in the envelope function of the experimental data, as schematized in Figure 5.3a. It is clear from these calculations, based on Eqs. 4.1 and 4.4 and neglecting the optical interference effects, that the nonlinear chromophore orientation will have a significant effect on the form of our signal. In order to understand

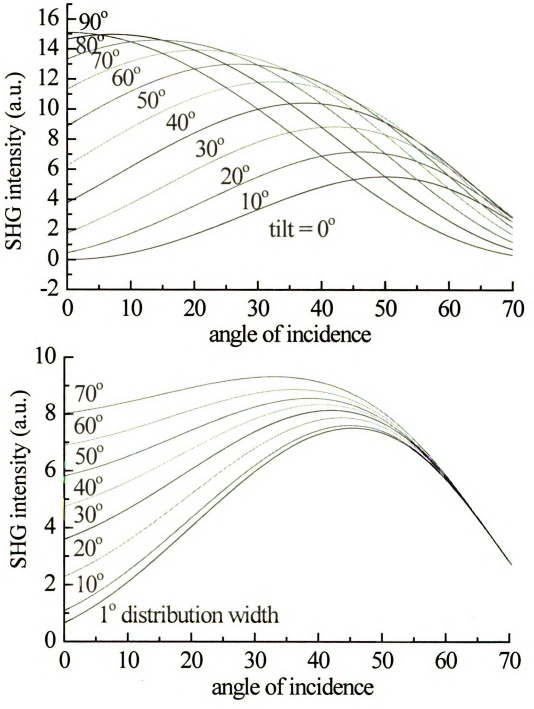

Figure 4.3 (a) Calculated SSHG envelope function for a series of chromophore tilt angles, as indicated in the plot. (b) Dependence of the envelope function on orientational distribution width. The distribution function is assumed to be Gaussian and the chromophore average orientation is along the surface normal axis.

the limits inherent to the interpretation of our data, we need also to consider the effect of the chromophore orientational distribution width on the envelope function. We show the effect of increasing orientational distribution width on the calculated envelope function in Figure 4.3b. This calculation is for a chromophore orientational distribution centered around the substrate normal. The broadening of the function near 0° tilt angle is reflective of the change in orientational distribution while the invariance of the signal near 70° demonstrates that, at high angles, the SSHG signal is dominated by optical considerations as described in Eqs. 4.4. Based on these calculations, it is clear that the unambiguous resolution of chromophore tilt angle and distribution width is limited by the S/N ratio of our data.

In the interpretation of many second harmonic generation measurements, it is common practice to assume that the electric dipole term in $\chi^{(2)}$ is much larger than the electric quadrupole and higher order terms. While this approximation holds for many experimental conditions, it is not universally the case. For the data we report here, the electric quadrupole term plays a significant role in determining the form of the experimental signal. Guyot-Sionnest and Shen have investigated the contributions of dipolar and quadrupolar terms to the second order nonlinear susceptibility of surfaces and interfaces.[63] Their work focused on the distinct contributions from the structural and electric field discontinuities that exist where the incident electric field propagates across the interface. In their model, the electric dipole contribution to the $\chi^{(2)}$ response is determined by the structural properties of the interface and they term it a local, intrinsic response. The electric quadrupole term results from the discontinuity experienced by the electric field as it propagates through the interface, and it is termed a nonlocal response

because it depends explicitly on the bulk properties of the two phases of matter comprising the interface. Using Guyot-Sionnest and Shen's terminology, the second order nonlinear susceptibility for an interface is given by[63]

$$\chi_{s}^{(2)}{}_{yzy} = \left(\int_{l} \chi_{yzy}^{D}(z)s(z) - \frac{\partial}{\partial z}[\chi_{zyzy}^{Q}(z)s(z)] + \chi_{A,yzzy}^{D}(z)\frac{\partial}{\partial z}s(z) \right) dz \qquad \textbf{Equation 4.6}$$

where $s(z) = 1/\varepsilon_I$, i=1,2, and ε is the optical frequency dielectric constant. Before the electric field is incident upon the interface ($z < 0$), $s(z)=1/\varepsilon_1$ and after the interface ($z > 0$), $s(z)=1/\varepsilon_2$. Between these two limits, s(z) varies continuously from $1/\varepsilon_1 \rightarrow 1/\varepsilon_2$ through the interface. $\chi^{(2)}{}_s$ is the total second order susceptibility and the integration is over the thickness on the interfacial region. The first term in Eq. 4.6 is the electric dipole term associated with the structural properties of the interface, the second is the nonlocal term associated with the induced electric quadrupole moment as the electric field propagates through the interfacial dielectric gradient, and the third term arises from the magnetic dipole moment. The theory is based on the simplest case; an interface between two transparent, nonmagnetic, isotropic media, 1 and 2. For these conditions, the first two terms in Eq. 4.6 will contribute most significantly to the observed $\chi^{(2)}{}_s$.

Because the interface electric dipole contribution to the nonlinear susceptibility is an intrinsic property of the material, it can be assumed constant over a range of experimental conditions. The discontinuity in the electric field as it propagates through the interface will depend on the difference in ε between the two bulk media and this quantity can be varied systematically. Guyot-Sionnest and Shen performed a series of surface SHG measurements using a fused silica substrate immersed in bulk liquids with varying dielectric constants.[63] In this way, the term $\partial/\partial z(s(z))$ could be made small,

revealing the role of the electric dipole term, χ^D, for this substrate. They determined from those experiments that the susceptibility of the air-fused silica interface is $\chi^{(2)}_s \sim 2.7\text{x}10^{-17}$ esu/cm^2, with $\chi^D \sim 5.7\text{x}10^{-18}$ esu/cm^2.[63] Although they did not explicitly perform the subtraction owing to the presence of the magnetic dipole term in Eq. 4.6, we estimate from their findings is that $\chi^Q \sim 2.1\text{x}10^{-17}$ esu/cm^2.

With the theoretical framework established by Guyot-Sionnest and Shen in place, we can see from the data in Figure 4.2 that the envelope function points to a signal maximum at normal incidence. For the fused silica substrate, the electric quadrupole term is dominant and the envelope function maximum near normal incidence suggests that the quadrupolar component lies in the plane of the substrate, and not perpendicular to it. We expect the electric dipole contribution to $\chi^{(2)}$ to be aligned with the surface normal. This finding can be understood in the context of the greatest electric field gradient at the interface being parallel to the interface. Thus a discontinuity in the incident electric field at the interface will be most pronounced in the plane of the interface. We can estimate the resulting "tilt" angle for the bare substrate if we assume that 20% of the total $\chi^{(2)}$ response is from the electric dipole term, normal to the surface and 80% of the response is from the electric quadrupole term, in the surface plane. The "tilt" angle recovered experimentally should be ~72° with respect to the surface normal for fused silica. We extract a best fit tilt angle of 63° from our experimental data. As discussed above, the extraction of tilt angle and orientational distribution information from our data is S/N limited, so to within the accuracy of these determinations, we view the agreement as good.

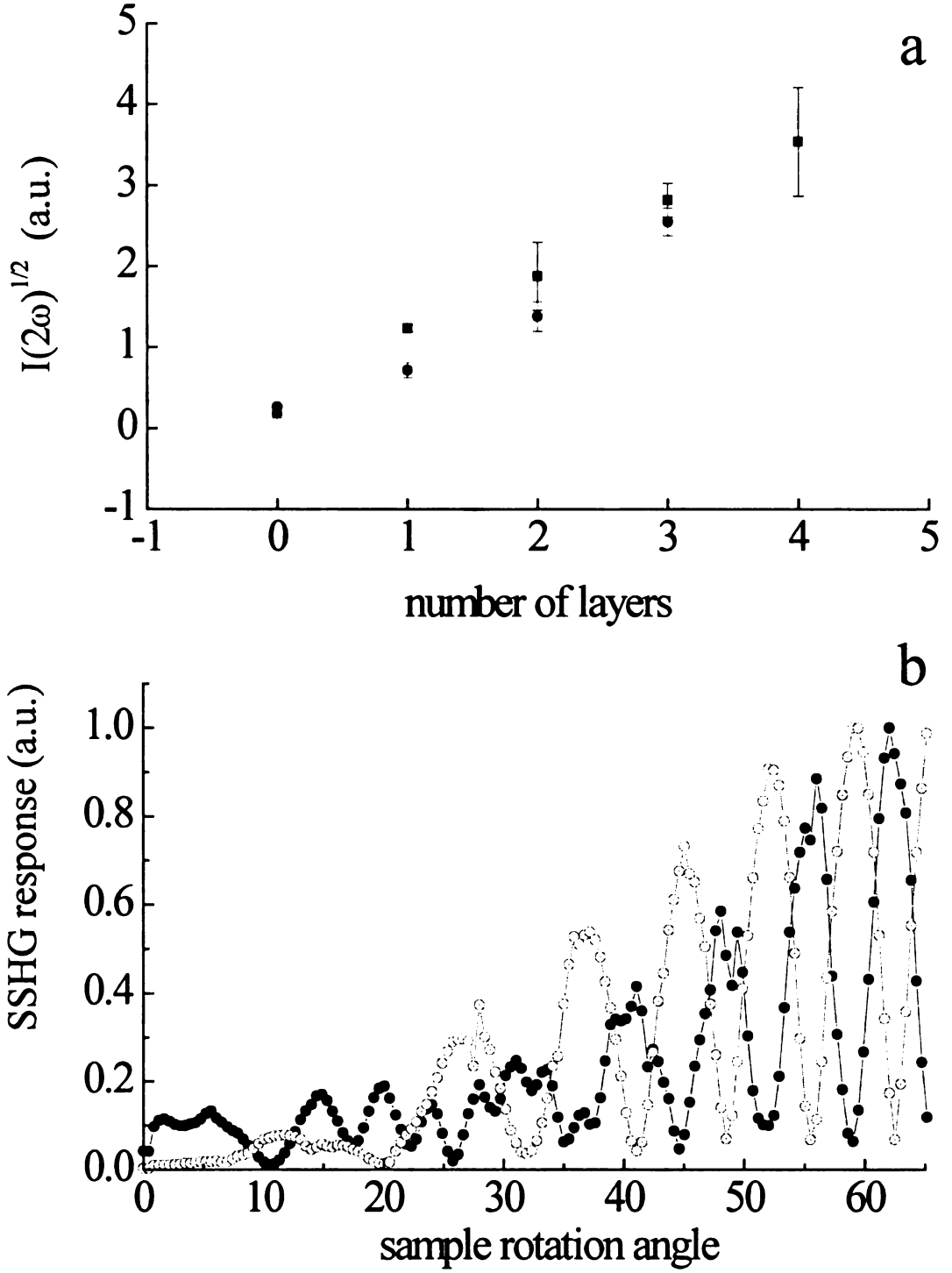

Figure 4.4 (a) Plot of the [SHG Intensity]$^{1/2}$ vs. the number of chromophore layers. (b) Angle-dependent SSHG signals from chromophores **1** (•) and **2** (o). These data are dominated by substrate response at small angles and chromophore response at high angles.

We consider next the nonlinear optical properties of multilayers of each of the chromophores. Katz *et al.* has reported previously on the second order nonlinear response of chromophore **1**.[33] Our data are consistent with his and we observe a square-law dependence of the second harmonic intensity with increasing number of layers for both chromophores. This is an expected result for a system where the nonlinear medium is significantly thinner than the coherence length of the incident light source. The data we present in Figure 4.4a demonstrate this relationship and show that the system is sufficiently ordered to allow the square-law relationship to be manifest for both chromophores. We estimate $\chi^{(2)} = 4.0 \times 10^{-16}$ esu/cm^2-layer for **1** based on the experimental signal relative to that of the quartz substrate. Katz *et al.* reported a value of $\beta = 150 \times 10^{-30}$ esu for a 4-layer stack of **1** characterized by an order parameter of 0.2.[33] Assuming a layer density of 1.6×10^{14} cm^{-2} [45] and the same layer order, our data correspond to a value of 200×10^{-30} esu.

There are many possible molecular and bulk contributions to the nonlinear response of the interfaces we study here and, based on the subtle differences in the linear response of **1** and **2**, it is possible that the magnitude of their $\chi^{(2)}$ responses could be different. From the data shown in Figure 4.4a, it is clear that the magnitudes of the $\chi^{(2)}$ responses for chromophores **1** and **2** are the same to within the experimental uncertainty. While the magnitudes are equal, the sign of the nonlinear response for these two chromophores is opposite owing to their complementary orientations, and this condition is apparent in the phase relationship of the angle-dependent SSHG data (Figure 4.4b).[52]

The experimental angle-dependent SSHG data for each chromophore can be modeled using Eqs. 4.1 – 4.5. We present the correspondence between the calculated

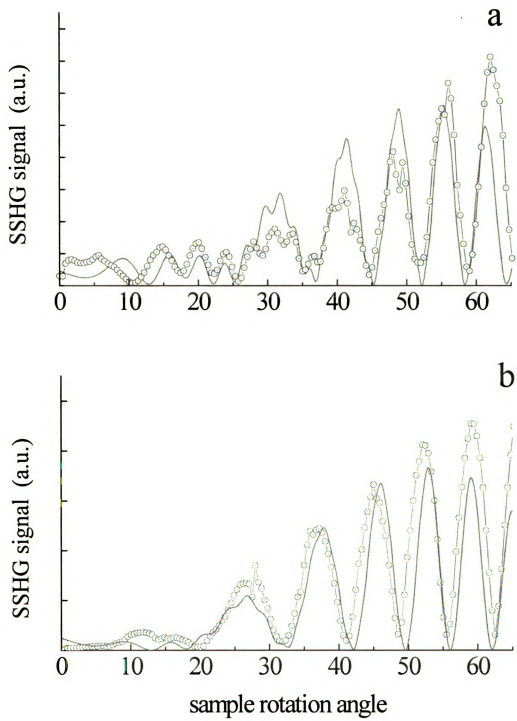

Figure 4.5 (a) Comparison of experimental SSHG data to the model presented in Eqs. 4.1-4.5 for chromophore **1**. (b) Comparison of experimental data with model presented in Eqs. 4.1-4.5 for chromophore **2**.

response and the experimental response for a single layer of chromophore **1** in Figure 4.5a and for a single layer of chromophore **2** in Figure 4.5b. For both chromophores, the agreement between experiment and model is reasonable. For small sample rotation angles, the signal has a measurable contribution from the SiO_x substrate while at higher rotation angles the chromophore response dominates. For the chromophores, it is likely that the electric dipole contribution to their $\chi^{(2)}$ response is dominant, owing to their structures and the fact that their response as a function of angle shows directly the orientation dependence. As discussed above, the manner in which we acquire SSHG data is not amenable to precise orientation angle or distribution determinations, but it is clear from the experimental signals that the largest $\chi^{(2)}$ susceptibility terms for chromophore layers lie close to the substrate normal.

We now turn to the issue of assessing the nonlinear response of multilayer assemblies that contain both chromophores. For a bilayer system, there are two possible structural permutations; [SiO_x-**1**-**2**] and [SiO_x-**2**-**1**]. Before comparing their nonlinear responses, it is important to ensure that the formation of these bilayers does not give rise to anomalous changes in their linear response. The absorption spectra of both bilayers are identical to the linear responses of the individual chromophores. We present the $\chi^{(2)}$ data for these two bilayer structures in Figures 4.6a and 4.6b. The data include $\chi^{(2)}$ responses of the bare substrate before deposition for comparison. The most striking feature of these data is that the responses of the two complete bilayers are not the same. This result is reproducible and cannot be accounted for in the context of simple additivity of the constituent electric dipole contributions. If electric dipole or any other contribution(s) intrinsic to the chromophores and the substrate accounted for the overall

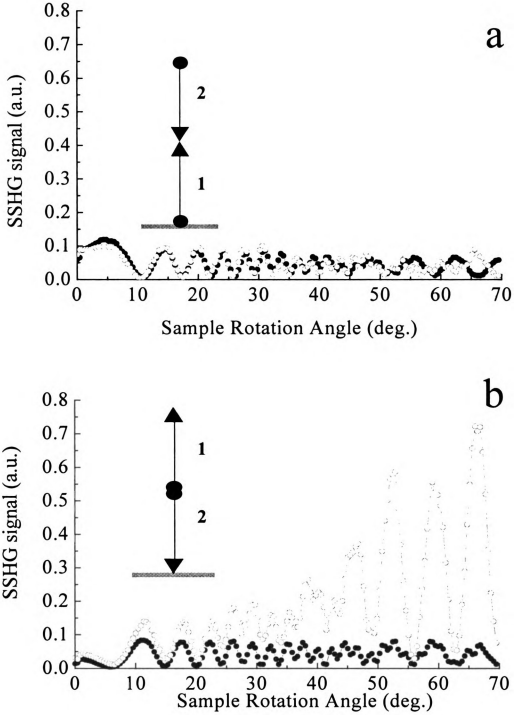

Figure 4.6 Surface SHG of (a) [SiO_x-**1-2**] and (b) [SiO_x-**2-1**] bilayers showing the cancellation of SHG signal with the adsorption of the second layer. The orange traces are data on the bilayer structures and the black circles are SSHG data for the bare SiO_x substrates.

$\chi^{(2)}$ response, the two bilayer structures would necessarily produce identical nonlinear responses, with any difference between the bilayer and bare substrate responses being attributable to vacancy and/or orientational defects. There may be some hint of this effect in the data in Figure 4.6a for high rotation angles, but this issue remains under investigation. We note that the cancellation we observe in these data demonstrates the feasibility of our approach to $\chi^{(2)}$ background nulling. Because the interlayer linking chemistry is the same for both bilayer structural permutations and the formation constant for ZP materials is characteristically so large, there is no reason to expect a difference for the bilayer responses based on differences in the efficiency of layer formation.

The fact that the bilayer data in Figures 4.6 are not identical demonstrates the importance of subtle structural contributions to the overall nonlinear response of the system. The only structural difference between the two bilayers lies in the region near where the two layers are connected through ZP linkages. It is known that the zirconium bisphosphonate solid state structure possesses a center of inversion about the metal ion, ruling out an electric dipole allowed contribution to the signal from this moiety. At first glance, one could invoke the phosphate/phosphonate asymmetry to account for a $\chi^{(2)}$ response, but a more detailed examination of the bilayer structure reveals that this asymmetry is oriented in the same direction for both bilayer structures. The only structural difference between the two bilayers is the polarizability, and thus the hyperpolarizability, of the organic functionalities attached to the phosphate and phosphonate moieties. For [SiO_x-**1**-**2**], the interlayer **1**-**2** connection is of the form indicated in Figure 4.7a and for [SiO_x-**2**-**1**] the analogous structure is shown in Figure 4.7b. As indicated above, the net dipolar contributions should be the same for both

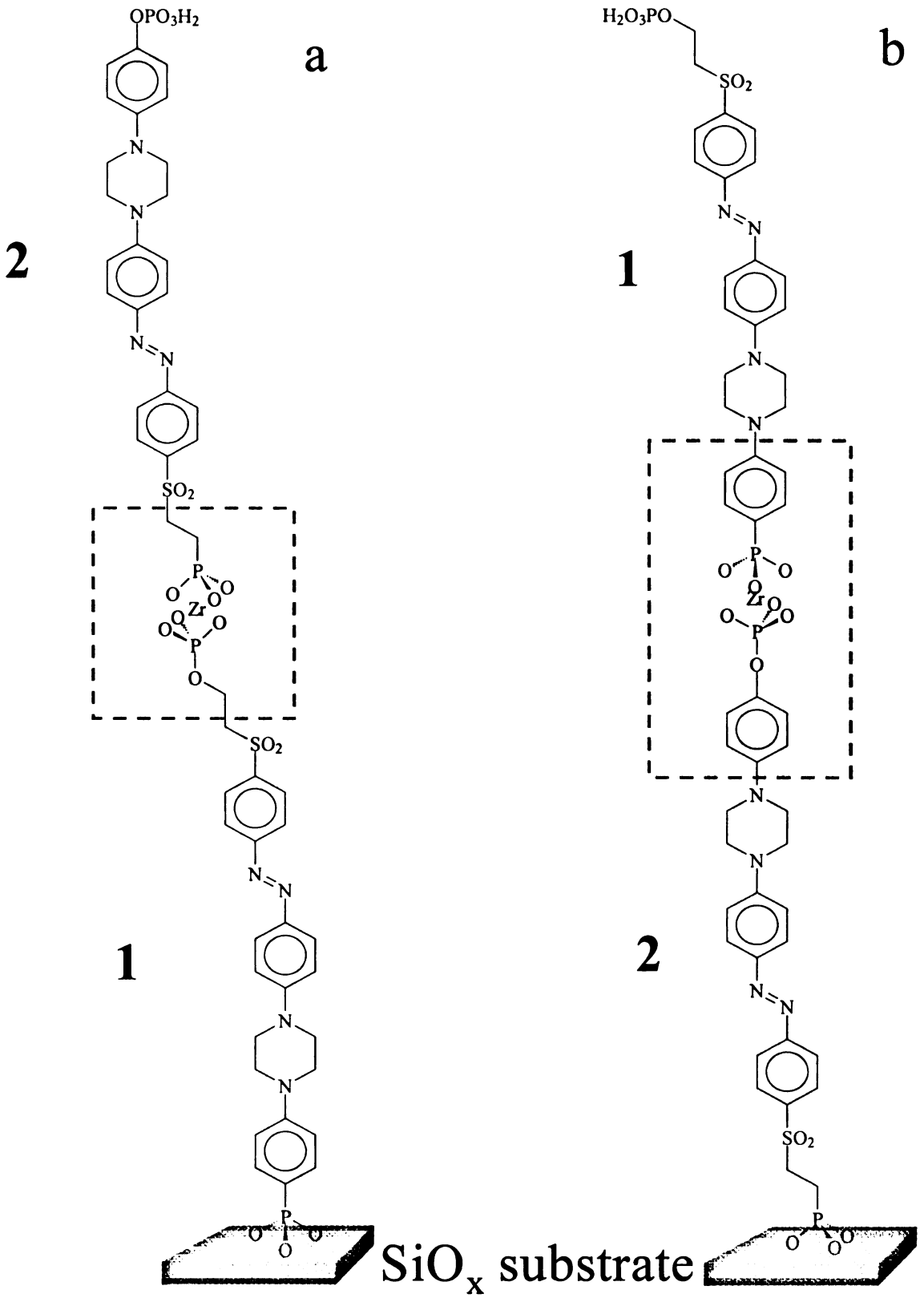

Figure 4. 7 (a) Structure of [SiO_x-**1**-**2**] bilayer. (b) Structure of [SiO_x-**2**-**1**] bilayer. Note the structural difference between the interlayer linkages for the two assemblies (boxed).

structures, but the quadrupole moment for [SiO_x-**1**-**2**] should be substantially less than that for [SiO_x-**2**-**1**]. The electric quadrupole moment for [SiO_x-**2**-**1**] should be oriented along the chromophore tilt axis and both of these structurally-based predictions are consistent with the experimental data. Unfortunately, there is no reliable means to estimate the magnitude of the nonlinear responses associated with these interlayer connecting structures. The central point is, however, that the nonlinear response of these bilayers cannot be accounted for simply by adding the dipolar contributions of the component parts.

4.4 Conclusions

We have characterized Zr-phosphate/phosphonate (ZP) self-assembled multilayer structures using surface second harmonic generation measurements. We have used two $\chi^{(2)}$-active chromophores with complementary structures and have assembled bilayers with controlled orientation relative to the substrate. The nonlinear optical responses of the SiO_x substrate and of multilayers of each of the chromophores have been characterized. For the substrate we find substantial contributions to the nonlinear response from the electric quadrupole contributions to the total $\chi^{(2)}$ term, in agreement with the work of Guyot-Sionnest and Shen.[63] For each chromophore, multilayer structures provide the expected dependence of second harmonic signal on number of layers and, based on the magnitudes of these signals, the electric dipole term likely dominates the chromophore $\chi^{(2)}$ responses. Using these same chromophores, we have formed bilayers to produce two different, canceling structural motifs, each with a local center of inversion about the ZP interlayer bonding plane. The $\chi^{(2)}$ responses of the two

bilayer systems are measurably different, revealing the limitations of accounting for nonlinear optical responses simply in terms of additive contributions from the constituents. The differences in the nonlinear responses of the two systems can be accounted for through cancellation of the electric dipole contribution to $\chi^{(2)}$, with the residual difference arising from the electric quadrupole contribution. This higher order response is associated with the region centered around the interlayer linking group. Our data underscore the complex and non-additive issues associated with the design and construction of layered interfaces and, in principle, provide a means to measure the vacancy defect density in layered materials. Clearly the chromophores we have used in this report are not ideal candidates for vacancy defect density measurements, but simple synthetic means can be used to improve their utility for this application. These data also raise the issue of the thickness of interface that SSHG measurements are sensitive to, and we anticipate future work in this area to shed new light on this matter.

4.5 Literature Cited

1. Katz, H. E.; Scheller, G.; Putvinski, T. M.; Schilling, M. L.; Wilson, W. L.; Chidsey, C. E. D.; *Science* **1991**, *254*, 1485.
2. Li, D.; Ratner, M. A.; Marks, T. J.; Zhang, C. H.; Yang, J.; Wong, G. K.; *J. Am. Chem. Soc.* **1990**, *112*, 7389.
3. Kepley, L. J.; Crooks, R. M.; Ricco, A.; *Anal. Chem.* **1992**, *64*, 3191.
4. Swalen, J. P.; Allara, D. L.; Andrade, J. P.; Chandross, E. A.; Garoff, S.; Israelachvilli, J.; McCarthy, T. J.; Murray, R.; Pease, R. F.; Rabolt, J. F.; Wynne, K. J.; Tu, H.; *Langmuir* **1987**, *3*, 932.
5. Calvert, J. M.; Georger, J. H., Jr.; Peckerer, M. C.; Perhsson, P. E.; Schnur, J. M.; Scheon, P.; E.; *Thin Films* **1992**, *114*, 9188.
6. Dulcey, C. S.; Georger, J. H.; Krauthamer, V.; Stenger, D. A.; Fare, T. L.; Calvert, J. M.; *Science* **1991**, *252*, 551.
7. Kumar, A.; Biebuyck, H. A.; Abbott, N. L.; Whitesides, G. M.; *J. Am. Chem. Soc.* **1992**, *114*, 9188.
8. Vrancken, K. C.; Van Der Voort, P.; Gillis-D'Hammers, I.; Vansant, E. F.; Grobet, P.; *J. Chem. Soc., Faraday Trans.* **1992**, *88*, 3197.
9. Pfleiderer, B.; Albert, K.; Bayer, E.; *J. Chromatogr.* **1990**, *506*, 343.
10. Ulman, A.; *Chem. Rev.* **1996**, *96*, 1533.
11. Dubois, L. H.; Nuzzo, R. G.; *Annu. Rev. Phys. Chem.* **1992**, *43*, 437.
12. Xia, Y.; Whitesides, G. M.; *Angew. Chem. Int. Ed.* **1998**, *37*, 551.
13. Karpovich, D. S.; Blanchard, G. J.; *Langmuir* **1994**, *10*, 3315.

14. Schessler, H. M.; Karpovich, D. S.; Blanchard, G. J.; *J. Am. Chem. Soc.* **1996,** *118,* 9645.

15. Kohli, P.; Taylor, K. K.; Harris, J. J.; Blanchard, G. J.; *J. Am. Chem. Soc.*, **1998,** *120,* 11962.

16. Gun, J.; Iscovici, R.; Sagiv, J.; *J. Colloid Interface Sci* **1984,** *101,* 201.

17. Maoz, R.; Sagiv, J.; *J. Colloid Interface Sci.* **1984,** *100,* 465.

18. Maoz, R.; Sagiv, J.; *Thin Solid Films* **1985,** *132,* 135.

19. Hong, H.-G.; Sackett, D. D.; Mallouk, T. E.; *Chem. Mater.* **1991,** *3,* 521.

20. Thompson, M. E.; *Chem. Mater.* **1994,** *6,* 1168.

21. Katz, H. E.; Wilson, W. L.; Scheller, G.; *J. Am. Chem. Soc.* **1994,** *116,* 6636.

22. Yonemoto, E. H.; Saupe, G. B.; Schmehl, R. H.; Hubig, S. M.; Riley, R. L.; Iverson, B. L.; Mallouk, T. E.; *J. Am. Chem. Soc.* **1994,** *116,* 4786.

23. Katz, H. E.; Bent, S. F.; Wilson, W. L.; Schilling, M. L.; Ungashe, S. B.; *J. Am. Chem. Soc.* **1994,** *116,* 6631.

24. Frey, B. L.; Hanken, D. G.; Corn, R. M.; *Langmuir* **1993,** *9,* 1815.

25. Yang, H. C.; Aoki, K.; Hong, H.-G.; Sackett, D. D.; Arendt, M. F.; Yau, S.-L.; Bell, C. M.; Mallouk, T. E.; *J. Am. Chem. Soc.* **1993,** *115,* 11855.

26. Vermeulen, L.; Thompson, M. E.; *Nature* **1992,** *358,* 656.

27. Ungashe, S. B.; Wilson, W. L.; Katz, H. E.; Scheller, G. R.; Putvinski, T. M.; *J. Am. Chem. Soc.* **1992,** *114,* 8717.

28. Cao, G.; Rabenberg, L. K.; Nunn, C. M.; Mallouk,; T. M. *Chem. Mater.* **1991,** *3,* 149.

29. Katz, H. E.; Schilling, M. L.; Chidsey, C. E. D.; Putvinski, T. M.; Hutton, R. S.; *Chem. Mater.* **1991**, *3*, 699.

30. Katz, H. E.; Scheller, G.; Putvinski, T. M.; Schilling, M. L.; Wilson, W. L.; Chidsey, C. E. D.; *Science* **1991**, *254*, 1485.

31. Putvinski, T. M.; Schilling, M. L.; Katz, H. E.; Chidsey, C. E. D.; Mujsce, A. M.; Emerson, A. B.; *Langmuir* **1990**, *6*, 1567.

32. Rong, D.; Hong, H.-G.; Kim, Y.-I.; Krueger, J. S.; Mayer, J. E.; Mallouk, T. E.; *Coord. Chem. Rev.* **1990**, *97*, 237.

33. Lee, H.; Kepley, L. J.; Hong, H.-G.; Akhter, S.; Mallouk, T. E.; *J. Phys. Chem.* **1988**, *92*, 2597.

34. Lee, H.; Kepley, L. J.; Hong, H.-G.; Mallouk, T. E.; *J. Am. Chem. Soc.* **1988**, *110*, 618.

35. Katz, H. E.; *Chem. Mater.* **1994**, *6*, 2227.

36. Horne, J. C.; Huang, Y.; Liu, G.-Y.; Blanchard, G. J.; *J. Am. Chem. Soc.*, **1999**, *121*, 4419.

37. Horne, J. C.; Blanchard, G. J.; *J. Am. Chem. Soc.*, **1999**, *121*, 4427.

38. Sabatini, E.; Rubinstein, I.; *J. Phys. Chem.*, **1987**, *91*, 6663.

39. Sabatini, E.; Rubinstein, I.; Moaz, R.; Sagiv, J.; *J. Electroanal. Chem.*, **1987**, *219*, 365.

40. Finklea, H. O.; Snider, D. A.; Fedyk, J.; Sabatini, E.; Gafni, Y.; Rubinstein, I.; *Langmuir*, **1993**, *9*, 3660.

41. Finklea, H. O.; Snider, D. A.; Fedyk, J.; *Langmuir*, **1990**, *6*, 371.

42. Sabatini, E.; Cohen-Boulakia, J.; Bruening, M. L.; Rubinstein, I.; *Langmuir*, **1993**, *9*, 2974.

43. Janek, R. P.; Fawcett, W. R.; Ulman, A.; *Langmuir*, **1998**, *14*, 3011.

44. Shen, Y. R.; The Principles of Nonlinear Optics, John Wiley and Sons, Inc., 1984.

45. Flory, W. C.; Mehrens, S. M.; Blanchard, G. J.; *J. Am. Chem. Soc., preceding article.*

46. Heinz, T. F.; Tom, H. W. K.; Shen, Y. R.; *Phys. Rev. A.*, **1983**, *28*, 1883.

47. Bloembergen, N.; Chang, R. K.; Jha, S. S.; Lee, C. H.; *Phys. Rev.*, **1968**, *174*, 813.

48. Naujok, R. R.; Higgins, D. A.; Hanken, D. G.; Corn, R. M.; *J. Chem. Soc. Faraday Trans.*, **1995**, *91*, 1411.

49. Daschbach, J. L.; Fischer, P. R.; Gragson, D. E.; Demarest, D.; Richmond, G. L.; *J. Phys. Chem.*, **1995**, *99*, 10690.

50. Lupo, D.; Prass, W.; Scheunemann, U.; Laschewsky, A.; Ringsdorf, H.; Ledoux, I.; *J. Opt. Soc. Am. B*, **1988**, *5*, 300.

51. Berkovic, G.; Shen, Y. R.; Marowsky, G.; Steinhoff, R.; *J. Opt. Soc. Am. B*, **1989**, *6*, 205.

52. Sato, O.; Baba, R.; Hashimoto, K.; Fujishima; A.; *J. Electroanal. Chem.*, **1991**, *306*, 291.

53. Kajikawa, K.; Takezoe, H.; Fukuda, A.; *Chem. Phys. Lett.*, **1993**, *205*, 225.

54. Herman, W.; Hayden, L. M.; *J. Opt. Soc. Am. B*, **1995**, *12*, 416.

55. Maker, P. D.; Terhune, R. W.; Nisenhoff, M.; Savage, C. M.; *Phys. Rev. Lett.*, **1962**, *8*, 21.

56. Jerphagnon, J.; Kurtz, S. K.; *J. Appl. Phys.*, **1970**, *41*, 1667.

57. Bloembergen, N.; Pershan, P. S.; *Phys. Rev.*, **1962**, 128, 606.

58. Kajzar, F.; Messier, J.; Zyss, J.; Ledoux, I.; *Opt. Comm.*, **1983**, 45, 133.

59. Pedrotti, F. L.; Pedrotti, L. S.; Introduction to Optics, Prentice-Hall, Inc., 1987, pp. 472-487.

60. Simpson, G. J.; Rowlen, K. L.; *J. Am. Chem. Soc.*, **1999**, *121*, 2635.

61. Simpson, G. J.; Rowlen, K. L.; *J. Phys. Chem. B*, **1999**, *103*, 1525.

62. Simpson, G. J.; Rowlen, K. L.; *J. Phys. Chem. B*, **1999**, *103*, 3811.

63. Guyot-Sionnest, P.; Shen, Y. R.; *Phys. Rev. B.*, **1987**, *35*, 4420.

Chapter 5

UNDERSTANDING THE SPATIAL DEPENDENCE OF THE NONLINEAR RESPONSE USING SELF-ASSEMBLED MULTILAYERS

Summary

We report on the structure-dependence of second harmonic generation (SHG) in Zr-phosphate/phosphonate (ZP) self-assembled multilayer structures using two $\chi^{(2)}$-active chromophores separated by $\chi^{(2)}$-inactive layers. The chromophores are identical save for their terminal functional groups, allowing for control over nonlinear chromophore orientation with respect to the surface to produce bilayer structures with inversion symmetry. We have shown previously that the $\chi^{(2)}$ response of such structures can cancel if the interlayer linking functionality does not produce an explicit $\chi^{(2)}$ response. We report here on the dependence of the $\chi^{(2)}$ response of structurally opposing multilayers spaced apart by pre-determined distances using centrosymmetric alkanebisphosphonates. Our data show that the nonlinear response of multilayer stacks, even when each layer is of molecular dimension, is more complex than that of a single $\chi^{(2)}$-active layer.

5.1 Introduction

Self-assembled monolayer and multilayer (SAM) thin films continue to receive a great deal of attention in the materials community because of their potential relevance to a variety of applications, including nonlinear optical device design.[1-27] The reason for this interest is that SAMs are easy to synthesize, require mild conditions for formation, and are structurally and thermally robust once formed. In addition, it is possible to grow highly oriented multilayer assemblies, allowing for the possibility of efficient second harmonic generation and other phenomena that depend on $\chi^{(2)}$. For SAMs to be used in applications that are sensitive to surface conditions, the nature of structural defects inherent in layer synthesis needs to be understood.

The interest in defect determination is not new.[28-31] There is a rich literature on the characterization of defects in self-assembled alkanethiol monolayers on gold. In that work, the primary means of defect characterization is electrochemical.[32-37] For multilayer films and films deposited on non-conducting substrates, electrochemistry is not a viable technique and we are left to devise alternative means for the examination of defects. Whitesides has used chemical modifications to detect vacancy defects.[38] Beebe and coworkers use "molecular corrals" to elucidate information defects from surface structures.[39] A major goal of our work has been to develop ways to quantify defects on a molecular scale in multilayer films. Our approach is to utilize surface second harmonic generation (SSHG) measurements in conjunction with oriented layer growth. For the $\chi^{(2)}$ chromophores we use, the functional chemistry of their termini allow for orientational control in the growth of these films. By constructing films with specific orientation relative to the substrate in each layer, a bilayer film can be assembled such that a center

of symmetry is enforced across the interlayer linking functionality. This structural arrangement effectively nulls the second order nonlinear response from portions of the assembly where the bilayer structure exists and, in principle, the recovered SSHG signal exists as a consequence of vacancy or orientational defects in the bilayer structure. We have demonstrated this effect in the previous chapter.

The chromophore used for our SSHG measurements, (4-(4-(4-(4-((2-hydroxyethyl)sulfonyl)-phenyl)azo)phenyl)piperazinyl)phenyl)phosphonic acid, **1**, was developed by Katz *et al.* for its rigid structure and large nonlinear response.[40] We have detailed the synthesis and characterization of the complementary chromophore, **2**, (2-(4-(4-(4-(4-hydroxyphenyl)piperazinyl)phenyl)azophenyl)sulfonyl)-ethylphosphonic acid in Chapter 2.[41] The molecular structure of these chromophores is shown in Figure 1.1. The similar absorption and layer-forming characteristics of both chromophores make them ideal candidates for SSHG investigations. The results presented in Chapter 4 have shown that the SSHG responses of bilayer structures of **1** and **2** grown on fused silica are decreased substantially due to symmetry about the ZP linkage with the residual $\chi^{(2)}$ response arising from the structure of the interlayer linking moiety.[42] For bilayers of the form [SiO_x-**1**-**2**], complete cancellation was observed while for bilayers [SiO_x-**2**-**1**] there was a residual SSHG signal. The origin of this residual signal is the formation of a polarizable interlayer linking moiety that is absent in the [SiO_x-**1**-**2**] layer structure. Subsequent to that study we have investigated the dependence of the SSHG signal on the structure of the multilayer assembly, and it is that work we report in this chapter.

The $\chi^{(2)}$ cancellation effects we see for relatively simple bilayer structures are not obtained for structurally more complex systems. Despite the fact that each layer in these

interfacial assemblies is of molecular dimension, achieving an understanding of the experimental $\chi^{(2)}$ response requires understanding of the structural complexity of the interface. The focus of this chapter is on reporting and understanding the experimental SSHG response for several multilayer assemblies.

5.2 Experimental

Chemicals. All chemicals used were obtained in the highest purity grade available and were used as received except for triisopropyl phosphite, which was purified by drying over sodium under an inert atmosphere, followed by vacuum distillation.[43]

Synthesis. **1,12-dodecanediylbisphosphonic acid**[44] 20.0 mL of purified triisopropyl phosphite (81.1 mmol) was added to 11.41 g of 1,12-dibromododecane (34.8 mmol) under Ar. The solution was refluxed for 18 hours at 150 °C, then cooled, and excess triisopropyl phosphite and isopropyl bromide were removed by vacuum distillation. 50 mL 12M HCl was added to the vessel and the solution was refluxed for 5 hours at 150 °C. Upon cooling, crystals precipitated from solution and were collected by vacuum filtration. The crystals were dissolved in ethanol and recrystallized. The product was collected by vacuum filtration and dried, yielding 9.45 g (82%) of white product. Pure by ^{1}H NMR.

Chromophore Deposition. The chromophores were synthesized according to the literature procedure (**1**)[40] or as described in Chapter 2 of this thesis (**2**), and were deposited on zirconated substrates from a saturated solution (~ 0.2 mM) of the appropriate chromophore dissolved in 1:4 DMF:EtOH. Deposition of each layer was from a solution containing either **1** or **2**, but not both. The temperature of each deposition

solution was maintained slightly below boiling while the zirconated substrates were immersed for 10 minutes, followed by rinsing with warm ethanol and drying with N_2. Subsequent phosphorylation and zirconation of the chromophore-containing surfaces was performed as described above. Before measurement of adlayers for $\chi^{(2)}$ activity, terminal OH groups were phosphorylated. To monitor layer adsorption, the UV-visible absorbance spectrum of the sample was measured after each deposition cycle, and in all cases linear growth was observed.

Spacer Layer Deposition. The alkyl bisphosphonate was deposited on zirconated substrates from a ~61mM solution using 1:4 DMF:EtOH as before. The temperature of the deposition solution was maintained slightly below boiling while the zirconated substrates were immersed for 10 minutes, followed by rinsing with warm ethanol and drying with N_2. Zirconation of the surfaces was performed as described above.

Measurements. ^{1}H NMR spectra were taken with a Varian Gemini-300 MHz NMR spectrometer. Optical absorption measurements were made using a Hitachi U-4001 UV-visible absorption spectrometer.

Surface Second Harmonic Generation Laser System. The laser system used for SSHG has been described in detail in Chapter 3.

5.3 Results and Discussion

The purpose of this chapter is to investigate the surface SHG response of multilayer assemblies greater structural complexity than those reported in the Chapter 4. In that work, structural cancellation of the surface SHG signal was demonstrated for a specific molecular configuration. The SSHG signal could be treated and understood in

the context of a single thin layer of $\chi^{(2)}$-active material at the interface between two bulk , $\chi^{(2)}$-inactive materials. We demonstrated that the chemical identity of the $\chi^{(2)}$-active interface layer can play a critical role in determining the form and magnitude of the experimental signal, as expected. In this work we have investigated structurally more complex interfaces and report that their SSHG responses cannot be understood in the same context as those reported in the previous chapter. The initial intention of this work was to establish the persistent length of layer organization by spacing the chromophores **1** and **2** away from one another and the substrate by varying distances using $\chi^{(2)}$-inactive alkylbisphosphonate layers. We will first consider the experimental data and then discuss the methods by which it can be interpreted.

We have investigated six structural permutations of multilayer assemblies and have recorded the SSHG response of each layer at each step in the assembly procedure. The structures we have investigated are shown schematically in Figures 5.1, 5.3, and 5.5 and their integrated SSHG responses are reported in Table 5.1. The corresponding angular dependent experimental data are shown in Figures 5.2, 5.4, and 5.6. For these measurements there is no explicit attempt to separate quadrupolar from dipolar contributions to the experimental signal. There are several unexpected results contained in these data. The first is that the structurally-based SSHG cancellation seen for bilayers of chromophores **1** and **2** is not seen for multilayer assemblies containing more than two molecular layers. The second unexpected finding is that the magnitude of the SSHG response for a given chromophore is found to depend on its spacing from the dielectric substrate. There are two qualitative approaches to the interpretation of these data and we outline them below.

Table 5.1. Experimental susceptibility values extracted from our data.

esux10^{-17}	SiO_x- 1S2	SiO_x- 1SS2	SiO_x- 2S1	SiO_x- 2SS1	SiO_x- SS12	SiO_x- SS21
SiO_x	2.70	2.70	2.70	2.70	2.70	2.70
Layer 1	12.7	29.1	16.8	32.0	0.39	3.33
Layer 2	11.2	26.2	2.15	2.70	2.72	0.99
Layer 3	206	73.8	197	1.50	26.4	4.44
Layer 4	-	252	-	204	77.2	28.9
cap	23.8		166			

In their work on understanding SSHG experiments, Guyot-Sionnest and Shen demonstrated that the SSHG response of a blank fused silica substrate contained contributions from both structural discontinuities and from variations in the dielectric response of the media at the interface which led to nonlinearities in the electric field as it traversed the interface.[45] They expressed their findings in an equation that takes into account both dipolar and quadrupolar contributions to the experimental signal.

$$\chi^{(2)}_{s,yzy} = \left(\int_l \chi^{D}_{yzy}(z)s(z) - \frac{\partial}{\partial z}[\chi^{Q}_{zyzy}(z)s(z)] + \chi^{D}_{A,yzzy}(z)\frac{\partial}{\partial z}s(z) \right) dz \qquad \textbf{Equation 5.1}$$

where $s(z) = 1/\varepsilon_i$ (i=1,2, ε = the optical frequency dielectric constant). Before the electric field is incident upon the interface ($z < 0$), $s(z)=1/\varepsilon_1$ and after the interface ($z > 0$), $s(z)=1/\varepsilon_2$. Between these two limits, s(z) varies continuously from $1/\varepsilon_1 \rightarrow 1/\varepsilon_2$ through the interface. $\chi^{(2)}_s$ is the total second order susceptibility and the integration is over the thickness on the interfacial region. The first term in Eq. 5.1 is the electric dipole term associated with the structural properties of the interface, the second is the nonlocal term

associated with the induced electric quadrupole moment as the electric field propagates through the interfacial dielectric gradient, and the third term arises from the magnetic dipole moment. The theory is based on the simplest case; an interface between two transparent, nonmagnetic, isotropic media, 1 and 2.

An assumption inherent in this treatment is that the $\chi^{(2)}$-active layer is characterized by a single (complex) dielectric constant, and the nonlinearity experienced by the electric field is the result of a continuous or simple step-wise variation in the dielectric response of the medium from one boundary condition to the other. Indeed, this treatment is implicit in essentially all of the current explanations of SSHG phenomena and, in Eq. 5.1, the term s(z) describes this variation in the dielectric across the interface. There are thus two ways to treat the structurally more complex systems we report on here. We can either consider the function s(z) to be a non-monotonic function across the interface or we can consider these systems to be multilayer stacks, with each layer possessing its own s(z) functionality. The difference between these two approaches lies in the treatment of the Fresnel factors at each interface. If we consider the $\chi^{(2)}$ active portion of the interface to be a single layer with a complicated s(z) profile, there is no need to explicitly consider the Fresnel factors at each layer. For a multilayer assembly, however, the Fresnel factors come into play at each interface.

The fundamental difference between these two approaches lies in the fact that the explicit multilayer treatment considers the $\chi^{(2)}$ response of the interface to be a simple linear superposition of the nonlinear response of each layer, with the Fresnel factors for each interface determining the transmission of the fundamental and second harmonic

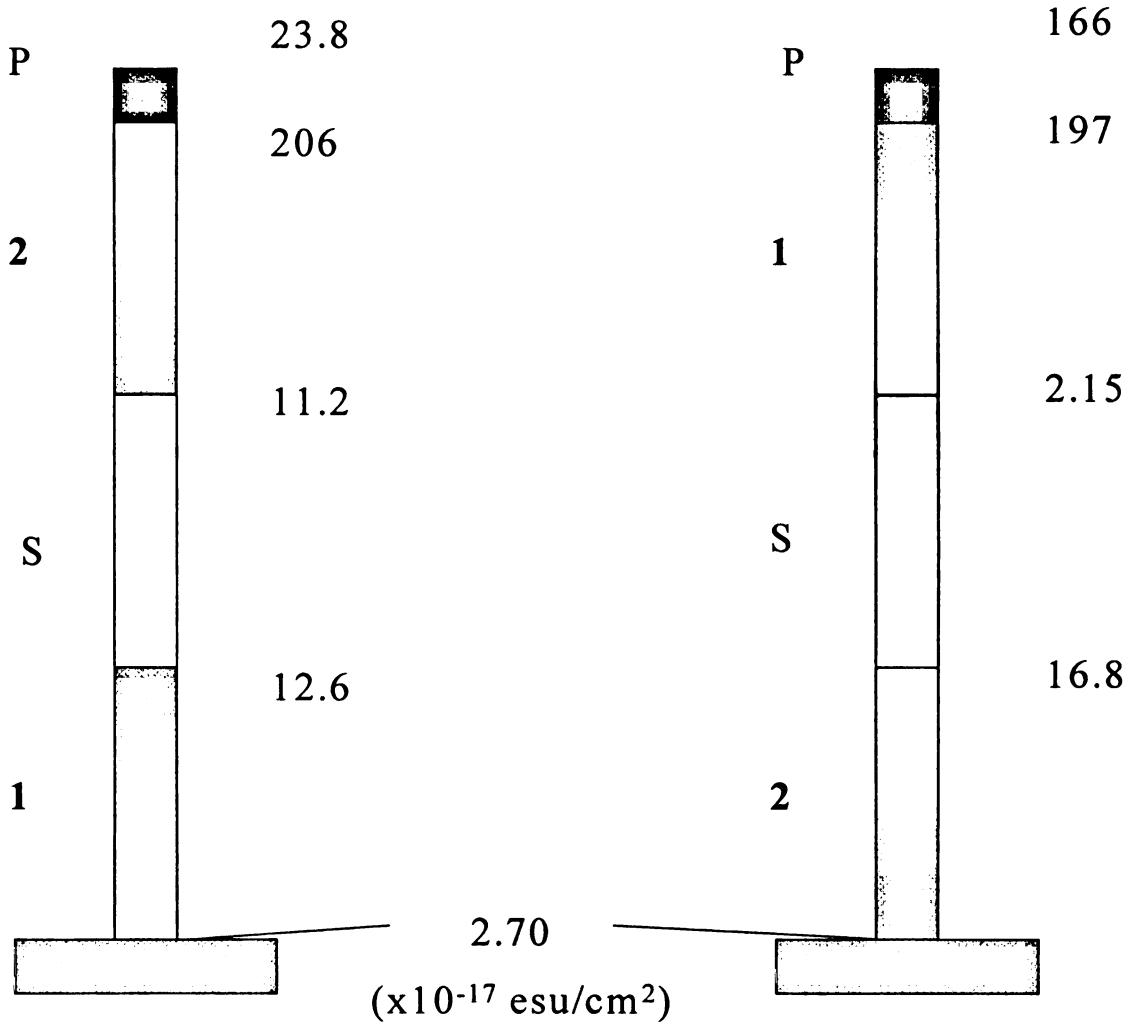

Figure 5.1 Schematic of the assemblies of chromophores **1** and **2** spaced apart with one $\chi^{(2)}$-inactive layer of 1,12-dodecanediylbisphosphonate. The shading of the chromophore layers represents the induced dipole moment. The experimental susceptibility values, referenced to the known value for quartz, are located adjacent to the appropriate layer for each step in the assembly.

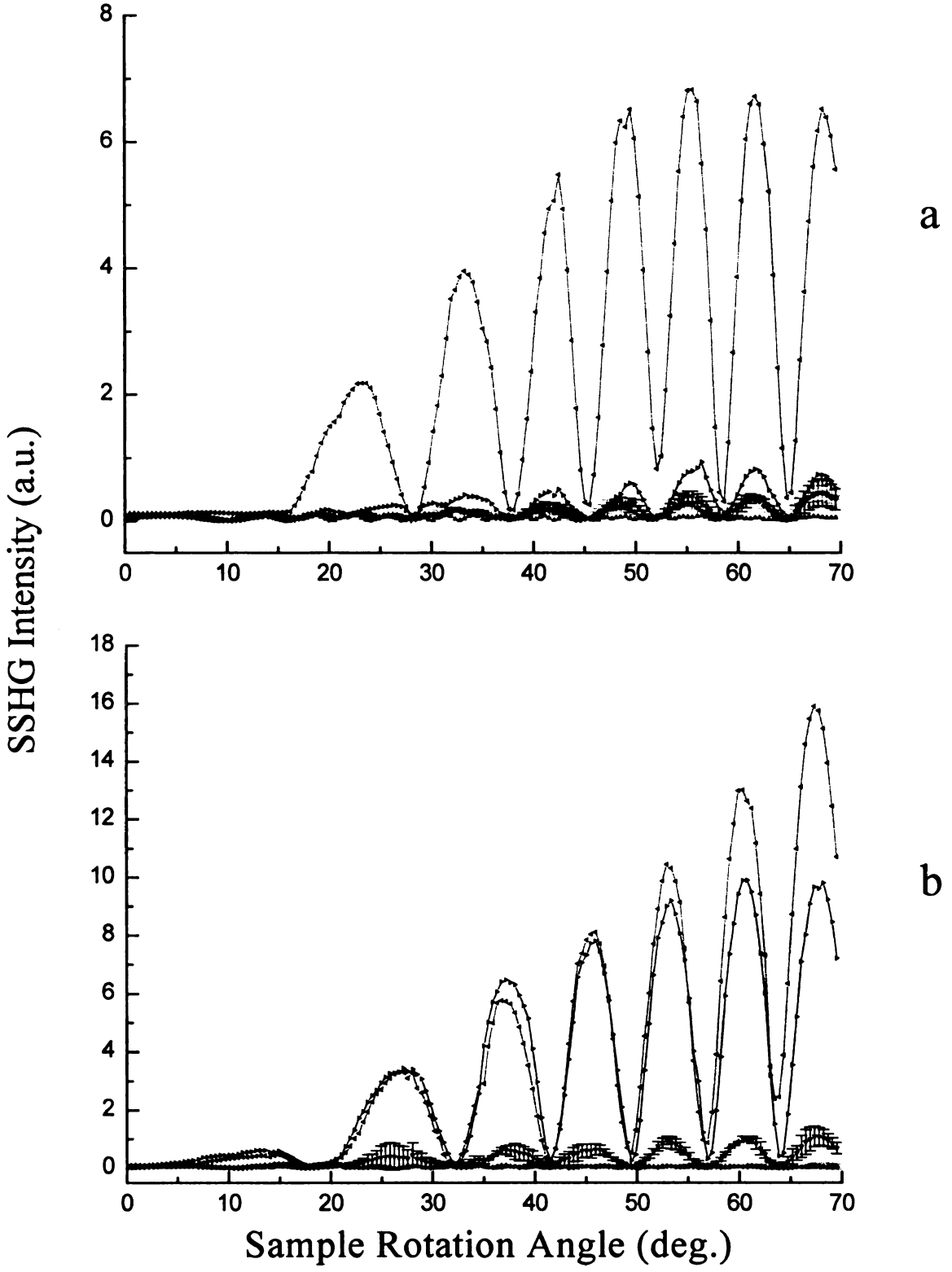

Figure 5.2 Surface SHG intensities for the build up of chromophores **1** and **2** spaced apart with one layer of $\chi^{(2)}$-inactive 1,12-dodecanediylbisphosphonate on fused silica substrates (a) SiO_x; SiO_x–**1**; SiO_x–**1**-S; SiO_x–**1**-S-**2**; SiO_x–**1**-S-**2**-P (b) SiO_x; SiO_x–**2**; SiO_x–**2**-S; SiO_x–**2**-S-**1**; SiO_x–**2**-S-**1**-P. The P is the addition of a phosphonic acid capping layer.

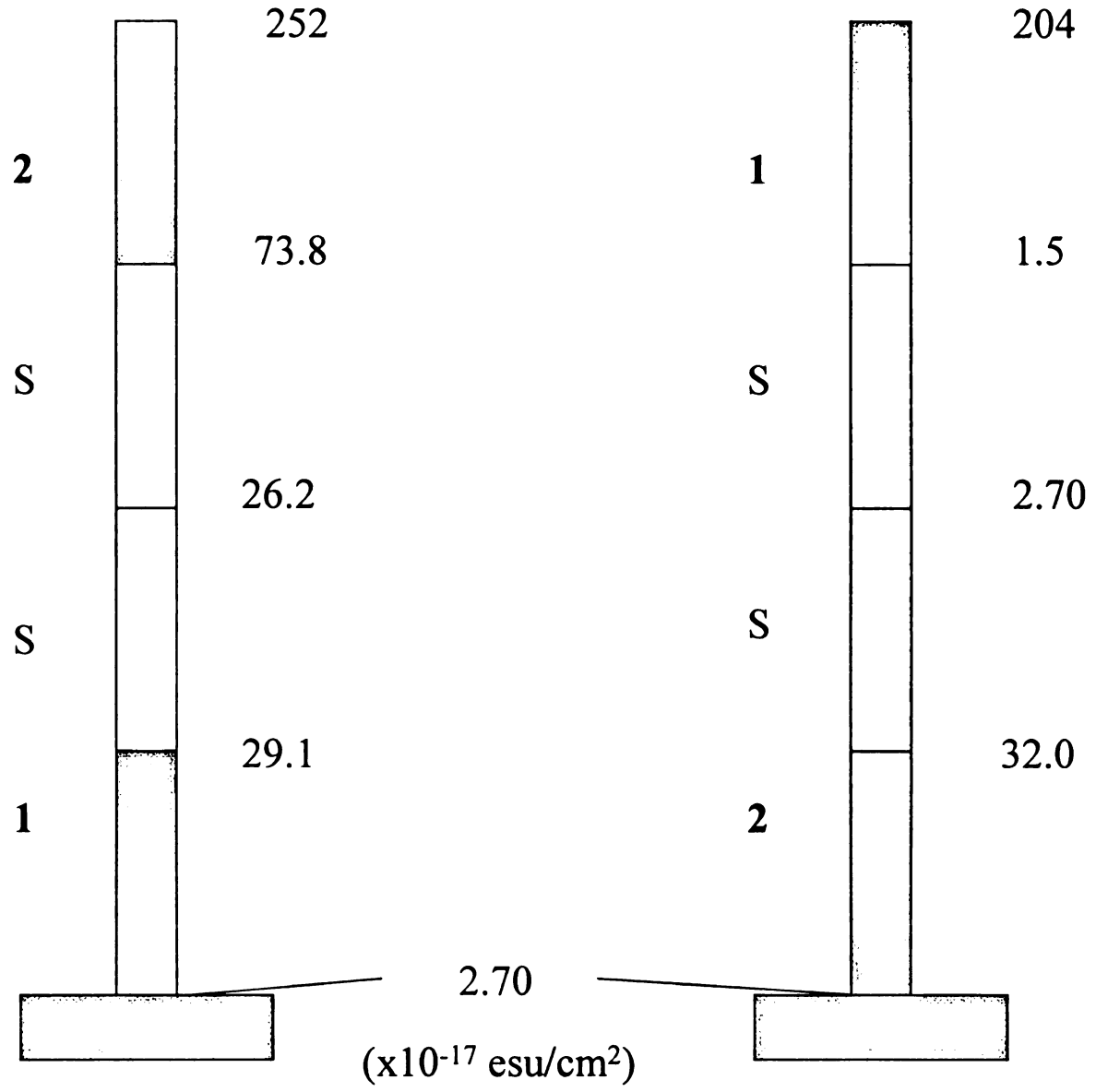

Figure 5.3 Schematic of the assemblies of chromophores **1** and **2** spaced apart with two $\chi^{(2)}$-inactive layers of 1,12-dodecanediylbisphosphonate. The shading of the chromophore layers represents the induced dipole moment. The experimental susceptibility values, referenced to the known value for quartz, are located adjacent to the appropriate layer for each step in the assembly.

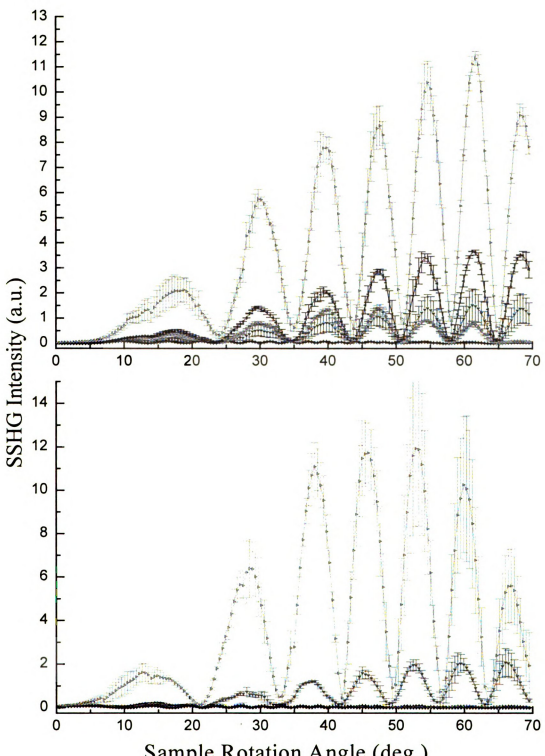

Figure 5.4 Surface SHG intensities for the build up of chromophores **1** and **2** spaced apart with two layers of $\chi^{(2)}$-inactive 1,12-dodecanediylbisphosphonate on fused silica substrates (a) SiO_x; SiO_x–**1**; SiO_x–**1**-S; SiO_x–**1**-S-S; SiO_x–**1**-S-S-**2** (b) SiO_x; SiO_x–**2**; SiO_x–**2**-S; SiO_x–**2**-S-S; SiO_x–**2**-S-S-**1**.

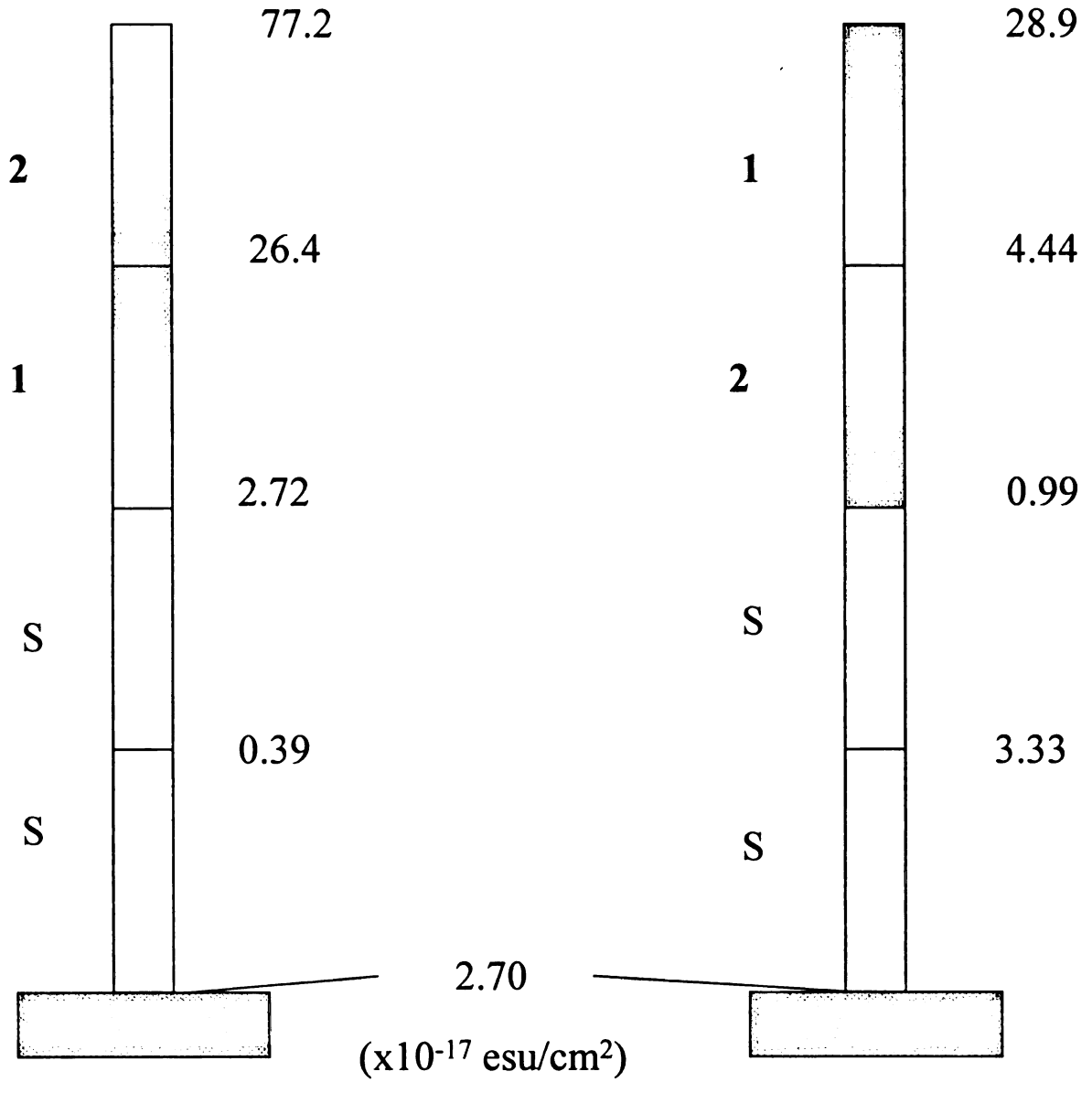

Figure 5.5 Schematic of the assemblies of chromophores **1** and **2** spaced away from the fused silica substrate with two $\chi^{(2)}$-inactive layers of 1,12-dodecanediylbisphosphonate. The shading of the chromophore layers represents the induced dipole moment. The experimental susceptibility values, referenced to the known value for quartz, are located adjacent to the appropriate layer for each step in the assembly.

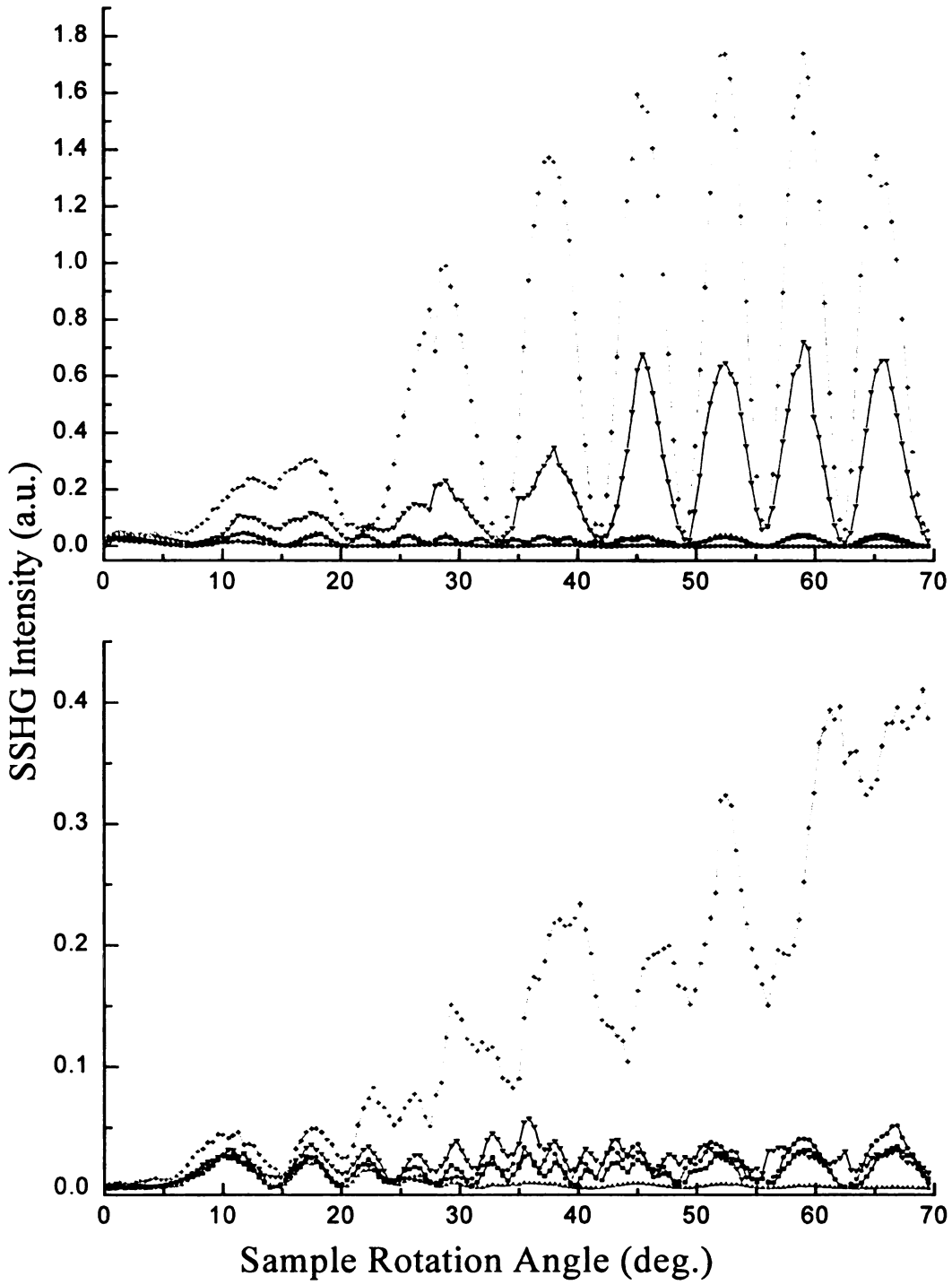

Figure 5.6 Surface SHG intensities for the build up of chromophores **1** and **2** spaced away from the fused silica substrate with two layers of $\chi^{(2)}$-inactive 1,12-dodecanediylbisphosphonate (a) SiO_x; SiO_x–S; SiO_x–S-S; SiO_x–S-S-**1**; SiO_x–S-S-**1**-**2** (b) SiO_x; SiO_x–S; SiO_x–S-S; SiO_x–S-S-**2**; SiO_x–S-S-**2**-**1**.

electric fields through the assembly. Implicit in this treatment is that there are no substantial inter-layer effects. This approximation is suspect, as we demonstrated experimentally in the preceding chapter. Treating the multilayer assembly in the context of a single layer with a non-monotonic dielectric response function, s(z), is potentially appealing in the sense that it eliminates the use of the Fresnel factors that can produce misleading results if the complex dielectric response of each layer is not known with certainty. This approach is also attractive in the sense that it offers the connection between the depth profile of the interface and its net nonlinear response. While it would be appealing to model s(z) from the experimental data, this is not a tractable task because we cannot determine *a priori* the relative contributions of the dipolar and quadrupolar terms in the effective $\chi^{(2)}$ response. Because these two contributions depend differently on the function s(z), and we measure experimentally the single quantity $\chi^{(2)}$, the unambiguous resolution of s(z) is not possible. Notwithstanding this limitation, we can gain some insight into the factors that contribute to s(z) from the experimental data.

The first experiments in the series we report here are for three layer systems, where the two opposing bilayer structures are each modified by the insertion of a $\chi^{(2)}$-inactive alkane bisphosphonate spacer. Because the length of the alkane bisphosphonate spacer layer (20 Å)[44] is substantially less than the coherence length of the laser light source ($\geq$ 3cm), we expect to recover cancellation of the chromophore dipolar contributions to the $\chi^{(2)}$ response. We do not observe this condition experimentally. As shown it Table 5.1 and schematized in Figures 5.1,5.3, and 5.5, there are two notable features regarding these data. The first is that cancellation is not obtained between chromophores **1** and **2** and the second is that the magnitude of the $\chi^{(2)}$ response for the

chromophores is different by a factor of ~10, depending on their position with the interface. For either chromophore in close proximity to the surface, we recover a SSHG signal that is ~ 7 times larger than that of the fused silica substrate. For these same chromophores spaced away from the substrate by ~ 50 Å, we recover SSHG signals that are ~ 70 times larger than the substrate. The difference in these responses must not be due to simple chemical structural effects. We recover essentially the same layer-dependent responses for the case where the chromophore layers are separated by two spacer layers, ~ 40 Å, demonstrating that the anomalous response we observe is not associated with a simple optical interference phenomenon.

In an effort to resolve whether our experimental data are the result of chromophore separation, we constructed the two canceling chromophore bilayer structures, with chromophores in adjacent layers, on a substrate where two spacer layers had been chemisorbed to isolate the chromophores from the fused silica. The results of these experiments are similar to those for the preceding ones; we do not observe structural cancellation, and the $\chi^{(2)}$ responses of the chromophores appear to correlate with the spacing from the silica substrate.

As discussed above, we need to consider the function s(z) in Eq. 5.1 to understand these data. For an interface of single composition, the dielectric response is considered to vary smoothly between its two boundary conditions. Guyot-Sionnest and Shen indicate that $s(z)_i = 1/\varepsilon_i$, and that s(z) varies smoothly across the interface. In their treatment it was implicit that ε was real, but for our systems, where the second harmonic electric field is in resonance with the red edge of the absorption spectra of the chromophores, ε will necessarily be complex. In addition, the dielectric response of the ZP interlayer linking

moiety is not the same as that of the organic layer constituents. We are thus left with a function s(z) which is, in general, complex and does not vary in a simple manner across the interface. The role of the ZP functionality is underscored by changes in the $\chi^{(2)}$ response of multilayers capped with phosphoric acid, as indicated in Table 5.1. While we can estimate the spatial variation of s(z) for our layered assemblies, there is still significant ambiguity remaining in the modeling of the experimental phenomena. This ambiguity remains because of the undetermined relative contributions from the various contributions to $\chi^{(2)}$ (Eq. 5.1), and the uncertainty that exists in the experimental values of n and k for the individual layer constituents.

5.4 Conclusions

We have determined that there is a strong interface structural dependence on the experimental SSHG signal recovered from systems expected to exhibit cancellation. By spacing two complementary chromophores apart using one or two layers of 1,12-dodecanediylbisphosphonic acid, the SSHG intensity is seen to deviate from expectations and increase anomalously for each structural motif. The different SSHG signal responses of each layer before and after phosphorylation indicates a contribution to the overall response from the Zr-phosphate/phosphonate linkage adjacent to different functional groups. The immediate horizons in this work are the development of models to account for complex spatial variations in s(z) and to treat these interfaces as explicit multilayer assemblies. Comparing the predictions of each of these models will allow us to determine the most appropriate way to treat our data.

5.5 Literature Cited

1. Nelson, Bryce P.; Frutos, Anthony G.; Brockman, Jennifer M.; Corn, Robert M.; *Anal. Chem.*, **1999**, 71, 3928.

2. Frutos, Anthony G.; Weibel, Stephen C.; Corn, Robert M.; *Anal. Chem.*, **1999**, 71, 3935.

3. Xia, Y. N.; Whitesides, G. M.; *Annu. Rev. Mater. Sci.*, **1998**, 28, 153.

4. Collier, C. P.; Wong, E. W.; Belohradsky, M.; Raymo, F. M.; Stoddart, J. F.; Kuekes, P. J.; Williams, R. S.; Heath, J. R.; *Science*, **1999**, 285, 391.

5. Katz, H. E.; Scheller, G.; Putvinski, T. M.; Schilling, M. L.; Wilson, W. L.; Chidsey, C. E. D.; *Science*, **1991**, 254, 1485.

6. Marowsky, G.; Lupke, G.; Steinoff, R.; Chi, L. F.; Mobius, D.; *Phys. Rev. B*, **1990**, 41, 4480.

7. Palto, S. P.; Blinov, L. M.; Yudin, S. G.; Grewer, G.; Schonholl, M.; Losche, M.; *Chem. Phys. Lett.*, **1993**, 202, 308.

8. Kepley, L. J.; Crooks, R. M.; Ricco, A.; *Anal. Chem.* **1992**, 64, 3191.

9. Swalen, J. P.; Allara, D. L.; Andrade, J. P.; Chandross, E. A.; Garoff, S.; Israelachvilli, J.; McCarthy, T. J.; Murray, R.; Pease, R. F.; Rabolt, J. F.; Wynne, K. J.; Tu, H.; *Langmuir* **1987**, 3, 932.

10. Calvert, J. M.; Georger, J. H., Jr.; Peckerer, M. C.; Perhsson, P. E.; Schnur, J. M.; Scheon, P.; E.; *Thin Films* **1992**, 114, 9188.

11. Dulcey, C. S.; Georger, J. H.; Krauthamer, V.; Stenger, D. A.; Fare, T. L.; Calvert, J. M.; *Science* **1991**, 252, 551.

12. Kumar, A.; Biebuyck, H. A.; Abbott, N. L.; Whitesides, G. M.; *J. Am. Chem. Soc.* **1992**, 114, 9188.

13. Vrancken, K. C.; Van Der Voort, P.; Gillis-D'Hammers, I.; Vansant, E. F.; Grobet, P.; *J. Chem. Soc., Faraday Trans.* **1992**, 88, 3197.

14. Pfleiderer, B.; Albert, K.; Bayer, E.; *J. Chromatogr.* **1990**, 506, 343.

15. Yonemoto, E. H.; Saupe, G. B.; Schmehl, R. H.; Hubig, S. M.; Riley, R. L.; Iverson, B. L.; Mallouk, T. E. *J. Am. Chem. Soc.* **1994**, 116, 4786.

16. Katz, H. E.; Bent, S. F.; Wilson, W. L.; Schilling, M. L.; Ungashe, S. B. *J. Am. Chem. Soc.* **1994**, 116, 6631.

17. Frey, B. L.; Hanken, D. G.; Corn, R. M. *Langmuir* **1993**, 9, 1815.

18. Yang, H. C.; Aoki, K.; Hong, H.-G.; Sackett, D. D.; Arendt, M. F.; Yau, S.-L.; Bell, C. M.; Mallouk, T. E. *J. Am. Chem. Soc.* **1993**, 115, 11855.

19. Vermeulen, L.; Thompson, M. E. *Nature* 1992, 358, 656.

20. Ungashe, S. B.; Wilson, W. L.; Katz, H. E.; Scheller, G. R.; Putvinski, T. M. *J. Am. Chem. Soc.* **1992**, 114, 8717.

21. Cao, G.; Rabenberg, L. K.; Nunn, C. M.; Mallouk, T. M. *Chem. Mater.* **1991**, 3, 149.

22. Katz, H. E.; Schilling, M. L.; Chidsey, C. E. D.; Putvinski, T. M.; Hutton, R. S. *Chem. Mater.* **1991**, 3, 699.

23. Putvinski, T. M.; Schilling, M. L.; Katz, H. E.; Chidsey, C. E. D.; Mujsce, A. M.; Emerson, A. B. *Langmuir* **1990**, 6, 1567.

24. Rong, D.; Hong, H.-G.; Kim, Y.-I.; Krueger, J. S.; Mayer, J. E.; Mallouk, T. E.; *Coord. Chem. Rev.*, **1990**, 97, 237.

25. O'Brien, J. T.; Zeppenfeld, A. C.; Richmond, G. L.; Page, C. J.; *Langmuir,* **1994,** 10, 4657.

26. Ansell, M. A.; Zeppenfeld, A. C.; Yoshimoto, K.; Cogan, E. B.; Page, C. J.; *Chem. Mater.,* **1996,** 8, 591.

27. Katz, H. E. *Chem. Mater.* **1994,** 6, 2227.

28. Langmuir, I.; *Trans. Faraday Soc.*; **1920,** 15, 62.

29. Kleinfeld, Elaine R.; Ferguson, Gregory S.; *Chem Mater.*, **1996,** 8, 1575.

30. Chidsey, C. E. D., Loiacono, D. N.; *Langmuir*, **1990,** 6, 682.

31. Seshadri, K.; Froyd, K.; Parikh, A. N. Allara, D. L.; Lercel, M. J.; Craighead, H. G.; *J. Phys. Chem.*, **1996**, 100, 15900.

32. Sabatini, E.; Rubinstein, I.; *J. Phys. Chem.*, **1987**, *91*, 6663.

33. Sabatini, E.; Rubinstein, I.; Moaz, R.; Sagiv, J.; *J. Electroanal. Chem.*, **1987**, *219*, 365.

34. Finklea, H. O.; Snider, D. A.; Fedyk, J.; Sabatini, E.; Gafni, Y.; Rubinstein, I.; *Langmuir*, **1993**, *9*, 3660.

35. Finklea, H. O.; Snider, D. A.; Fedyk, J.; *Langmuir*, **1990**, *6*, 371.

36. Sabatini, E.; Cohen-Boulakia, J.; Bruening, M. L.; Rubinstein, I.; *Langmuir*, **1993**, *9*, 2974.

37. Janek, R. P.; Fawcett, W. R.; Ulman, A.; *Langmuir*, **1998**, *14*, 3011.

38. Zhao, Xiao-Mei; Wilbur, James L.; Whitesides, George M.; *Langmuir*, **1996**, 12, 3257.

39. Patrick, David L.; Cee, Victor, J.; Purcell, Timothy, J.; Beebe, Thomas B. Jr.;

Langmuir, **1996**, 12, 1830.

40. Katz, H. E.; Wilson, W. L.; Scheller, G.; *J. Am. Chem. Soc*, **1994**, *116*, 6636.

41. Flory, W. C.; Mehrens, S. M.; Blanchard, G. J.; *J. Am. Chem. Soc.*, in review.

42. Flory, W. C.; Blanchard, G. J.; *J. Am. Chem. Soc.*, in review.

43. Perrin, D. D.; Armarego, W. L. F.; Perrin, B. R.; *Purification of Individual Organic Chemicals, Pergmon Press*, Oxford, **1980**, 449.

44. Horne, J. C.; Blanchard, G. J.; *J. Am. Chem. Soc.*, **1996**, 118, 12788.

45. Guyot-Sionnest, P.; Shen, Y. R.; *Phys. Rev. B.*, **1987**, *35*, 4420.

Chapter 6

Future Directions

This dissertation has demonstrated that there are a minimal amount of defects within zirconium phosphate/phosphonate multilayer assemblies. With the development of the SHG laser system and the synthesis of chromophores **1** and **2**, there are a variety of directions that this work can take. The system can be modified to image surfaces. A variety of layer motifs can yield a large body of data further investigating these systems and the spatial effects that the two chromophore layers can have with respect to the SSHG signal obtained.

Modification of the SSHG system to image the surfaces would improve the amount of knowledge obtainable from ZP systems. Nonlinear surface imaging is a technique that has recently been employed for use as a measuring tool of interfaces.[1-3] SSHG imaging measurements can yield information about the surface morphology on a μm scale. Images are acquired using two fundamental beams temporally intersecting at the sample. The SHG signal from the sample is collected using CDD detectors, and the sample is then translated normal through the beam thereby forming an SHG images of the area scanned. The SHG images can be collected using either transmission or reflection modes. Control over the input polarization of each of the beams will allow selective control of the electric field polarization with respect to the chromophores nonlinear transition moment, and more specifically, access to the tensor elements of the $\chi^{(2)}$ optical susceptibility.

By using both SSHG intensity and SSHG imaging measurements in characterizing SAMs, a wealth of information can be acquired. Insight into the

chromophore layer's nonlinear susceptibility, tilt angle, and the angular distribution can be ascertained from the direct SHG intensity data, while information relating to surface morphology on a μm scale can be obtained using SSHG imaging experiments.

One possible avenue of exploration using these systems in tandem is the study of aggregation within a chromophore layer using SSHG as the measuring tool. It has been shown that varying the concentration of a chromophore within a single layer leads to island formation.[4,5] By using these nonlinear molecules in conjunction with SSHG, noninvasive characterization to the degree of this inhomogenaity can be assessed. By choosing an alkane bisphosphonate of the appropriate length and using this to 'dilute' the chromophore in solution, layers containing aggregated islands of the chromophore can be formed. The SSHG intensity and image from this assembly will be from these island defects and information about their properties can be elucidated in a more detailed manner then previously reported.

One may also be able to draw information about the assembly of the chromophores by mixing the chromophores in the same solution. Using a 1:1 solution of chromophores **1** and **2**, one would expect an even distribution of each on the surface since the formation properties are identical, based on the linear response presented in Chapter 2. The monolayer SSHG signal should be only the response of the substrate, because the distribution of signs of the nonlinear response within the 100 μm beam area. If a bilayer is synthesized from sequential deposition from this solution, the response should yield a signal that contains cancellation of the electric dipole moments in the bilayer as well as the monolayer, and half the signal intensity observed for [SiO_x-**2**-**1**] (Figure 4.6b) is expected due to the quadrupole moment contribution.

Based on the discussion from Chapter 5, a greater understanding of the response of the spatially modified surfaces needs to be achieved. Because the chromophores **1** and **2** both have absorption tails at 532 nm, both the real and imaginary components of the dielectric gradient contribute to the observed signal. It is this gradient of the dielectric properties that leads to the observed SSHG signal. It is believed that this is the first work that studies dielectric variance in thins films. By controlling the dielectric properties of a film, one can begin to understand the effects the imaginary component has in thin films.

6.1 Literature Cited

1. Florsheimer, M.; Kupfer, M.; Bossard, C.; Looser, H.; Gunter, P.; *Adv. Mater.*, **1992**, 4, 795.

2. Florsheimer, M.; Jundt, D. H.; Looser, H.; Sutter, K.; Gunter, P.; *J. Phys. Chem.*, **1994**, 98, 6399.

3. Florsheimer, M.; *Phys. Stat. Sol. A*, **1994**, 173, 15.

4. Horne, J.C.; Huang, Y.; Liu, G. Y.; Blanchard, G. J.; *J. Am. Chem. Soc.*, **1999**, 121, 4419.

5. Horne, J.C.; Blanchard, G. J.; *J. Am. Chem. Soc.*, **1999**, 121, 4427.

APPENDIX A

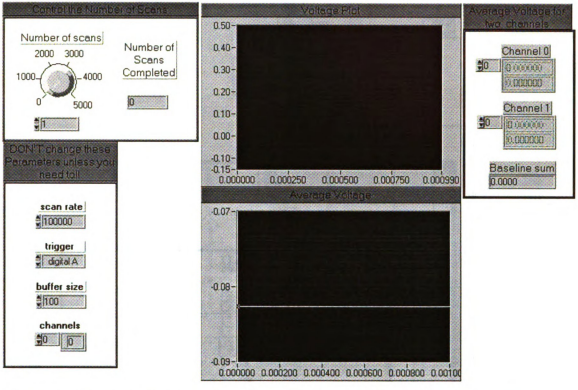

Figure 1A Front panel of the Labview® program written for the SSHG laser system.

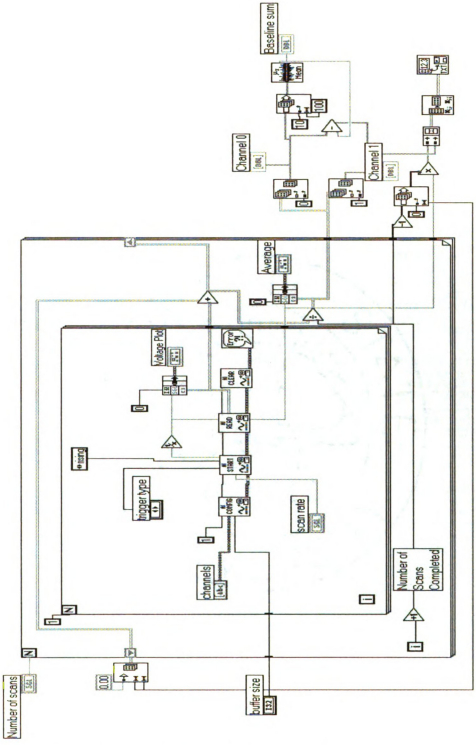

Figure 2A Icon based schematic of the Labview® Program.

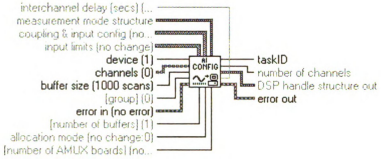

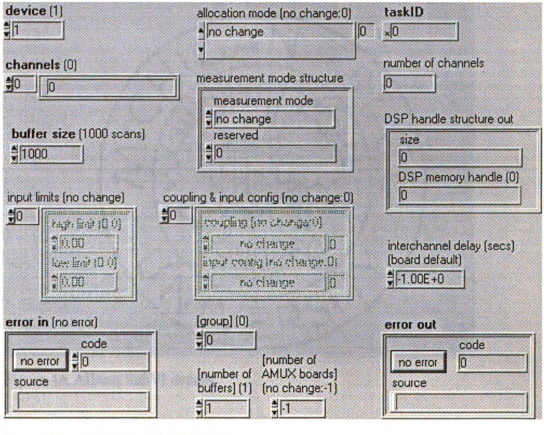

Figure 3A AIConfig SubVI details.

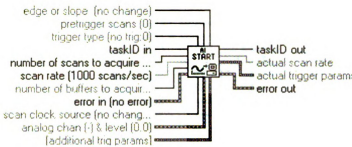

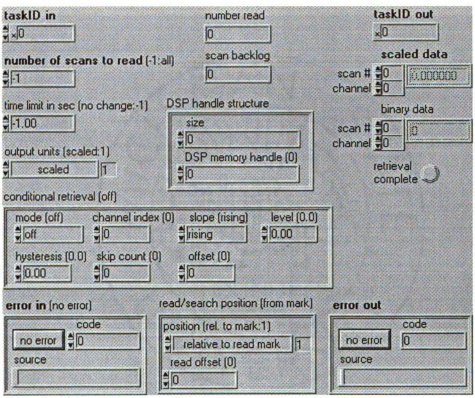

Figure 4A AIStart SubVI details.

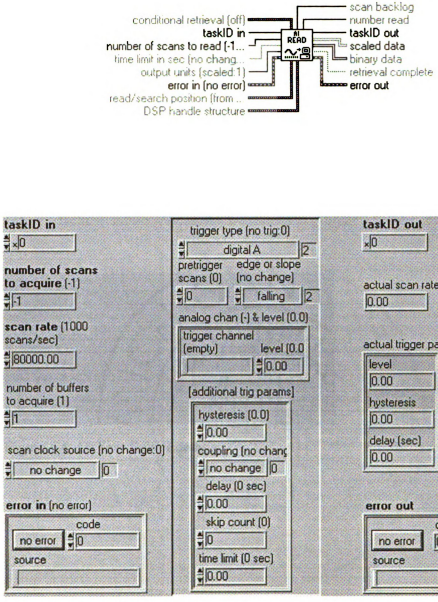

Figure 5A AIRead SubVI details.

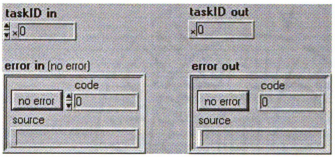

Figure 6A AIClear SubVI details.

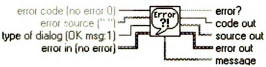

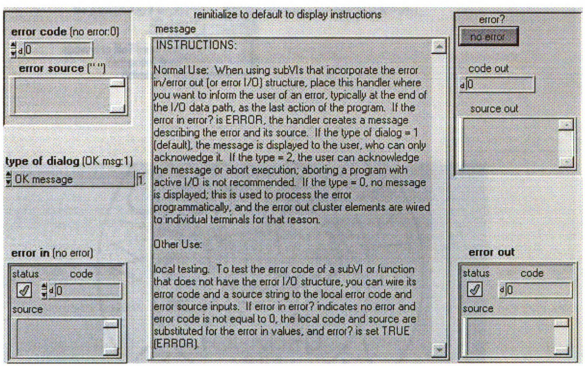

Figure 7A Error SubVI details.

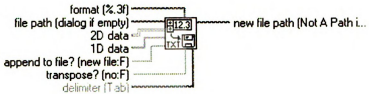

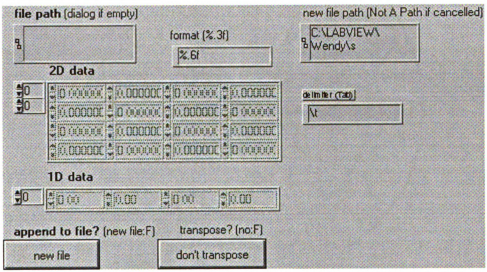

Figure 8A. Write to Spreadsheet SubVI details.